공학박사 학위논문

Development of Bipolar electrode based Membrane Capacitive Deionization System with Direct Energy Recovery

직접 에너지 회수 단계를 포함하는 Bipolar MCDI 시스템 개발

2022년 8월

서울대학교 대학원

화학생물공학부

전 성 일

Development of Bipolar electrode based Membrane Capacitive Deionization System with Direct Energy Recovery

by

Sung-il Jeon

Under the supervision of

Professor Jeyong Yoon, Ph. D.

A dissertation submitted in partial fulfillment of the requirements for

the Degree of Doctor of Philosophy

August 2022

SCHOOL OF CHEMICAL AND BIOLOGICAL

ENGINEERING

SEOUL NATIONAL UNIVERSITY

Development of Bipolar Electrode based Membrane Capacitive Deionization System with Direct Energy Recovery

직접 에너지 회수 단계를 포함하는 양극성 전극 기반 막 축전식 탈염 시스템 개발

지도교수 윤 제 용

이 논문을 공학박사 학위논문으로 제출함

2022년 6월

서울대학교 대학원

공과대학 화학생물공학부

전 성 일

전성일의 공학박사 학위논문을 인준함

2022년 6월

위 원 장 최 장 욱 (인)

부 위 원 장 윤 제 용 (인)

위 원 이 창 하 (인)

위 원 김 춘 수 (인)

위 원 강 경 석 (인)

Abstract

Development of Bipolar electrode based Membrane Capacitive Deionization System with Direct Energy Recovery

Sung-il Jeon

School of Chemical and Biological Engineering

The Graduates School

Seoul National University

For the transition to a carbon-neutral society to overcome the climate crisis, the development of energy-efficient and eco-friendly water securing technology is important. Membrane capacitive deionization (MCDI) technology is attracting attention as a suitable solution for these needs. In order for MCDI technology to be applied to actual industry, it is essential to expand the MCDI module and install the energy recovery technology. However, the conventional expansion method causes a large energy loss in controlling the system due to the increase in current. Besides, the energy recovery technology is also inefficient despite high development costs.

This dissertation is to develop a bipolar electrode-based MCDI (Bipolar

MCDI) with a direct energy recovery step. To prevent the problem on an industrial scale, two approaches were applied. The first is to connect the electrodes of the MCDI module in series, which is called bipolar electrode. Since Bipolar MCDI operates at low current and high voltage, this concept can reduce energy loss on an industrial scale. The second is to adopt a direct energy recovery method, which can reduce the energy consumption of the system with a small development cost. However, in order to successfully combine these two concepts, electrical safety must be secured. When two Bipolar MCDI modules operating at high voltage are directly connected for energy recovery, a current higher than the allowable current of the system may flow, which may result in an electrical explosion or damage to the device.

Therefore, this dissertation is studied as follows. First, an equivalent circuit model is proposed to simulate the charge/discharge and direct energy recovery steps. As a primary result, simulation results were in good agreement with the experimental results in not only the charge/discharge step but also the direct energy recovery step. In addition, it was confirmed that the direct energy recovery operates below the current of constant voltage operation, which indicates that the direct energy recovery of Bipolar MCDI can be safely performed with a constant voltage operation system.

Second, the operation characteristics of Bipolar MCDI with the direct

energy recovery stage are investigated. The optimized operation is applied to the pilot-scale process based on the investigation. As a major result, energy consumption was reduced by 43% and 41%, respectively, at the laboratory scale (2.4 V and 12 V systems) compared to the conventional constant voltage charge/discharge operation. In addition, the energy consumption was reduced by 40% without deterioration of the desalination performance even on the pilot scale.

This study successfully developed a Bipolar MCDI system for the industrial application of MCDI technology by adopting bipolar electrodes as an MCDI module expansion and direct energy recovery. The Bipolar MCDI system with direct energy recovery step developed through this study can be an energy-efficient alternative in an actual industrial environment, and the development process will help expand lab-scale research to industrial scale in the future.

Keywords: electrochemical ion separation; capacitive deionization; bipolar electrode; energy recovery; equivalent circuit

Student number: 2017-34898

Table of Contents

List of figures

List of tables

1. Introduction

1.1. Research Background

Recently, the world has declared carbon neutrality in order to fundamentally escape from the crisis of climate change and is demanding a transition from a carbon-based society to a carbon-neutral society [1–3]. In line with this era, desalination technology also needs to be converted from energy-intensive existing technology to low-energy and eco-friendly technology.

Membrane capacitive deionization (MCDI) derived from capacitive deionization (CDI), one of the electrochemical ion separation technologies, is attracting attention as a next-generation desalination technology [4]. By applying the electrical energy to a MCDI cell, the ions are removed from salt water to the electrode surface. In addition, the input energy can be recovered, making the technology more energy efficient [5]. This technology, which uses a DC voltage of 1.2 V or lower, is expected as a desalination technology suitable for the carbon-neutral era since this technology can be well suited to the existing grid as well as renewable energy [6].

In order for MCDI to be successfully applied throughout the industry, it is necessary to develop an efficient scale-up method and energy recovery technology. The MCDI modules extend their desalination capacity via stack-

up of the electrode as well as the extension of the electrode size [7,8]. Typically, the stacked electrodes are connected in parallel, which can be defined as a unipolar type [7,9]. For this unipolar MCDI, all electrode pairs require a terminal to connect with an external power supply, which increases the complexity of module assemblies with a larger number of stacked electrodes [8,10]. In addition, the current is proportionally increased with the number of electrodes in the stack since the total current of the system is distributed at one point to each electrode pair to apply the same voltage (e.g., 1.2 V) [11]. On the other hand, the invested energy in MCDI can be recovered, which is calculated by analyzing the voltage profile of the constant current discharge operation [12–15]. This extracted energy from the MCDI device can be utilized again for MCDI operation or other electric equipment [16]. To utilize this energy, it is considered to equip the control system with a DC-DC converter for energy recovery [6,17–28].

However, the current approach for industrial application of MCDI suffers from several limitations. For example, the operating current that increases with the stack-up of electrodes causes a lot of energy loss in their control system according to Joule's law. This energy loss was found to account for more than 40% of the total invested energy in the pilot system operating at 105 A [6]. Furthermore, the development cost of a control system

with the DC-DC converter for energy recovery will be expensive. Despite the cost, the energy recovery with the DC-DC converter showed a low energy recovery efficiency of 50% or less, not only on the lab scale but also on the pilot scale, so far [6,19,28].

To overcome this problem, two approaches can be considered. The first is to connect the electrodes of the MCDI module in series, which is called bipolar electrode-based MCDI (Bipolar MCDI). Since the Bipolar MCDI operates at low current and high voltage, this concept can reduce energy loss on an industrial scale. The second is to adopt a direct energy recovery method, which can reduce the energy consumption of the system with a small development cost. However, in order to combine these two concepts, electrical safety must be secured. When two Bipolar MCDI modules operating at high voltage are directly connected for energy recovery, a current higher than the allowable current may flow due to the high voltage difference and low resistance between the two modules. This poses an electrical explosion risk or damage to the device. For this reason, the combination of these two concepts has not been studied until now.

1.2. Objectives of the research

The purpose of the research in this dissertation is to develop a bipolar electrode-based membrane capacitive deionization (Bipolar MCDI) system with direct energy recovery to overcome the energy efficiency decrease due to scale-up. Bipolar MCDI is a type of MCDI that operates with high voltage and low current and uses a stack of electrodes connected in series. To achieve this goal, extensive studies were carried out over two parts.

First, the charging/discharging and direct energy recovery processes of a Bipolar MCDI system are simulated by using an equivalent circuit model to secure electrical safety. The simulation results were compared with the experimental results in constant voltage charging/discharging and direct energy recovery steps.

Second, the operation characteristics of the Bipolar MCDI with direct energy recovery are investigated for the lab-scale system (2.4 V and 12 V system). In addition, the pilot-scale process was subjected to the optimum operating method based on the investigation.

2. Literature Review

2.1. History of electrochemical ion separation based on energy storage technique

The electrochemical method for ion separation is attracting attention as the eco-friendly, energy-efficient, and cost-effective separation process in the carbon-neutral era. The electrochemical method separates the ions by the interaction between ions in the water and the electrode material, which is generated by the application of an external power source. Electrodialysis (ED) is a well-known electrochemical method that is used in the desalination and concentration processes to separate ions through a redox reaction on the electrode chamber [29–31].

Beyond ED technology, the electrochemical method based on the working principle of energy storage devices is being investigated in order to separate ions at a lower energy cost [22]. These processes are evaluated as very efficient ion separation technologies in terms of energy because they use a low potential of around 1.5 V and can recover the invested energy [32,33]. The first electrochemical ion separation based on the operating principle of an energy storage device is thought to be capacitive deionization (CDI), which was introduced in the 1960s under the name electrochemical demineralization [34–37]. Since then, various materials and cell structures

have been developed to improve ion separation capacity and energy efficiency, and they have been given various names, as shown in **Figure 2-1**.

Yoon group in Seoul National University (SNU) classified these technologies into electrochemical ion separation (EIONS) [38], they can be grouped into one technology category through their technical feature and relationship, as shown in **Figure 2-2**. For example, MCDI was derived from CDI with the introduction of an ion exchange membrane [39–41]. It was then expanded to the concept of decoupling the electrolyte and the salt water via an ion exchange membrane, giving rise to flow-electrode CDI (FCDI) [42–44] and multi-channel CDI (MC-CDI) [45–49]. Furthermore, it has evolved into a concept of performing a desalination process and a concentration process simultaneously by dividing the salt water channel with an ion exchange membrane, which is a rocking chair CDI (RCDI) [50]. This concept also inspired electrochemical ion separation based on the battery principle represented by desalination battery (DB) and developed into cation intercalation desalination (CID) and anion reactive battery desalination (ARBD), which simultaneously perform desalination and concentration [51–54]. Recently, these technologies have been investigated to use redox-active material as an electrolyte [55–59].

These EIONS technologies are typically composed of electrodes, an

electrolyte, and an external power source, with various materials introduced as needed [60–65]. The fact that the energy invested for ion separation can be recovered and utilized is considered a high advantage. Furthermore, because it can increase selectivity for specific ions by using an ion exchange membrane and modifying an electrode material, EIONS can be applied to not only the desalination process but also the ion-selective process for resource recovery [38].

In the following section, some notable events are reviewed to gain insight into future research prospects of EIONS.

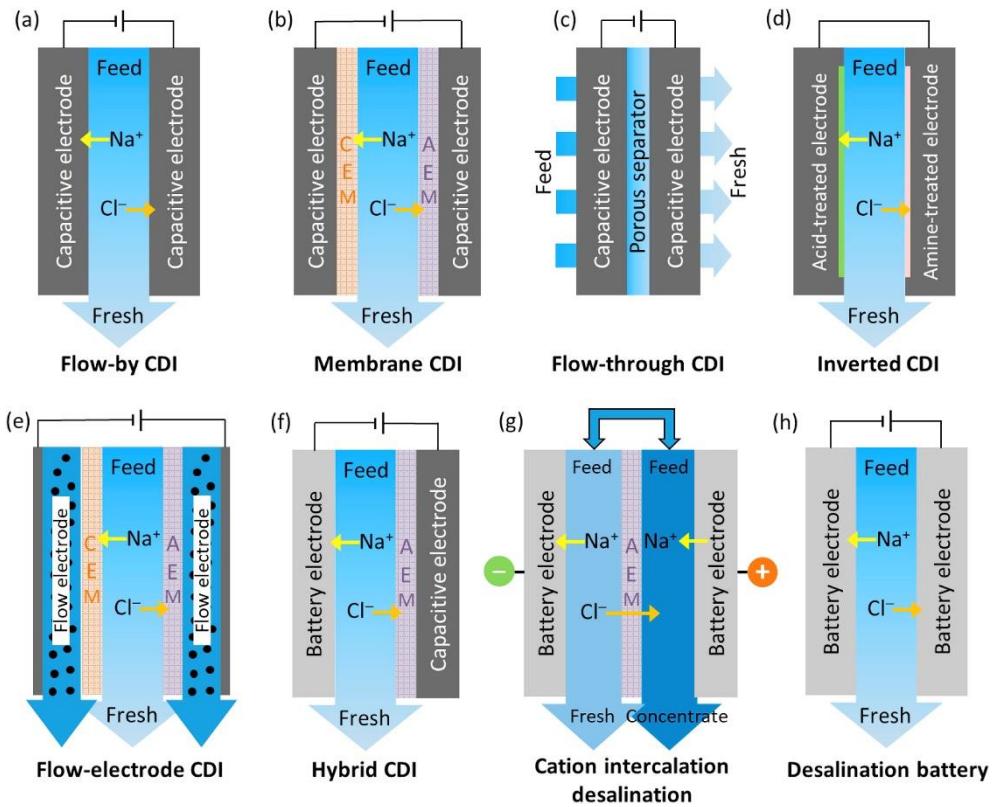

Figure 2-1. Various advanced architectures of capacitive deionization techniques [66].

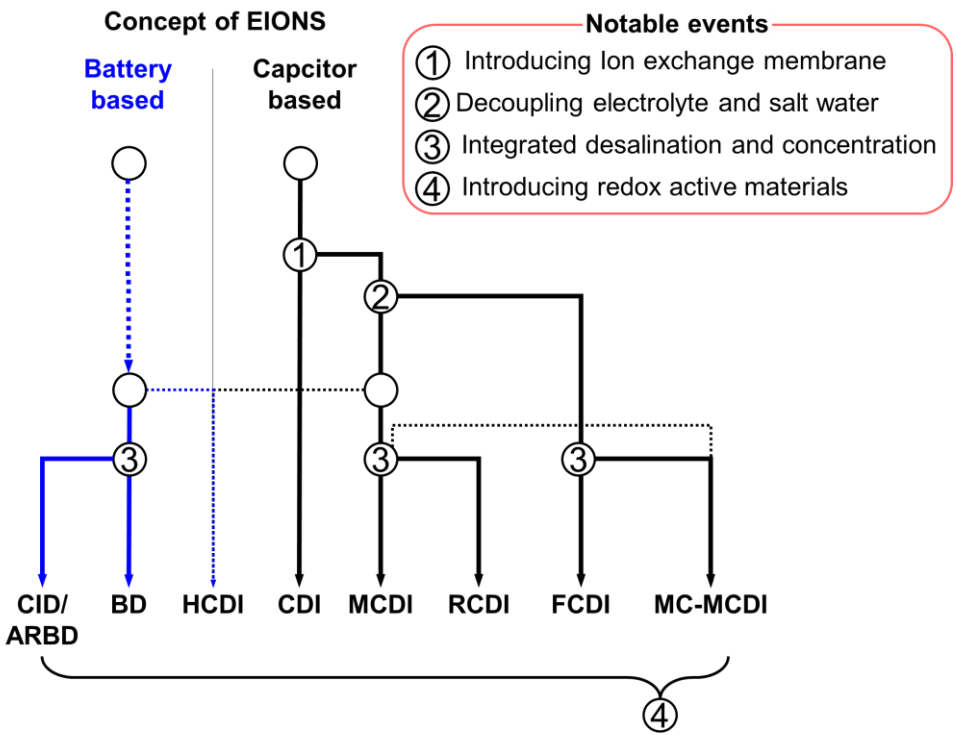

Figure 2-2. Technical history of electrochemical ion separation (EIONS). The figure refers to ph.D. Ahn's unpublished doctoral dissertation [67].

2.1.1 Introduction of ion exchange membrane into EIONS

CDI, an early technology of EIONS, works similarly to the operating principle of a supercapacitor, a typical energy storage device, as shown in **Figure 2-3** [32,68]. When a power source applies a voltage across both electrodes ions in the electrolyte are arranged to form an electric double layer on the electrode surface to match the charge neutrality of the electrode. (**Figure 2-3c and d)**. In the case of CDI, this deionized electrolyte is continuously discharged out of the reactor and fresh electrolyte (i.e., salt water) is continuously supplied into the reactor. (**Figure 2-3c)**. Discharging process of a supercapacitor and CDI transfers the stored energy into an external load by releasing ions into the electrolyte (**Figure 2-3e and f).** In CDI, the concentrated electrolyte during the discharging process by releasing ions is discharged out of the reactor (**Figure 2-3e)**. That is, CDI is generally operated in two stages of charging/discharging like a supercapacitor, and in this process, deionized water and concentrated water can be obtained respectively along with energy circulation. Also, the operation of most EIONS systems is similar to this.

However, the charge applied to CDI is not all stored on the surface of the electrode due to various phenomena occurring in the aqueous system (refer to **Figure 2-4**). For example, an electric charge can be consumed to

repulse co-ion rather than being used to adsorb the counter ion (co-ion repulsion). In addition, the charge can be consumed by swapping the co-ion of the electrode surface with the counter-ion of the bulk solution (ion swapping). These phenomena would cause no change or increase in ion concentration of bulk solution despite the invested electric charge since the counter ion is transferred from the opposite electrode to the bulk solution [4,69–73].

Moreover, not only the desired reaction (capacitive ion storage) but also parasitic reactions (faradaic reaction) can occur at the interface between the electrode and electrolyte, as shown in **Figure 2-4b**. According to the research of Yoon group in SNU, various reactions such as hydrogen peroxide revolution and carbon oxidation occur on the electrode surface [74]. These reactions could change the properties of the electrode surface which can adversely affect long-term performance, and eventually, the desalination and regeneration processes are reversed [74]. Waite group in the University of New South Wales (UNSW, Australia) has reviewed various reactions in CDI systems [75].

The introduction of an ion exchange membrane (or resin) between the electrode and a spacer was an innovative change of cell configuration that could partially solve this problem. As shown in **Figure 2-5a**, the ion exchange

membrane uses fixed charges in the backbone chain of the membrane to exclude ion transfer having the same charge and selectively permeate only ions with opposite charges. Since the concept was suggested through the patent of Andelman and Walker in 2004 [76], the research results were reported for the first time by Lee group of Korea Electric Power Research Institute (KEPRI) [39]. This system, called membrane capacitive deionization (MCDI), can reduce ion repulsion and ion swapping because the membrane covered on the electrode surface prevents these phenomena [39–41]. Hence, charge efficiency is greatly enhanced leading to an improvement in the deionization performance, although the ion exchange layer act as additional resistance to the system.

In addition, as shown in **Figure 2-5b**, the effect of suppressing parasitic reactions can be obtained by blocking the chain reaction of various electrode surface reactions through the ion exchange membrane and creating conditions unfavorable for these reactions in the interface between the electrode and bulk solution [74]. Therefore, the long-term performance and lifespan of MCDI are significantly improved compared to conventional CDI that suffer from various surface reactions [75].

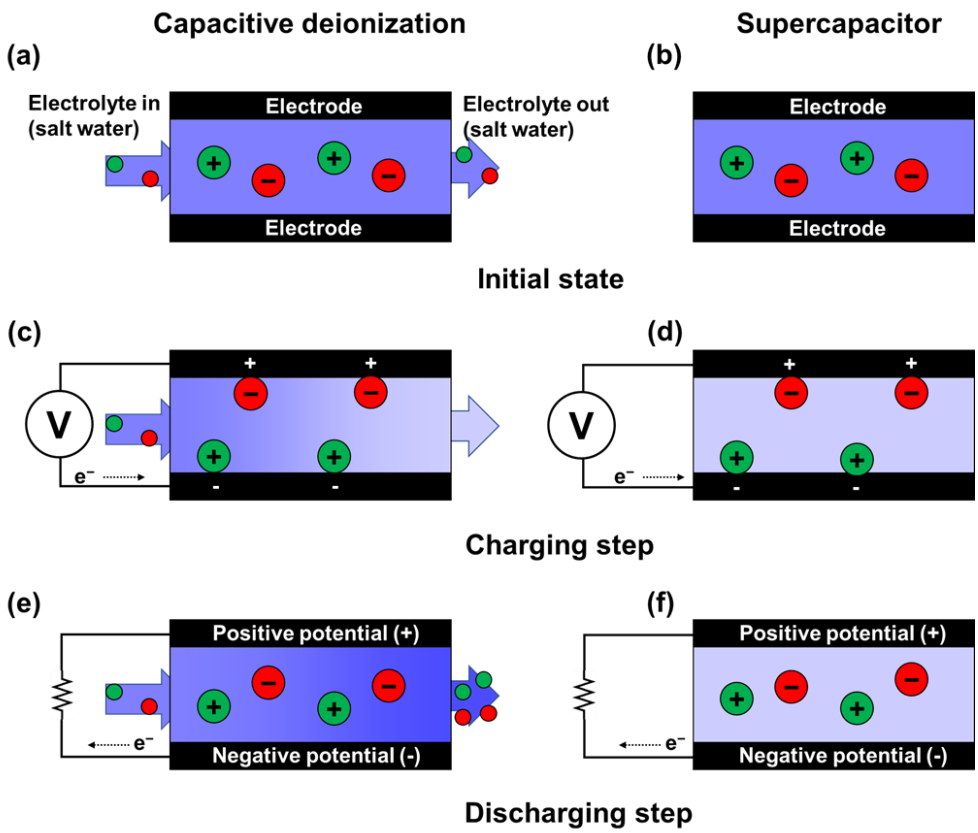

Figure 2-3. Fundamental operation difference of capacitive deionization (a, c, e), and a supercapacitor (b, d, f).

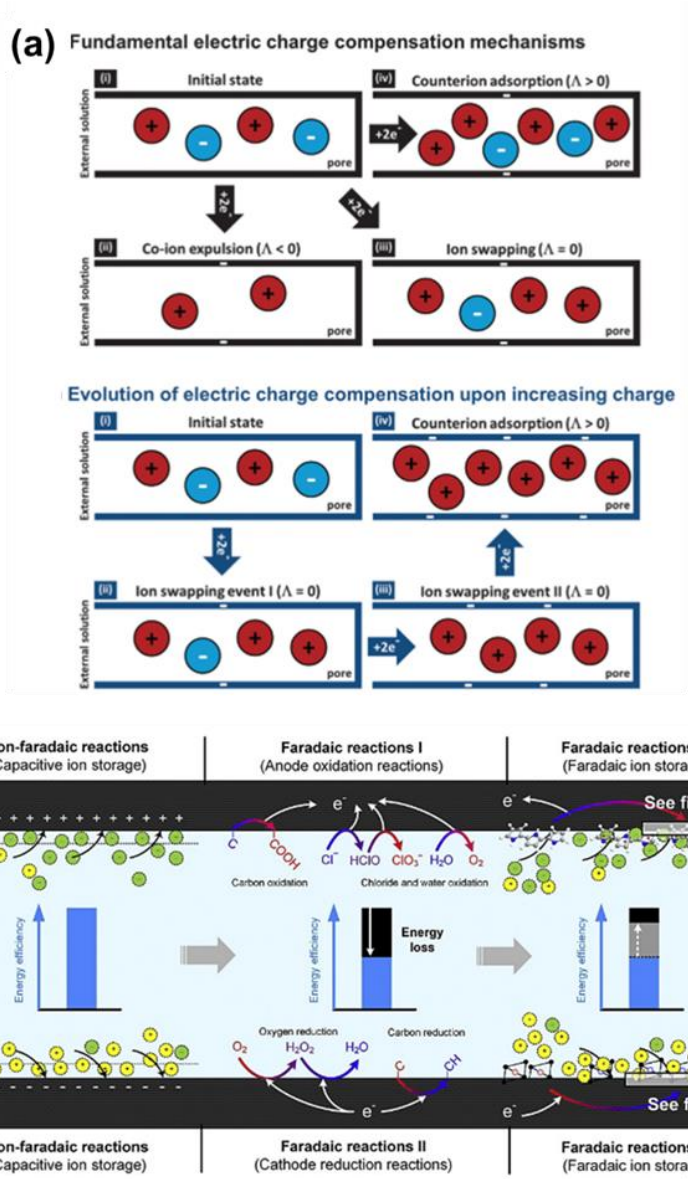

Figure 2-4. Various phenomena on the electrode surface that consume electric charge; (a) co-ion repulsion and ion swapping in micropore of the electrode [4], and (b) electrochemical reaction at the electrode and electrolyte interface [75]**.**

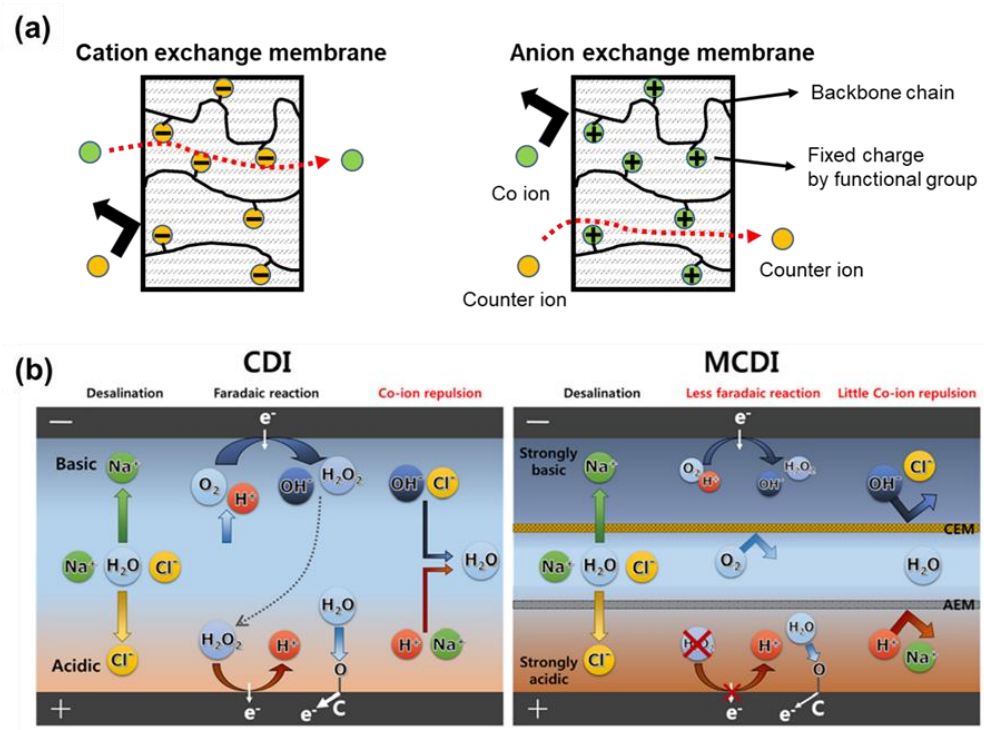

Figure 2-5. Schematic mechanism of ion exchange membrane and its representative effect on faradaic reaction in CDI system [74].

Meanwhile, there were also innovative changes that did not utilize ion exchange membranes to overcome the shortcomings of the conventional CDI. For example, as shown in **Figure 2-6a**, a change of cell structure in which the electrolyte straightly flows through from an electrode to another electrode enhances a desalination rate than conventional CDI configuration, which is called flow-through electrode CDI (FTE CDI). For the electrolyte stream, this architecture uses unconsolidated carbon material as electrode material such as activated carbon cloth [77–80] and carbon aerogel monoliths (HCAMs) [81]. Typical CDI cell has inevitably high cell resistance because an electrolyte having low ion concentration flows between the electrodes, which call flow-by cell. Hence, the CDI system is limited by the diffusive time scale based on the time required for ions to diffuse from the spacer channel into the electrode. By reducing this resistance and time, the flow condition of FTE cell has the advantage of faster system response (rate of desalination) than flow-by CDI [81].

On the other hand, to suppress performance degradation and enhance long-term stability, the anode and cathode electrodes were treated to contain negative and positive surface charges, respectively. In this system called inverted CDI (i-CDI), ions are adsorbed through short-circuiting and then desorbed by applying potential difference due to the difference in the surface

charge, which is opposite to the conventional CDI process (see **Figure 2-6b**). This system can prevent performance degradation by carbon oxidation [82,83]. Nevertheless, the introduction of the ion exchange membrane can be seen as the most important event in the history of EIONS research in that it is the starting point of various changes to be reviewed in the next section.

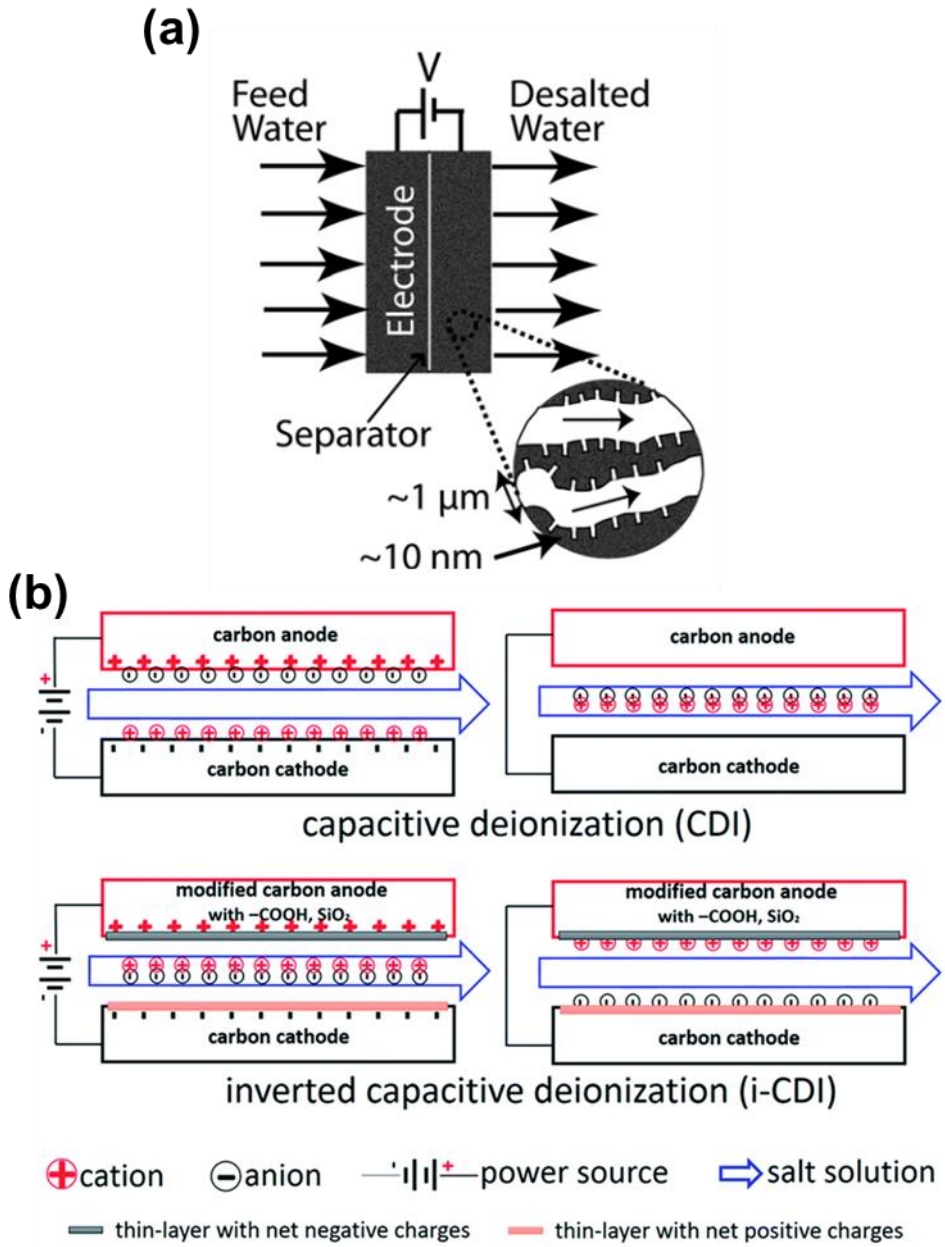

Figure 2-6. Schematic concept of (a) flow-through electrode capacitive deionization (FTE CDI) [81], and (b) inverted capacitive deionization (i-CDI) [83].

2.1.2 Decoupling electrolyte and salt water

In addition to the above-mentioned advantages, the introduction of the ion exchange membrane became a source from which new paradigms for the cell structure of EIONS can be initiated. A representative new paradigm is a decoupling electrolyte and salt water, where the ion exchange membrane could be used to construct a chamber for the electrode and electrolyte between the current collector and a feed water channel.

This new paradigm of CDI was opened with the use of flowable carbon suspensions (refer to **Figure 2-7**). This system, referred to as flow-electrode CDI (FCDI), employs carbon suspension instead of the conventional fixed electrode such as activated carbon film and carbon cloth [43,44]. Compared to the conventional CDI that have a limited capacity of static electrodes, FCDI enables continuous desalination for various feed concentrations and cell geometries as flow-electrodes provide a theoretically infinite amount of desalination capacity. Hence, the FCDI was able to treat seawater with 95% of ion removal [44], and it can easily be scaled up by increasing the size of the cell and tank containing the flow-electrode [84]. In particular, this system can adjust the ion concentration of the electrolyte, since the salt water channel and the electrode channel are separated by an ion exchange membrane. Namely, the environment around the electrode can be adjusted to be favorable

for the desired reaction as shown in **Figure 2-8a**. Yang et al. reported that desalination performance can be improved by increasing the concentration of the electrolyte [85]. Ma et al. reported that the redox active material can help the desalination performance by adding hydroquinone to the electrolyte [56]. Moreover, the decoupling of the electrolyte and salt water allows the recombination of separated ions into other ionic solutions. For example, as shown in **Figure 2-8b**, the AB solution and CD solution consisted of ion spice A and B, C and D can be simply changed to AD and CB solution [86]. In order to increase the desalination performance of FCDI, various studies were pursued to enhance the electrochemical properties of the electrodes through carbon surface modification [87,88] and the addition of carbon additives [89,90] and redox-active materials [56]. However, compared to the static electrodes, flow-electrodes are subject to high electrode resistance due to the large fraction of liquid content and poor contact between the suspended particles.

On the other hand, a system has been proposed that can take advantage of the fixed electrode and the decoupling electrolyte. This system, called multi-channel MCDI (MC-MCDI), creates an electrode chamber to separate the electrolyte and salt water, but employs the fixed electrode, as shown in **Figure 2-9** [45]. Through this architecture, the salt adsorption capacity of the

electrodes was enhanced significantly by flowing highly concentrated solvents in the side channels, which allows the formation of dense EDL leading to the high specific capacitance of the electrodes [91]. Also, the possibility of semi-continuous desalination was demonstrated by alternating desalination and regeneration steps using MC-MCDI [46]. Furthermore, by supplying an organic electrolyte into the side channel, the cell voltage could be extended up to 2.4 V which is beyond the water-splitting range. Since the capacitance of carbon electrodes depends on the magnitude of the cell voltage, higher desalination could be achieved [47].

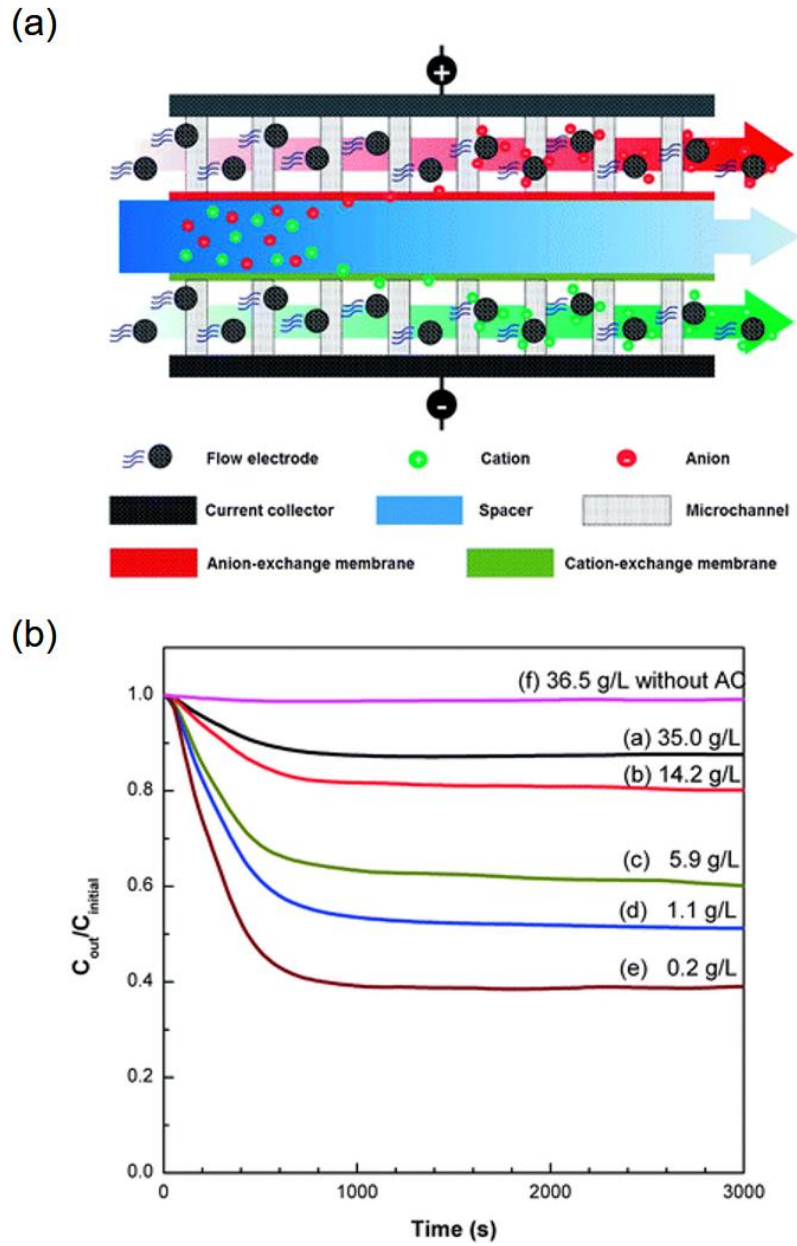

Figure 2-7. (a) Schematic of the flow-electrode capacitive deionization (FCDI). (b) Desalination performance of FCDI with continuous removal of salt ions in solutions with different salinity [44].

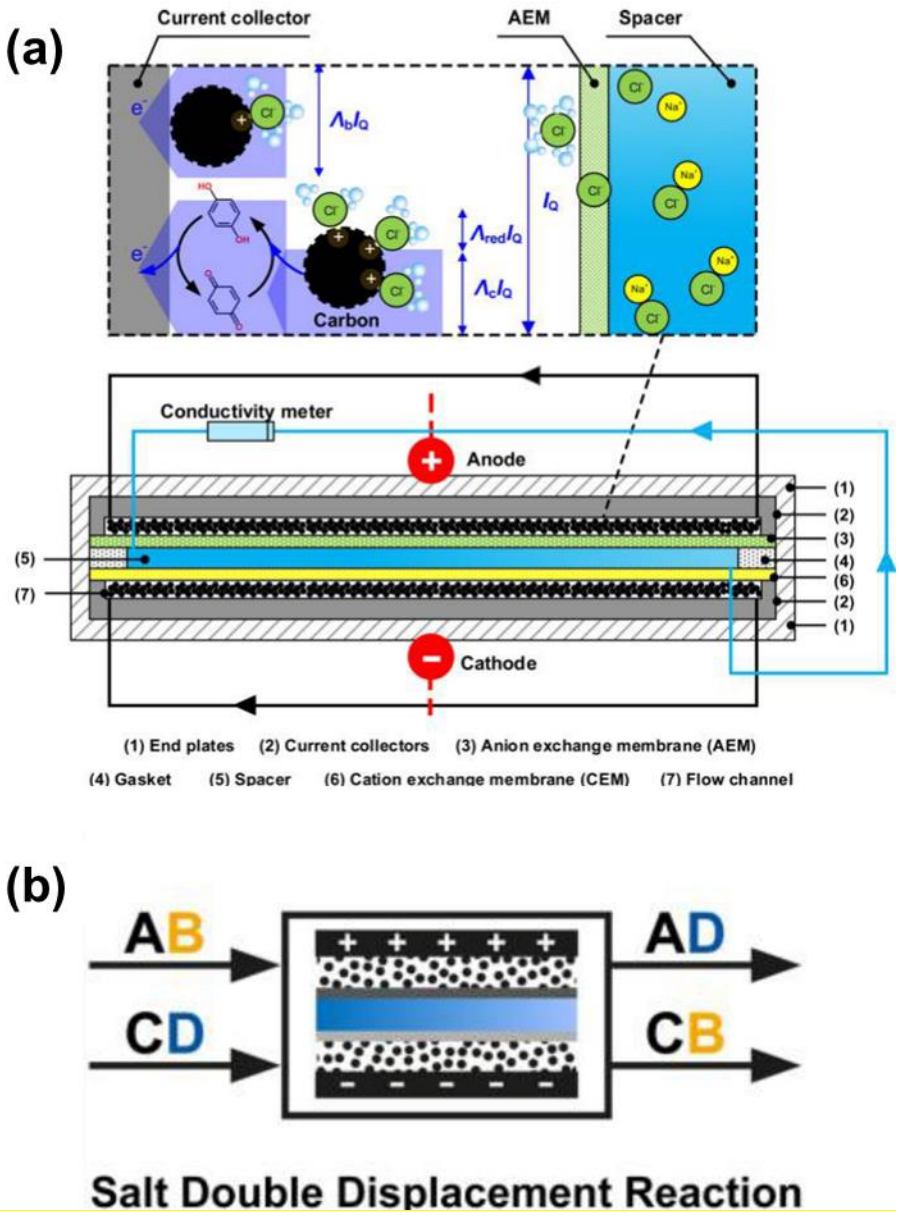

Figure 2-8. Schematic concept of (a) creating a favorable electrode environment for the desired reaction through the decoupled electrolyte and salt water channel [56], and (b) ion recombination process [86].

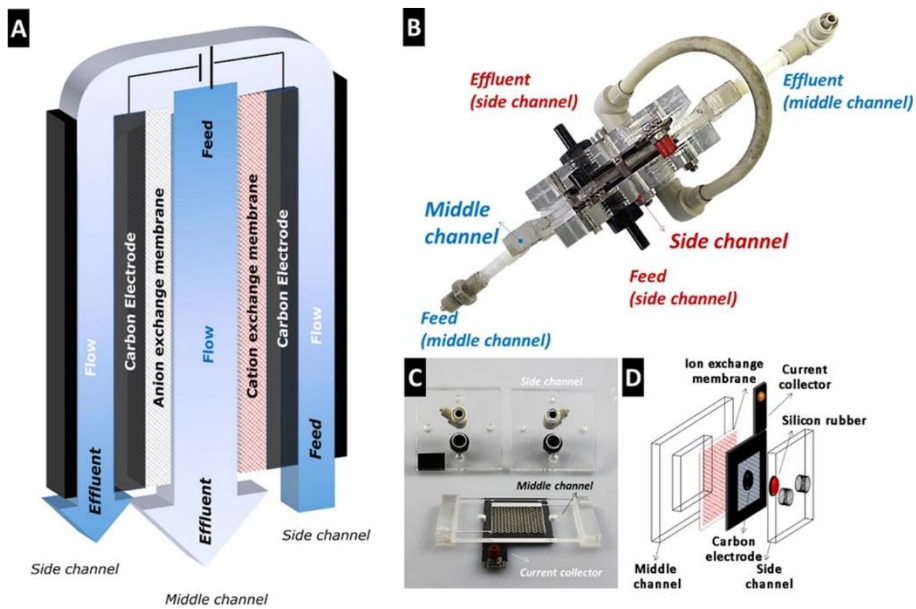

Figure 2-9. (a) Schematic diagram of a multi-channel membrane CDI (MC-MCDI) cell. Top view images of the (b) assembled and (c) dissembled cell. (d) Configuration scheme indicating half of the cell [45]**.**

2.1.3 Integration of desalination and concentration processes

Decoupling compartments through the ion exchange membrane led to the development of a new concept. The concept is to simultaneously implement the charging and discharging of the electrode (i.e., the desalination and regeneration process) via two salt water channels using the ion exchange membrane. For example, Rommerskirchen et al. employed two anion exchange membranes for the flow-electrode channel, and one cation exchange membrane to split the salt water channel to dilute and concentrate channel [92]. In this system, the cation moves from the dilute channel to the concentration channel. Simultaneously, the anion moves from the dilute channel to the positively polarized channel and from the negatively polarized channel to the concentration channel, since the flow-electrode circulates between both channels. Through this operation mode, this system was intended to complete the continuous desalination process.

This approach was later tried in EIONS with the fixed electrode, and accordingly, various technical concept was suggested. For example, Smith and Dmello applied this approach to desalination battery (DB) using Na intercalants such as $Na_{0.44}MnO_2$ and $NaTi_2(PO_4)_3$, which evolved under the various name such as Na intercalate desalination (NID), cation intercalate desalination (CID) and rocking chair desalination battery [51–53]. In the

capacitor-based EIONS, Lee et al. proposed this configuration, which is called rocking-chair CDI (RCDI)[50]. During the operation of this type of system, one electrode is charged by ions and another electrode is discharged. Then, the charging and discharging electrodes are reversed. Therefore, dilute water and concentrated water flow alternately via separated water channels, and the fresh water can be continuously obtained by controlling the external valve [51–53].

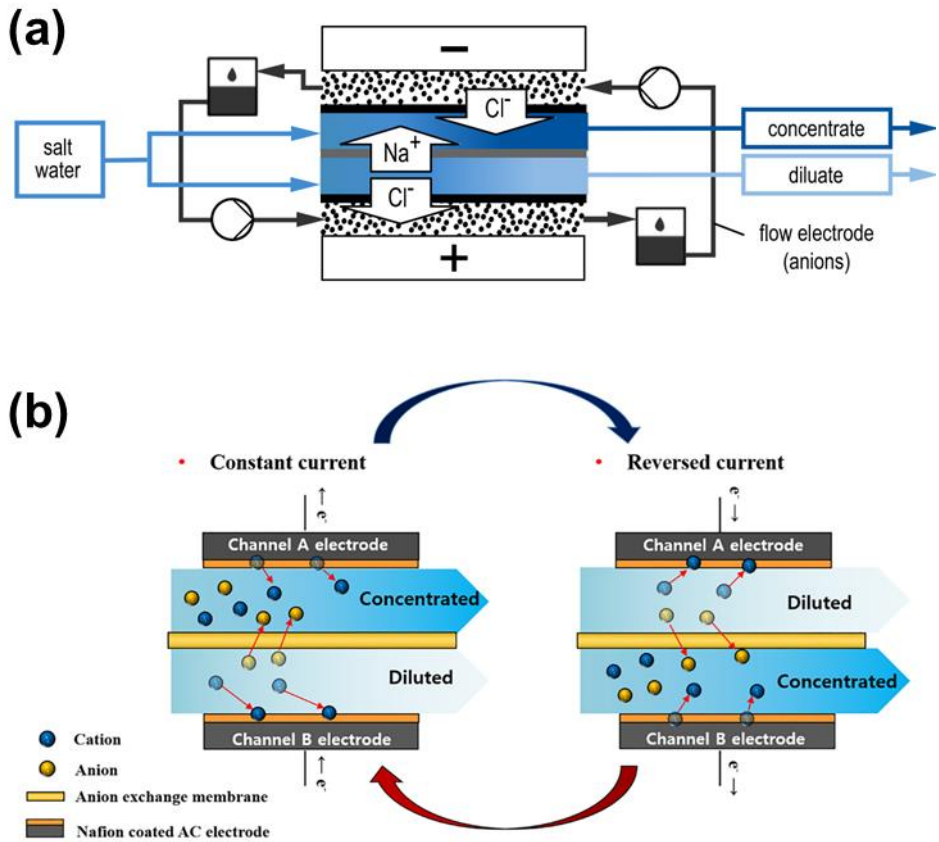

Figure 2-10. Schematic concept of integrating desalination and concentration process for continuous fresh water production in (a) flow-electrode based and (b) fixed electrode based EIONS [50,92].

2.1.4 Application of Redox-active electrolytes.

As mentioned above, the ion exchange membrane brought on innovative changes in EIONS. In addition to this, EIONS is expected to change into a form that applies a redox-active material because the current cell structure can decouple the electrolyte and salt water channels. In order to make a better condition for ion removal, various redox couple materials are considered as the electrolyte that is called the redox-active electrolyte. These materials have been extensively explored in redox flow battery and redox supercapacitor, and representative examples include I^-/I_3^-, Br^-/Br_3^- and $[Fe(CN)6]^{4-}/[Fe(CN)_6]^{3-}$ [93].

The redox-active electrolyte allows high charge and desalination capacity and fast kinetics and better stability [93,94]. For example, Ma et al. added hydroquinone to the electrolyte of flow-electrode for enhancement of electron transfer between the current collector and carbon particle [56]. Since Hydroquinone change to benzoquinone at the electrode-electrolyte interface and return to hydroquinone at the current collector-electrolyte interface, Hydroquinone can act as an electron shuttle led to high desalination performance (refer to **Figure 2-8a**). In addition, $[Fe(CN)6]^{4-}/[Fe(CN)_6]^{3-}$ was recently applied to MC-MCDI system, and it enhances the desalination performance of this system [57].

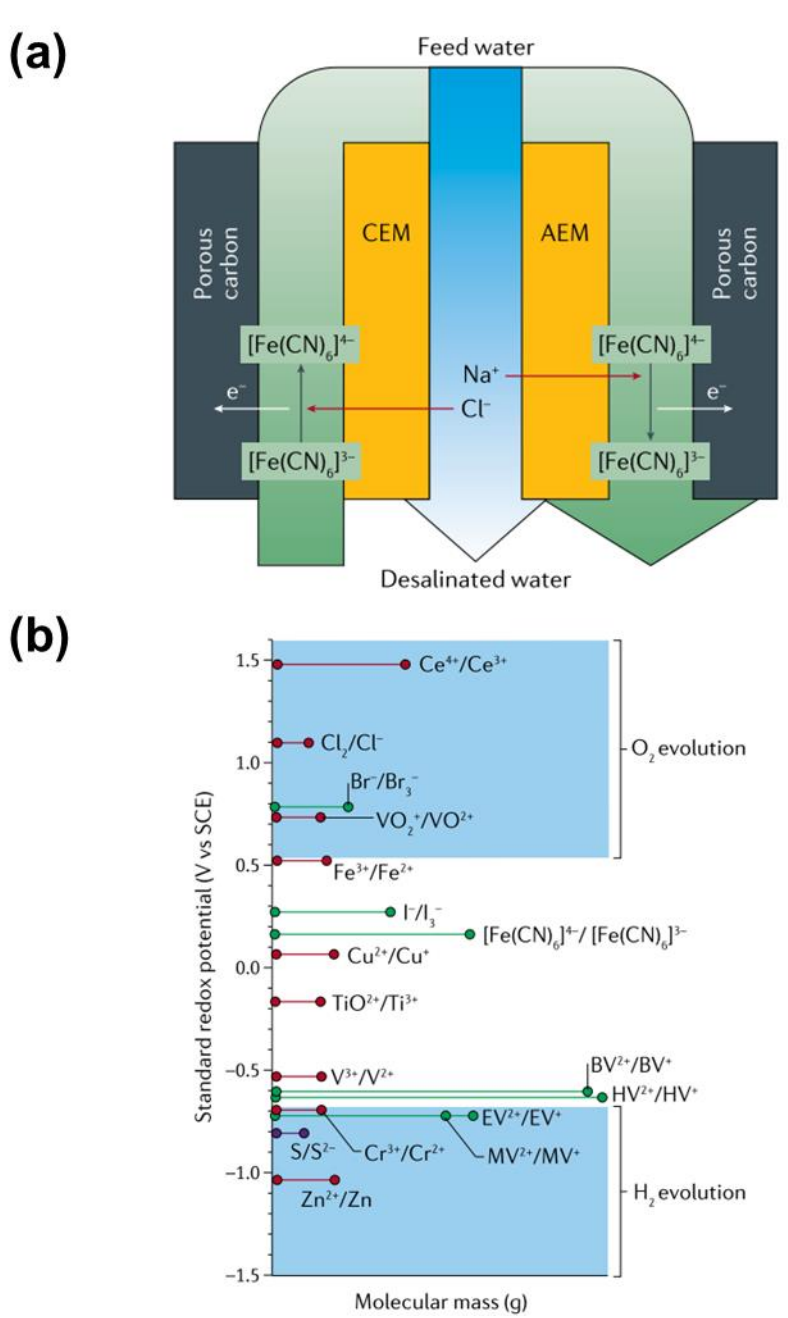

Figure 2-11. (a) Example of EIONS with redox-active electrolyte and (b) reduction potentials of various redox couple. In (b) the colors indicate stability in acidic (red), neutral (green), and basic (purple) condition [93].

2.2. Factors affecting the energy efficiency of EIONS system

In order for the EIONS system to move away from laboratory study and achieve high energy efficiency on an industrial scale, it is necessary to examine the energy consumption factors in the system and consider the impact of system expansion. As shown in **Figure 2-12**, in the EIONS system, the energy is invested in the EIONS module for ion removal and the control system for the operation of the system. The invested energy to the MCDI module is utilized for charge storage on the electrode that can be recoverable and dissipated by leakage current, parasitic reaction, and voltage drop through resistance [4,75,95]. The invested energy to the control system is consumed through voltage drop in the system, and operation of system equipment, which is generally negligible in the calculation of energy efficiency for lab scale. However, energy consumption in each part change with the operation method and system scale. In particular, the energy consumption in the control system will be not negligible on an industrial scale [5,6].

In this section, the effect of operation method and system scale on energy efficiency is reviewed with a focus on the MCDI system, which is closest to commercialization.

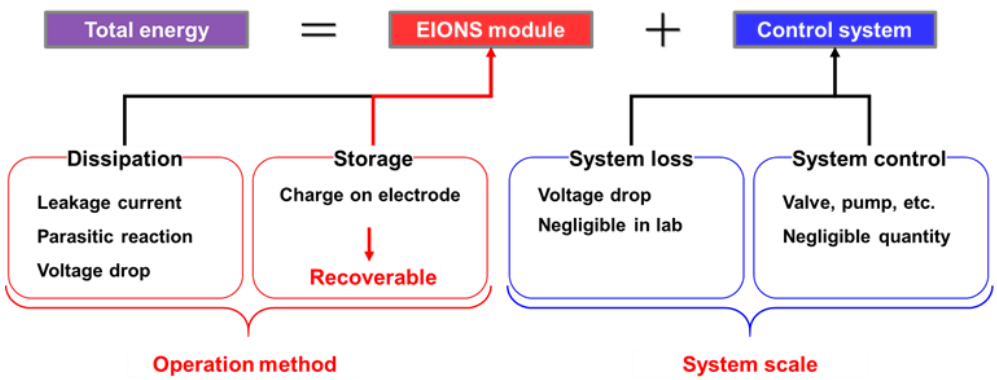

Figure 2-12. Factors affecting the energy efficiency of EIONS system.

2.2.1 Operation method

In general, the desalination process such as reverse osmosis or thermal method calculates the energy consumption by dividing invested energy by the volume of produced water (e.g., kWh/m^3, J/L), since it produces water with few ions. In contrast, the concentration of ions in the produced water can be controlled in EIONS such as CDI and MCDI, because it separates ions from the salt water. Therefore, the invested energy per removed ions (e.g., kWh/g, J/mg, J/mmole) is utilized as a major performance indicator of MCDI, which is specific energy consumption (SEC) [96].

$$\mathrm{SEC} = \frac{\mathrm{E_{in}}}{\Phi \int (C_{in} - C_{out}) dt} \tag{2-1}$$

Assuming that electric current (i) is used only for ion adsorption, invested energy (Ein) is determined by multiplying the operation voltage (V) and the amount of charge for ion removal.

$$\mathrm{E_{in}} = \int Vi(t)dt \ \ in\ constant\ voltage \tag{2-2}$$

In the past CDI research, the theoretical energy consumption was calculated by simply this approach, since constant voltage operation was common [7,8,22]. Therefore, it was considered that there would be competitiveness in terms of energy efficiency even in seawater desalination if more than 70% of the energy can be recovered under 1.2 V operation [22]. However, this evaluation is only allowed for constant voltage operation, and

it is expected that the energy consumption can be further reduced via other operation methods. The reason that the constant voltage operation was considered the most operation mode in the past is presumed to be because it was difficult to precisely control the applied voltage level [97].

The consideration of constant current operation in EIONS began after Andelman's study in 2011 compared it with constant voltage operation [32]. According to this study, the constant current operation theoretically consumed about 50% less energy than the constant voltage operation, but the energy consumption becomes similar to the constant voltage operation as the applied current density increases. Kang et al. reported that the constant voltage has a fast desalination rate, whereas constant current operation consumes 30% less energy despite similar charge efficiency [97]. Moreover, the constant current operation is more advantageous than the constant voltage operation in terms of energy consumption even without considering energy recovery [95,98,99].

However, WETSUS and the University of Wageningen group in the Netherland tried to analyze the energy consumption trends of constant voltage and constant current operation of CDI and MCDI under various operating conditions [100,101]. They concluded that there was no significant difference between the two operations method when energy recovery was not included [102]. In addition, Wang and Lin reported that energy efficiency depends on

the desalination objective and constant voltage operation is more energy efficient at a higher level of desalination [103].

According to the modified Donnan model, applied cell voltage (V_{cell}) is significantly higher than equilibrium cell voltage (V_{eq}) at the beginning of constant voltage operation. V_{eq} is the sum of the Donnan potential, the Stun potential, and the Donnan potential applied to both interfaces of the ion exchange membrane, it is the potential difference resulting from ions alignment at the electrode and bulk solution interface. Excess voltage (V_{ex}), which is a voltage applied excessively over V_{eq}, can be interpreted as a deviation from the equilibrium of the system or a driving force for ion transport [103]. In constant voltage operation, energy consumption per transferred charge is always determined by V_{cell}, since V_{ex} is independent of cell resistance as a function of charge density. In other words, when energy loss due to side reactions is not considered until the equilibrium state, energy consumption is determined by specifying the cell voltage [96]. On the other hand, in the case of the constant current operation, the energy consumed to transfer a unit charge is highly dependent on the current density and cell resistance. Therefore, this operation may be disadvantageous in terms of energy efficiency for a process requiring high desalination rates and high desalination efficiency [103].

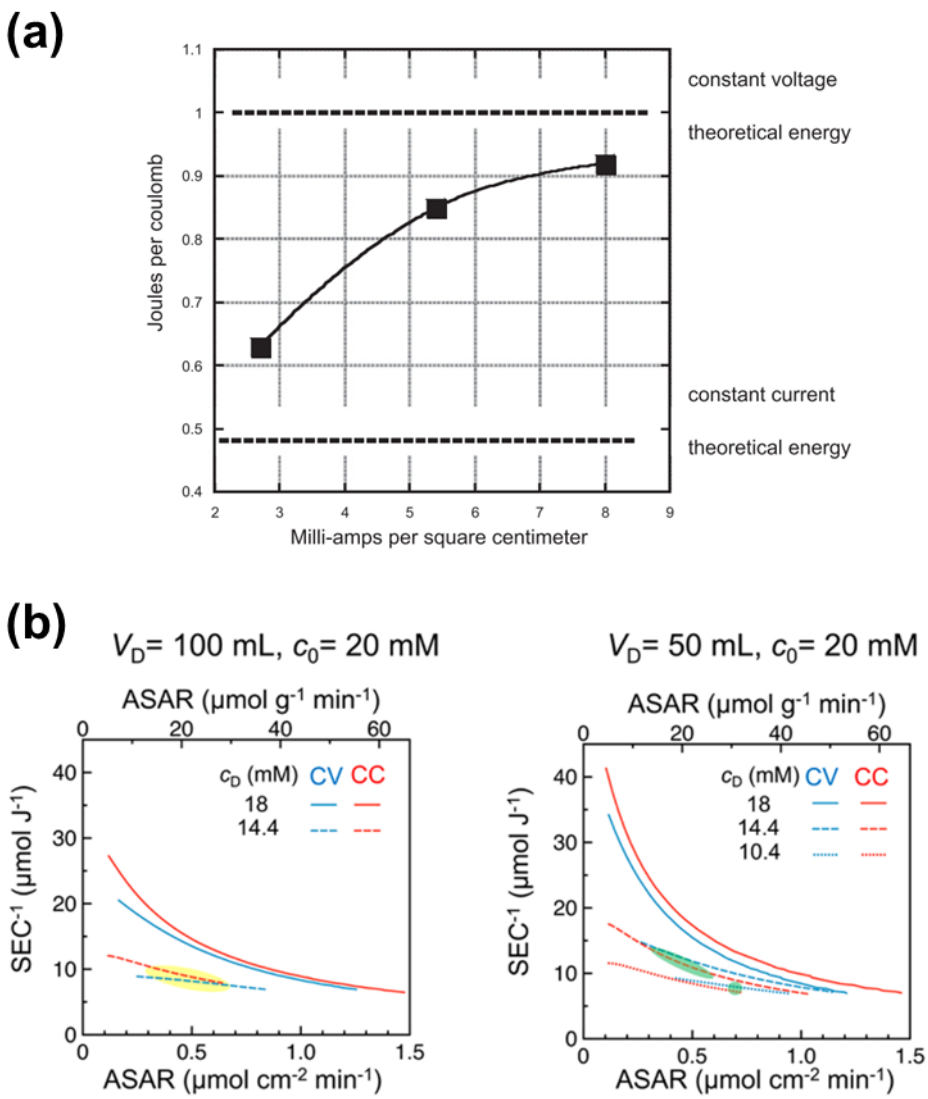

Figure 2-13. Comparison of energy consumption between constant voltage and constant current (a) with current density [32], and (b) average salt adsorption rate and concentration reduction [103].

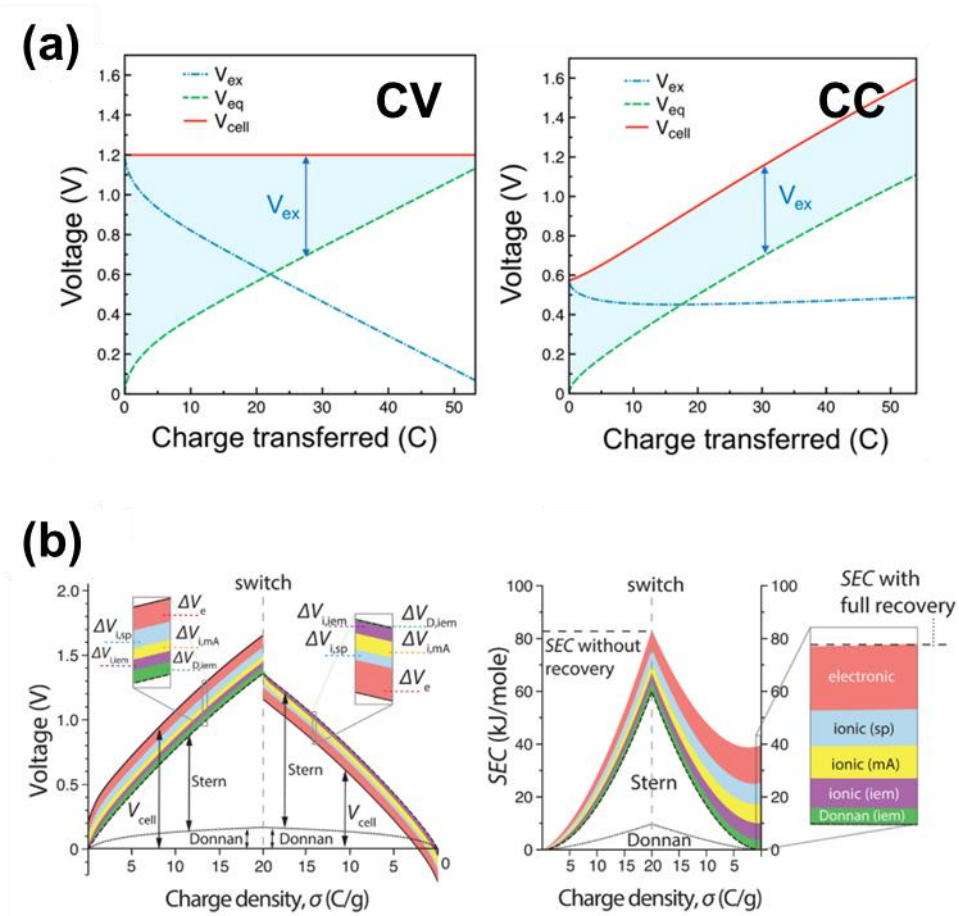

Figure 2-14. (a) Distribution of cell voltage (V_{cell}), equilibrium voltage (V_{eq}), and excess voltage (V_{ex})over the charging step in constant voltage (CV) operation and constant current (CC) operation [103]. (b) Distribution of resistance elements in V_{ex} of constant voltage operation and its effect on specific energy consumption (SEC) [96].

2.2.2 Energy recovery in CDI and MCDI

EIONS systems, especially CDI and MCDI store the energy invested for ion removal. This invested energy can be recovered by discharging like a supercapacitor. Shiue et al. in 2003 proposed a concept patent on CDI with an energy recovery system that connects a supercapacitor to a CDI cell [32]. Anderson et al. in 2010 proposed the concept of energy recovery using a DC-DC converter from two CDI units that alternately operates between charging and discharging, respectively [22].

An energy recovery study has been conducted since 2008 by Alkuran et al. They attempted to transfer the energy in charged CDI cell to the uncharged supercapacitor by using a buck-boost converter [17,21]. On the other hand, Pernia et al. in 2012 conducted energy transfer from charged CDI cell to uncharged CDI cell via a buck-boost converter [18,23,25]. These studies can be defined as an indirect method because they recover energy using a DC-DC converter. These early studies were conducted with a dummy cell system that simulated CDI using resistors and capacitors. Since the constant current operation began to attract attention, the study results of constant current discharge are beginning to replace the actual energy recovery [12,13,15]. In these studies, the recovered energy was calculated by integrating the reversely applied current and the voltage change of the CDI cell. The actual DC-DC

converter controls the voltage level to allow a constant mean current [16], the constant current operation can be considered as a case of using an ideal converter. Meanwhile, research on energy recovery through equivalent circuit modeling was also conducted [16,20].

Practical implementation of energy recovery using real MCDI and the buck-boost converter was conducted by Kang et al. in 2016 [28]. They transfer 50% of invested energy from charged MCDI to the supercapacitor. In addition, Chen et al. also reported 50% energy recovery efficiency using a similar system consisting of MCDI, buck-boost converter, and supercapacitor [19]. The indirect method of energy recovery has been applied to a pilot-scale MCDI process, which has the effect of deducing energy up to 37.5% [6].

On the other hand, Landon et al. in 2013 reported the energy recovery without a DC-DC converter, which can be called by direct method [104]. In this method, energy is transferred by directly connecting charged and uncharged MCDI modules, thereby energy can be partially recovered. To increase the amount of recovered energy, the charged and uncharged CDI module groups were connected in various sequences by Andres et al.[105,106].

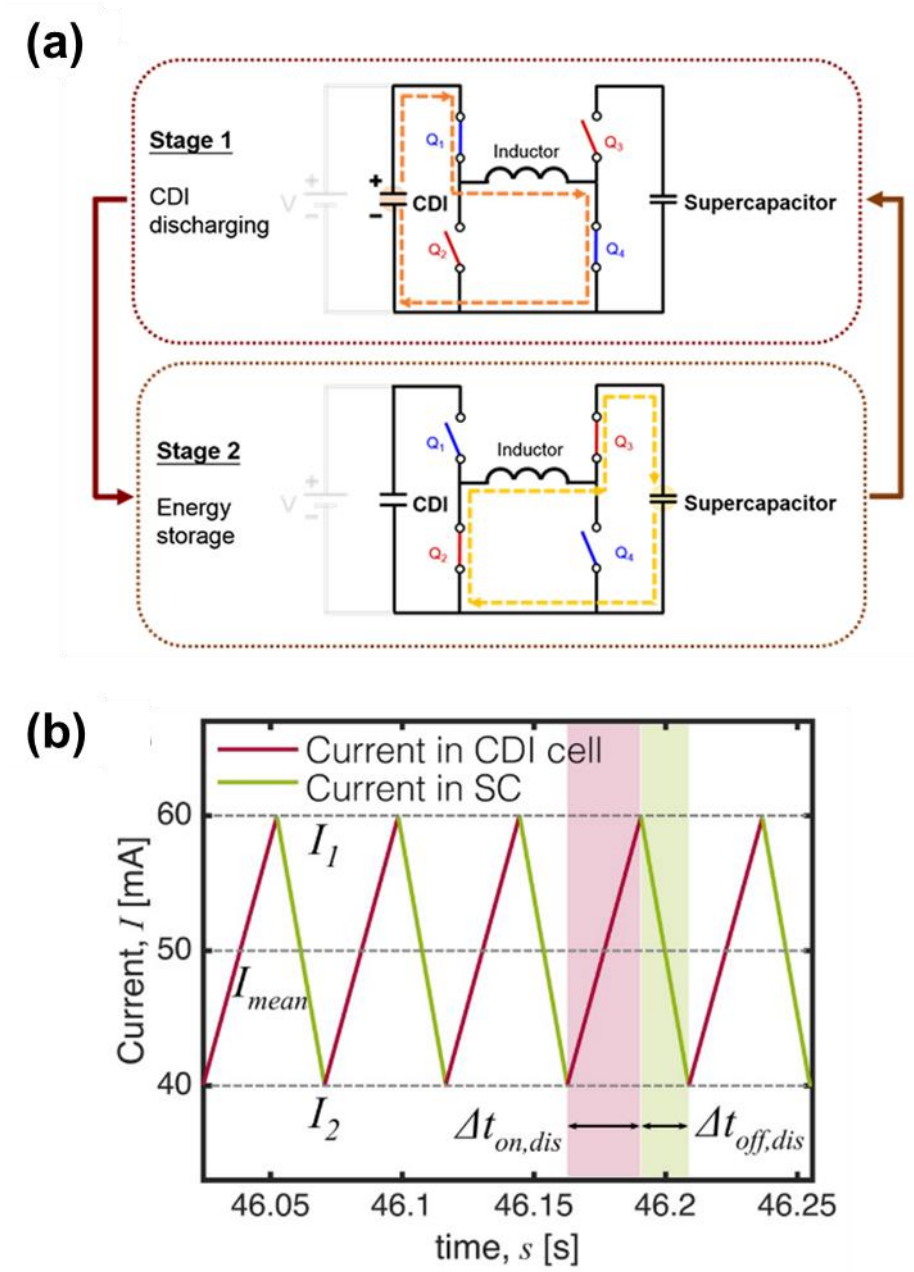

Figure 2-15. Schematic (a) diagram of energy recovery via indirect method [19], and (b) standard current profile over indirect energy recovery [16].

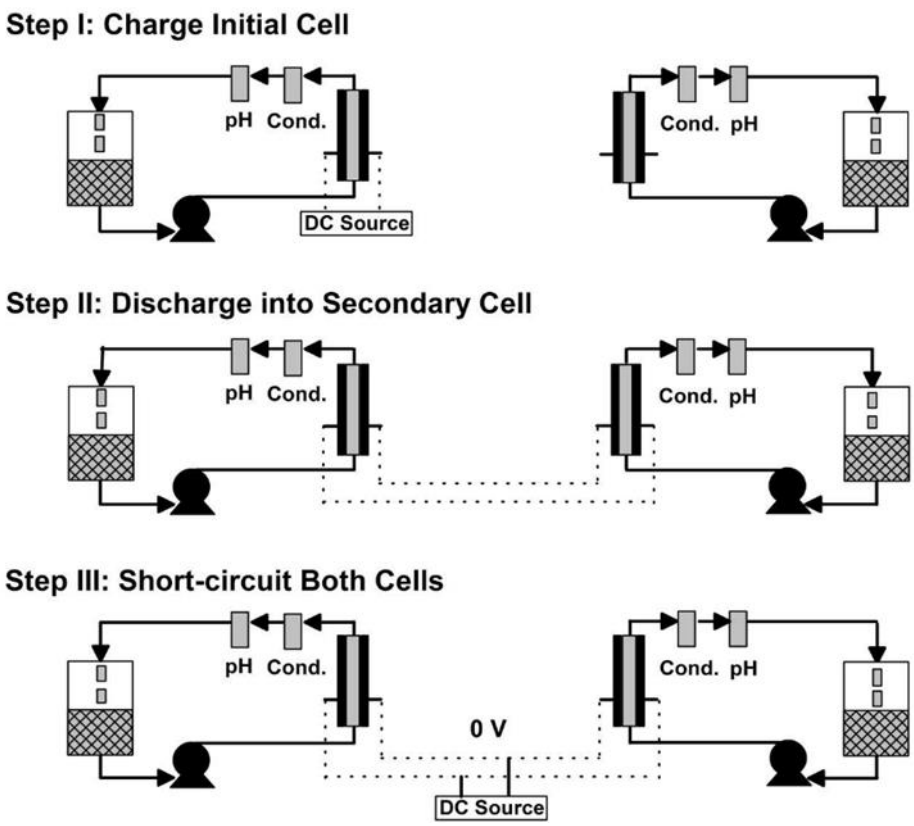

Figure 2-16. Concept of direct energy recovery between two MCDI modules [104].

2.2.3 Bipolar electrode for scaled-up MCDI system

In order for the MCDI system to be successfully applied to industry, it must show high energy efficiency even in large systems. According to the report of Tan et al. (refer to **Figure 2-17a**), more than 40% of the invested energy was lost in the control system [6]. This is energy loss due to resistance existing in the system which increases as the current increases according to Ohm's law. For example, as shown in **Figure 2-17b**, it can be seen that the energy loss is very high at the applied current for the pilot scale (approx. 150A), even if the system resistance is calculated as 0.001 Ω, which is the resistance of a typical conducting wire. To prevent such energy loss, it is necessary to find a way to operate the pilot system with a low current. Lee et al. proposed a bipolar electrode stack in CDI, in which CDI operated under low current, whereas required high voltage [11]. Chen et al reported that the bipolar electrode shows high desalination performance and can potentially be used to improve energy efficiency [107]. In addition, this stack exhibited a faster discharge rate than a conventional monopolar electrode stack [9]. This characteristic is because the electrodes are connected in series, and the current that flows from the first cell continuously flows to the following cell (refer to **Figure 2-18**).

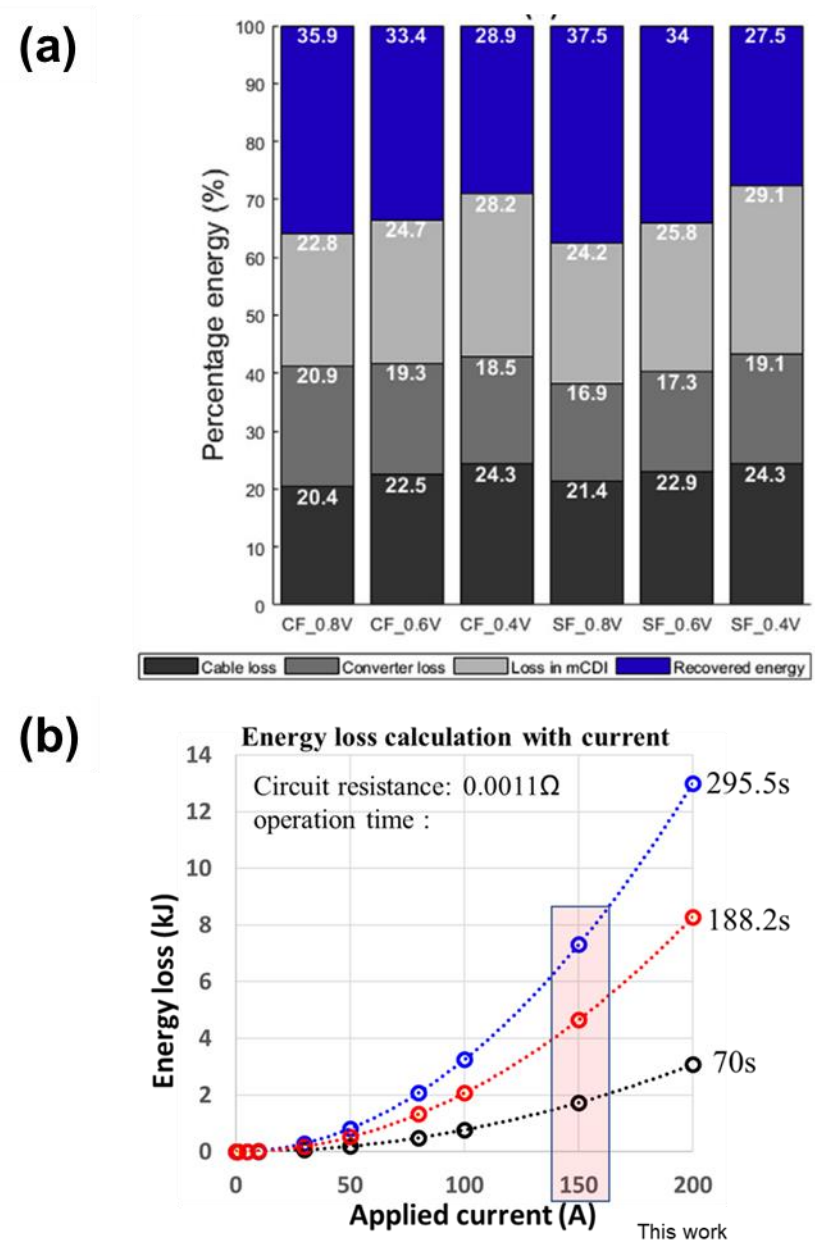

Figure 2-17. (a) Distribution of invested energy in pilot-scale MCDI system, and (b) energy loss in control system with applied current and operation time. In (b), energy loss was calculated by Joule's law ($E=i^2Rt$) referring to [6].

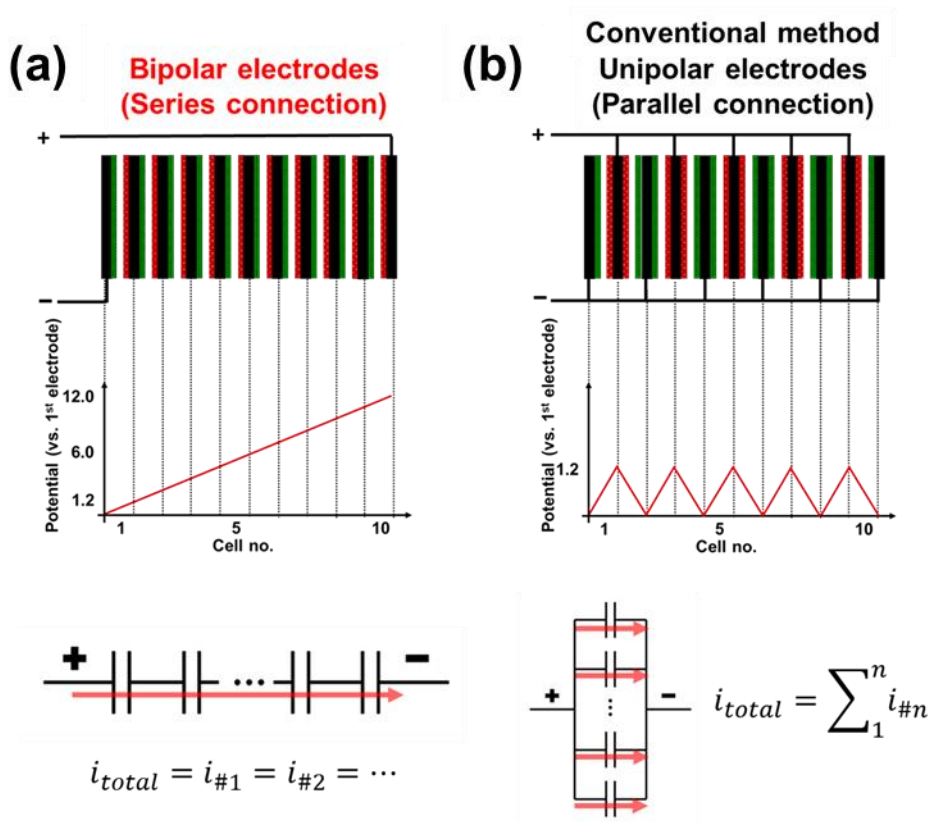

Figure 2-18. Schematic comparison of (a) bipolar electrode stack and (b) unipolar electrode stack.

3. Parameter estimation and simulation using equivalent circuit for Bipolar MCDI system with direct energy recovery

3.1. Introduction

The importance of securing clean water for human society has increased due to worldwide industrialization, population growth, and global climate change [1,2]. In addition, the world society is declaring the transition from a carbon-based society to a carbon-neutral society in to response the global crisis of climate change [3]. In a carbon-neutral society, energy-efficient water security technology will be even more important because water will be widely used as a raw material for various processes

Membrane capacitive deionization (MCDI), derived from capacitive deionization (CDI), is attracting attention as a next-generation desalination technology. By applying the electrical energy to the MCDI cell, the ions are removed from salt water to the electrode surface. Since CDI uses a DC voltage of 1.2 V or less, it is easy to link with renewable energy. Furthermore, the input energy can be recovered [5].

A commercial-scale MCDI system is generally composed of an MCDI module in which stacked unipolar carbon electrodes are connected in parallel (unipolar MCDI), and a control system to control it [5,7]. For energy recovery, it is considered to install a DC-DC converter in the control system for energy

recovery [6]. However, it has been confirmed that scaling up in this way has several problems. First, when the stacked electrodes are paralleled, the system current increases according to the scale, which leads to an increase in energy loss in the control system [6]. In addition, DC-DC converters have shown low energy recovery efficiency of less than 50% so far despite high development costs [6].

To overcome this problem, a scale-up method in which bipolar electrodes are stacked and connected in series (Bipolar MCDI), and a method of recovering energy through a direct connection between MCDI and an external load are considered. The energy recovery method through direct connection transfers energy by directly connecting the charged MCDI module with an electrochemical cell such as a supercapacitor or battery and a second MCDI. Since there is no need for a special device other than the switch circuit, the energy can be partially recovered at a low cost [104,105,108].

Meanwhile, among the scale-up methods of MCDI, the method of stacking bipolar electrodes and connecting them in series can operate at a low current. Unlike the conventional unipolar MCDI, which applies voltage by connecting all electrode pairs to an external power source, in this method, only the outermost electrode is connected to an external power source and a high voltage is applied. The inner electrodes connected in series

electrochemically are polarized by the electric field applied to the outer electrode pair to adsorb ions [42,43]. That is, it operates by increasing the voltage, not the current, as the stack increases [40,44].

Despite these advantages, studies that combine the two concepts have not yet been conducted due to the risk of electric explosion. Theoretically, the current is determined by the voltage and resistance between the two electrodes. The fact that a Bipolar MCDI module has a high voltage and a direct connection means a low resistance makes the related research difficult.

Therefore, this study aimed to simulate a Bipolar MCDI system with direct energy recovery using an equivalent circuit to demonstrate that direct energy recovery of Bipolar MCDI is possible. For this work, the two branches model, which is an equivalent circuit of the supercapacitor, was modified to represent a characteristic of a Bipolar MCDI system. The electrochemical parameters for charging and discharging were estimated by analyzing the current profile of the Bipolar MCDI with a modified two branches model. In addition, the direct energy recovery of Bipolar MCDI was simulated by substituting the estimated parameter values into the modified two branches model.

3.2. Experimental Section

3.2.1 Bipolar MCDI module configuration

Figure 3-1 shows a schematic illustration of the MCDI module with a bipolar configuration. In the Bipolar MCDI module, the bipolar carbon electrodes were coated with cation and anion exchange resins on both sides. The bipolar carbon electrodes were placed between a pair of conventional activated carbon electrodes with an anion exchange membrane and cation exchange membrane. The nonconductive nylon cloth was used as a spacer providing a water stream.

The outermost electrode pair of the lab-scale Bipolar MCDI module consisted of a pair of activated carbon electrodes (Siontech Co., Ltd., Republic of Korea), and ion exchange membranes (AEM/CEM Type 1, FUJIFILM Europe, Japan). One or nine sheets of the resin-coated bipolar electrodes (Siontech Co., Ltd., Republic of Korea) were inserted between the outermost electrode pair for the 2.4 V and 12 V modules, respectively. All components were cut to 10 cm in diameter and had a 1 cm hole in the center for water flow.

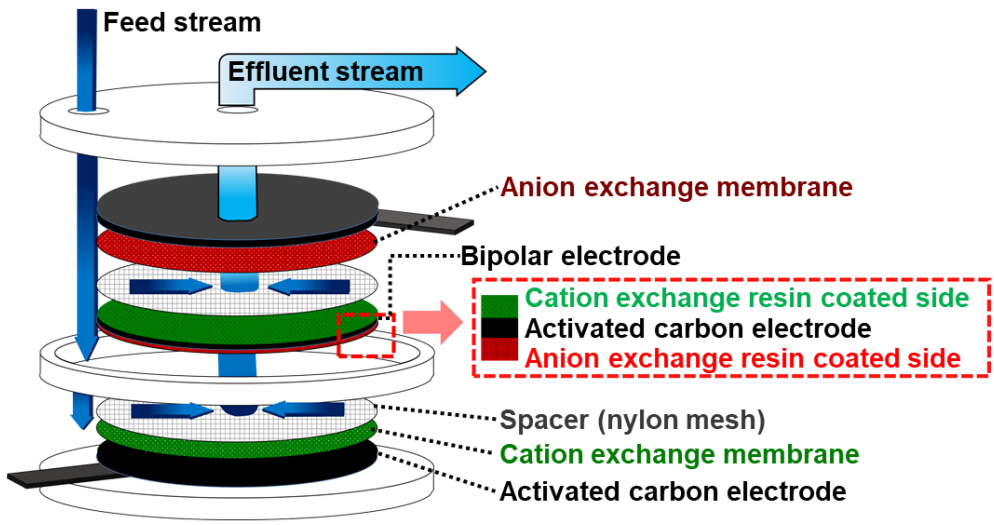

Figure 3-1. Schematic illustration of Bipolar MCDI module.

3.2.2 Charging and discharging tests of Bipolar MCDI

During the charging and discharging test, feedwater with 10.27 mM NaCl solution was supplied to 2.4 V and 12 V modules with flow rates of 8-, and 40- ml min^{-1}, respectively, by a gear pump (75211-15, Cole-Parmer, USA). The effluent concentration of the Bipolar MCDI module was measured using a conductivity meter (3574-10C, HORIBA, Japan).

For the charging test, a constant voltage of 2.4 V and 12 V was applied to 2.4 V and 12 V Bipolar MCDI modules, respectively, by using different devices due to the operating ranges of experimental devices. For example, a constant voltage of 2.4 V was applied, and the current was measured by using an automatic battery cycler (WBCS3000, WonaTech, Republic of Korea). In the case of 12 V, the voltage was applied by using a switching mode power supply (SMPS, PSF600-12, Fine Suntronix, Republic of Korea) and the current was measured by using a current probe (CP150, LeCroy, USA).

In the discharging test, the charged Bipolar MCDI modules were discharged by applying a constant voltage of zero voltage and connecting a standard resistor, supercapacitor, and second Bipolar MCDI module.

3.2.3 Parameter estimation and simulation using equivalent circuit

Since the Bipolar MCDI system is based on the electrochemical principle, this system can be modeled as lumped RLC (resistor-inductor-capacitor) networks which are called an equivalent circuit. This simplest model expressing electrode reactions including faradaic reaction and capacitive reaction is called a classical model, and a useful model for analysis of MCDI system (**Figure 3-2a**).

In this equivalent circuit, the voltage of the capacitor (v_c) changes by charge accumulated on the capacitor (q_c), and this voltage affects the current through a parallel resistor (R_P) as shown in Equations (3-1) and (3-2).

$$v_c = \frac{q_c}{C_{eq}}, \tag{3-1}$$

$$i_P = \frac{V_C}{R_P} \tag{3-2}$$

According to Kirchhoff's voltage law (KVL), the voltage of the circuit elements has the following relationship

$$V_a - v_{R_s} - v_C = 0, \tag{3-3}$$

$$V_a - (i_C + i_P)R_s - \frac{q_C}{C_{eq}} = 0 \tag{3-4}$$

Equation (3-4) is arranged by a first-order differential equation (first ODE), and the system current ($i(t)$) can be obtained by Equation (3-6).

$$\frac{dq_C}{dt} = \frac{V_a}{R_S} - \frac{R_S+R_P}{R_S R_P C_{eq}} q_C, \tag{3-5}$$

$$i(t) = \frac{V_a}{R_S+R_P}\left(1 + \frac{R_P}{R_S} e^{-\frac{t(R_S+R_P)}{R_S R_P C}}\right) \tag{3-6}$$

In order to increase the accuracy of estimation on the charging current, two branches model of supercapacitor was introduced and modified (Figure 3-2b). In this model, the branch consisting of the series resistor and the capacitor is added to the RC network of the classical model in parallel. Accordingly, Equation (3-4) is changed to Equation (3-7)

$$V_a - (i_{C1} + i_{C2} + i_P)R_s - \frac{q_C}{C_{eq}} = 0 \tag{3-7}$$

The equation is arranged by a second-order differential equation (second ODE), and the system current can be obtained by solving the equation. Thus, by analyzing this current with the equivalent circuit model, electrochemical parameters for charging and discharging Bipolar MCDI can be estimated. The estimation of parameters was conducted by following two steps for reducing a computational burden.

First, the discharging and charging current curves were fitted by using Equations (3-8) and (3-9), respectively, for the estimation of R_S and R_P. The general solution of the first ODE for the classical model and the second ODE

for the two branches model can be considered as

$$i(t) = a + be^{-\frac{t}{\tau}} \quad \text{for discharging parameter} \tag{3-8}$$

$$i(t) = a + be^{-\frac{t}{\tau_1}} + ce^{-\frac{t}{\tau_2}} \quad \text{for charging parameter} \tag{3-9}$$

Where a, b, and c can be obtained by curve fitting using Origin pro 2018 software (OriginLab co.). At applying a constant voltage, the current (*i(0)*) only flows through i_C in the classical model and i_{C1} in the modified two branches model due to the difference in resistance. Therefore, if the value of *i(0)* is known, R_S of the classical model and R_{S1} of the modified two branches model can be estimated by Ohm's law.

$$R_s = \frac{V_a}{i(0)} = \frac{V_a}{a+b}, \tag{3-10}$$

$$R_{s1} = \frac{V_a}{i(0)} = \frac{V_a}{a+b+c}, \tag{3-11}$$

After a long time with a constant voltage, the current ($i(\infty)$) only flow through i_p in the classical model and modified two branches model because the capacitors are fully charged. Therefore, if the value of $i(\infty)$ is known, R_P of the classical model and modified two branches model can be estimated by Ohm's law.

$$R_P = \frac{V_a}{i(\infty)} - R_S = \frac{V_a}{a} - R_S, \quad \text{for discharging model} \tag{3-12}$$

$$R_P = \frac{V_a}{i(\infty)} = \frac{V_a}{a} - R_{S1}, \text{ for charging model} \quad (3\text{-}13)$$

Second, for the estimation of C_1, C_2, and R_{S2}, the charging current was analyzed by using the parameter estimation tool of MATLAB & Simulink (Mathworks, Inc.). As shown in Figure 3-3a, the modified two branches model was entered in MATLAB & Simulink. Then, the parameters of C1, C2, and RS2 were estimated using the parameter estimation toolbox, which conducts iterative calculations with changing parameter sets until input data and simulation data match. In this study, we assumed that the C_{eq} in the classical model is the sum of C_1 and C_2 in the modified two branches model.

LTspice software (Analog Devices) was used for the simulation of the direct energy recovery step because it is simple to obtain simulation data. As shown in **Figure 3-3b**, the modified two branches model was applied in LTspice, and the estimated parameter was entered. By simulating the charging Bipolar MCDI with constant voltage, the initial voltage for discharging can be obtained. For the simulation of direct energy recovery, the initial voltage of Bipolar MCDI was entered from the result of the charging simulation.

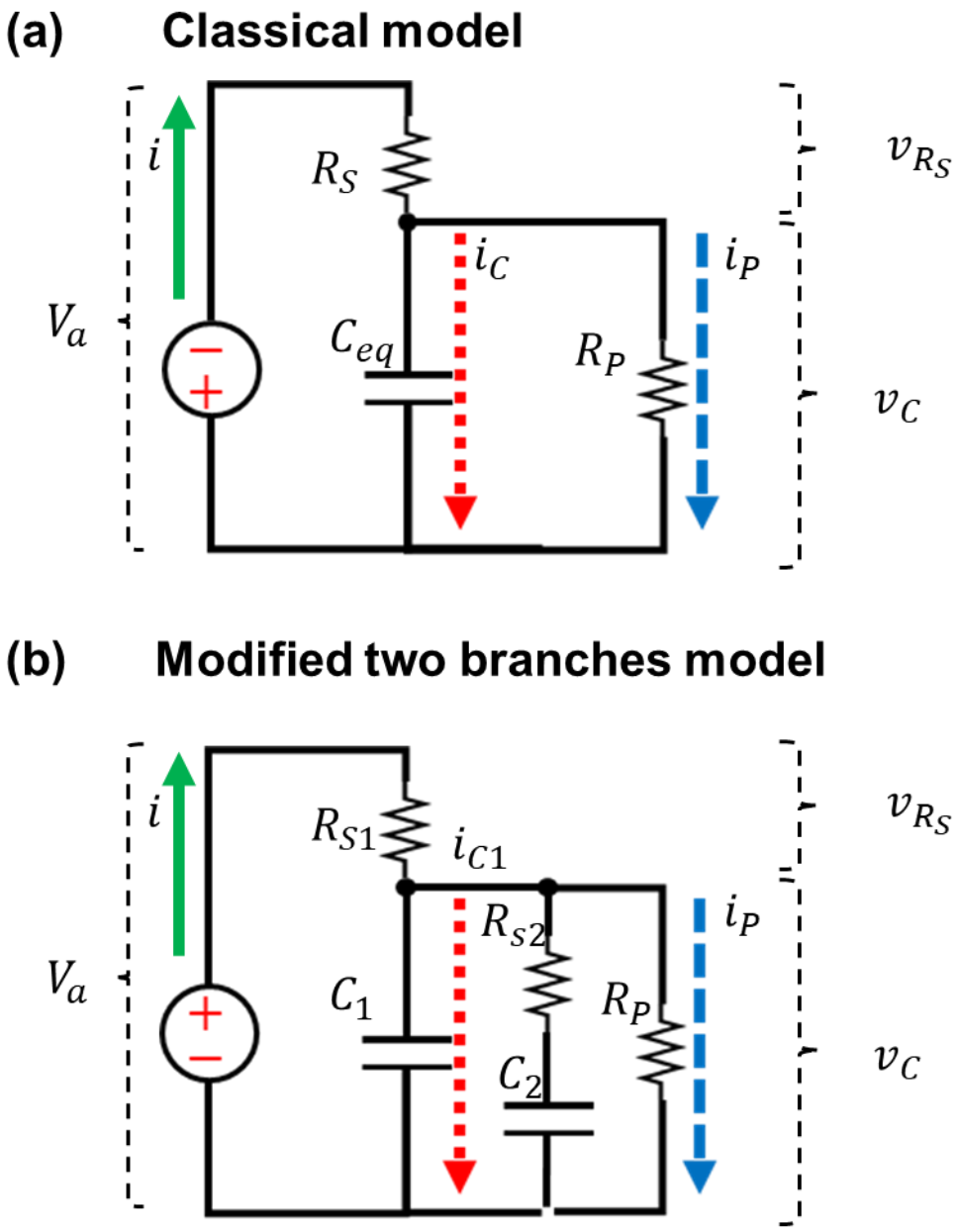

Figure 3-2. Schematic equivalent circuit diagram of (a) classical model and (b) modified two branches model. (C: capacitor, R: resistor, V_a: applied voltage, v_c: capacitor voltage, v_{rs}: voltage across resistor, i: current)

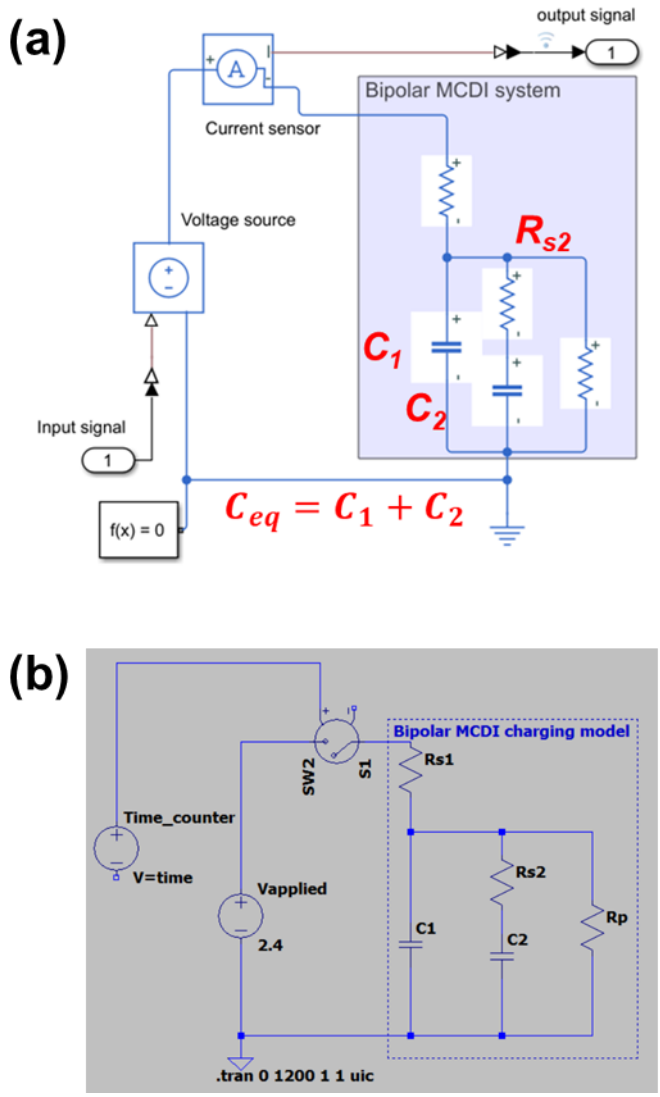

Figure 3-3. Modified two branches model in (a) MATLAB & Simulink for parameter estimation and (b) LTspice for simulation. (C: capacitor, R: resistor)

3.3. Results and Discussion

3.3.1 Model validation

In order to show the validity of the simulation using the equivalent circuit model, the simulation data and experimental data were compared. As shown in **Figure 3-4**, the classical model cannot imitate the charging current of constant voltage operation in Bipolar MCDI. The classical model could not express both the initial current and the late current decay behavior at the same time. In contrast with the classical model, the current profile simulated by the modified two branches model was well matched with the experimental data (**Figure 3-5a**). This result might be due to the local resistance difference inside the Bipolar MCDI (refer to **Figure 3-6**). From a microscopic point of view, the ionic charge will be difficult to access through the internal pores because the surface of the carbon electrode is geometrically complex. In addition, from a macroscopic point of view, the concentration of the electrolyte at the inlet and the outlet is different due to ion adsorption. Namely, some capacitor elements will have high resistance. For this reason, it is considered that the charging current of the Bipolar MCDI could not be simulated with the classical model. In contrast with the classical model, the modified two branches model has an additional RC branch in the network to consider the different resistance of capacitors. Because the capacitor elements

with different resistances are lumped by one resistor and two capacitors, this model could simulate the charging current of Bipolar MCDI. On the other hand, the discharging current under zero voltage was well matched with simulation data using the classical model (**Figure 3-5b**). The reason is probably that the ions in the electrolyte are enriched during the discharging process. Therefore, the modified two branches model was selected as the charging model, and the classical model was selected as discharging model.

Figure 3-7 shows the comparison between experimental and simulation results on of discharging current of Bipolar MCDI when the charged module is directly connected with the standard resistor of 24, 36, and 68 Ω and with the supercapacitor (75 F). As shown in **Figure 3-7a,** the cell voltage of Bipolar MCDI exponentially decayed when the charged Bipolar MCDI was connected to the external resistor. These experimental results were also well simulated by an equivalent circuit model. In addition, the voltage changes when connected to a supercapacitor were well simulated. The result indicates that the modified two branches model well represents the constant voltage charging of Bipolar MCDI, and it is appropriate to conduct the simulation by substituting the parameter estimated by this model into the discharging model.

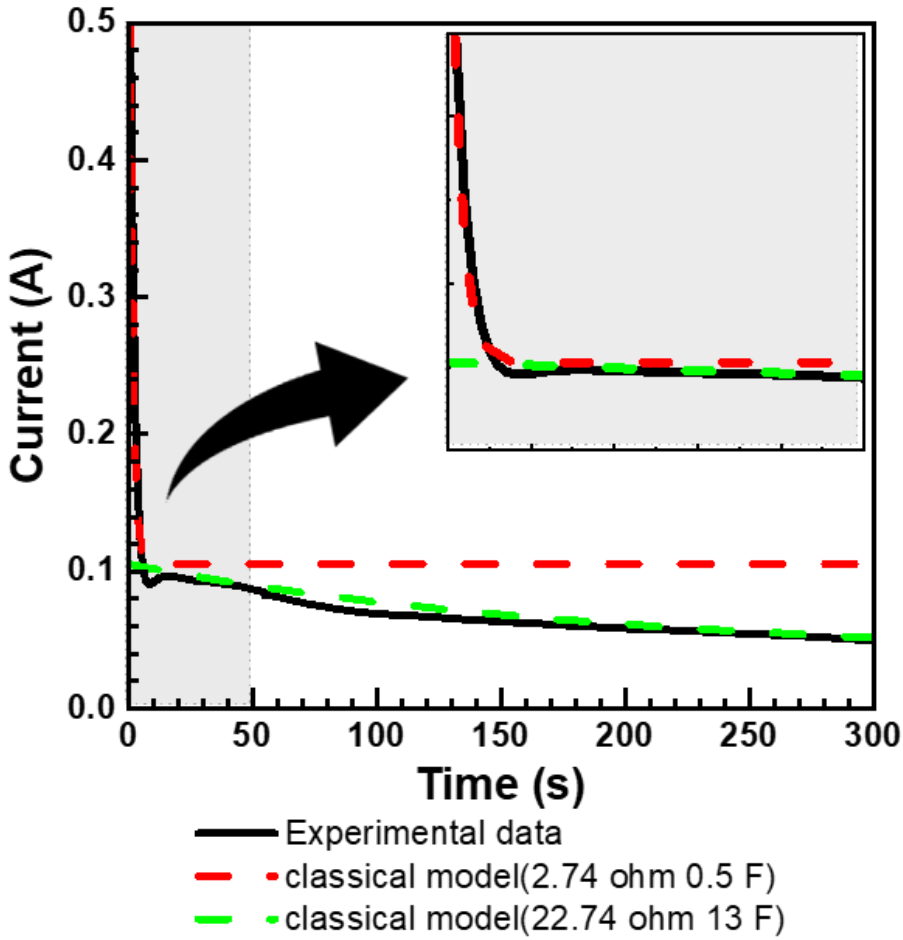

Figure 3-4. Comparison of experimental and simulation results of charging current with the classical model in Bipolar MCDI with a constant voltage of 2.4 V.

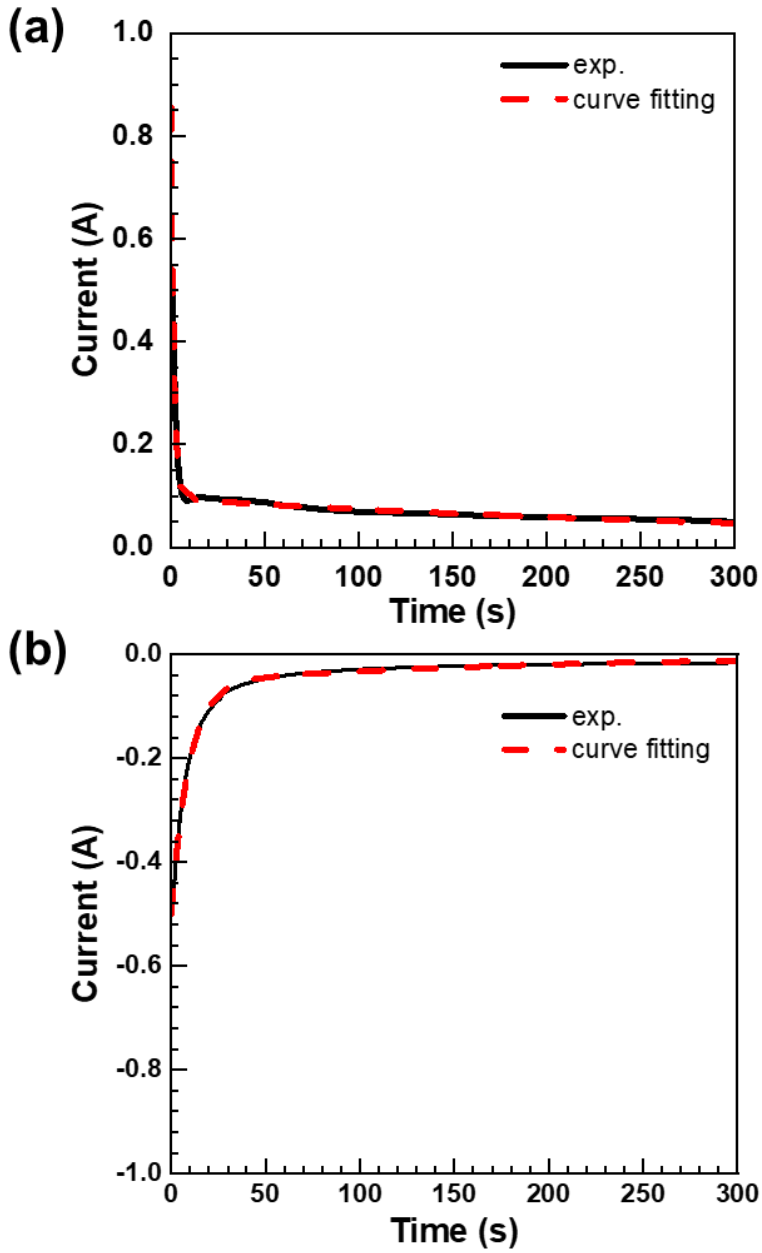

Figure 3-5. Representative comparison of simulation and experimental data: (a) charging current with modified two branches model under constant voltage of 2.4 V, and (b) discharging current with the classical model under constant voltage of 0 V.

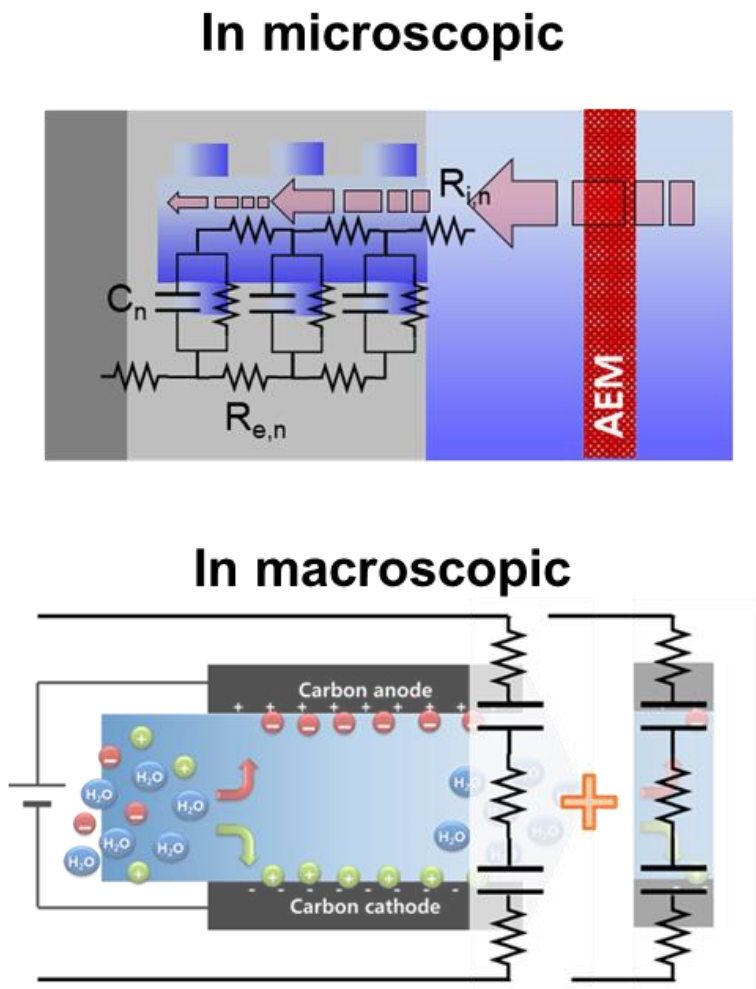

Figure 3-6. Schematic illustration of the difference in resistance of capacitor components according to the location in (a) microscopic and (b) macroscopic terms.

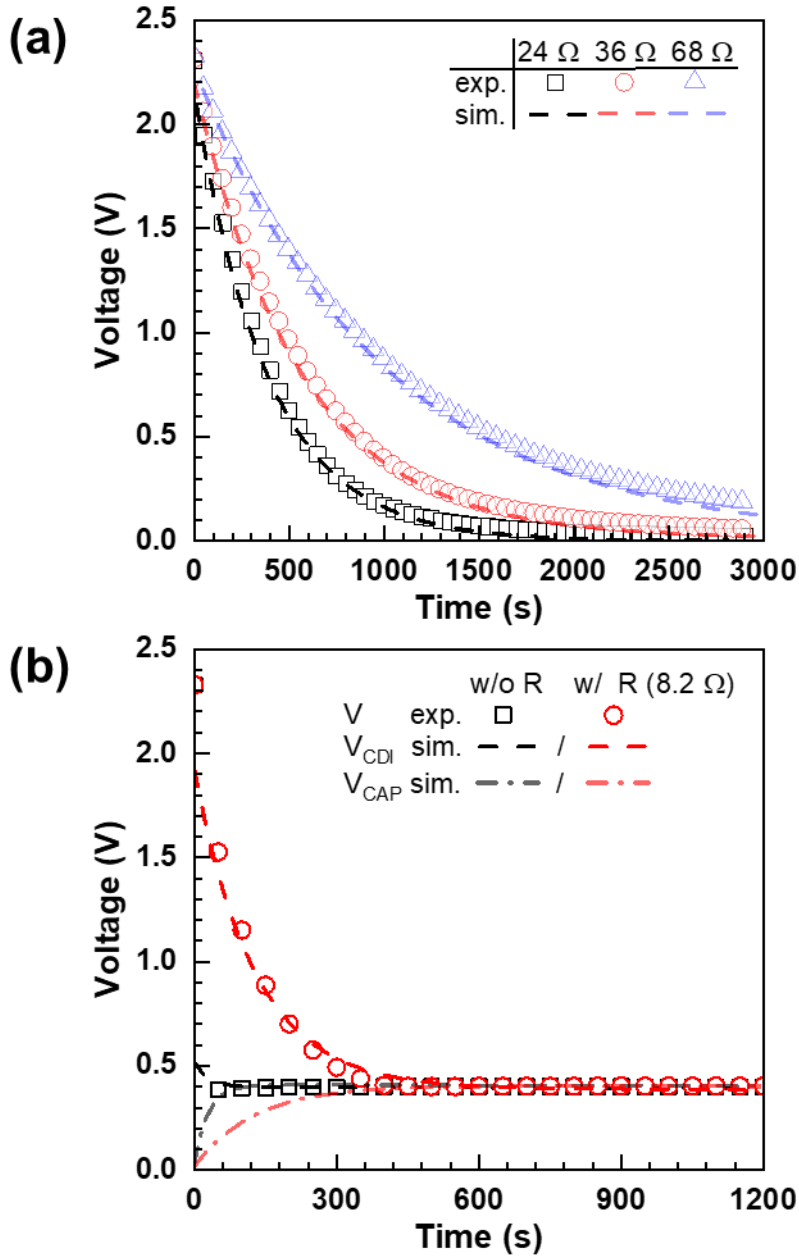

Figure 3-7. Comparison between experimental and simulation result on of discharging voltage of Bipolar MCDI when the charged module directly connected with the standard resistor of 24, 36, and 68 Ω and with supercapacitor (75 F).

3.3.2 Simulation of Bipolar MCDI charging with direct energy recovery

Figure 3-8 shows the charging current of 2.4 V and 12 V Bipolar MCDI system obtained by experiment and simulation.

As shown in **Figure 3-8a**, the charging current of 12 V Bipolar MCDI was measured to be almost similar to that of 2.4 V despite the increase in the number of electrode stacks. This result means the current does not increase as the stack number increases. Theoretically, the 12 V Bipolar MCDI is the same as five 2.4 V modules connected in series. Namely, the 12 V Bipolar MCDI module can be expressed as a series connection of five modified two branches model. This equivalent circuit can be lumped by one modified two branches model having 5- time higher resistance and 5- time lower capacitance since the RC elements are connected in series.

$$R_{total} = R_1 + R_2 + R_3 + R_4 + R_5 = 5R_1, \tag{3-14}$$

$$C_{total} = \left(\frac{1}{C_1} + \frac{1}{C_2} + \frac{1}{C_3} + \frac{1}{C_4} + \frac{1}{C_5}\right)^{-1} = \frac{1}{5}C_1 \tag{3-15}$$

This consideration is supported by the parameter estimation result. As shown in **Figure 3-8b**, the charging current is well fitted by the modified two branches model. By this fitting, the charging parameter of 12 V Bipolar MCDI can be obtained and summarized in **Table 3-1**. As shown in **Table 3-1**, the resistance components (R_{S1}, R_{S2}, and R_P) increased approximately 5- fold, and

the capacitance components (C_1 and C_2) decreased approximately 5- fold. The results indicate that the scale-up of the Bipolar MCDI system follows the electrical characteristics, and there will be no obvious risk of current increase even with the stack increase.

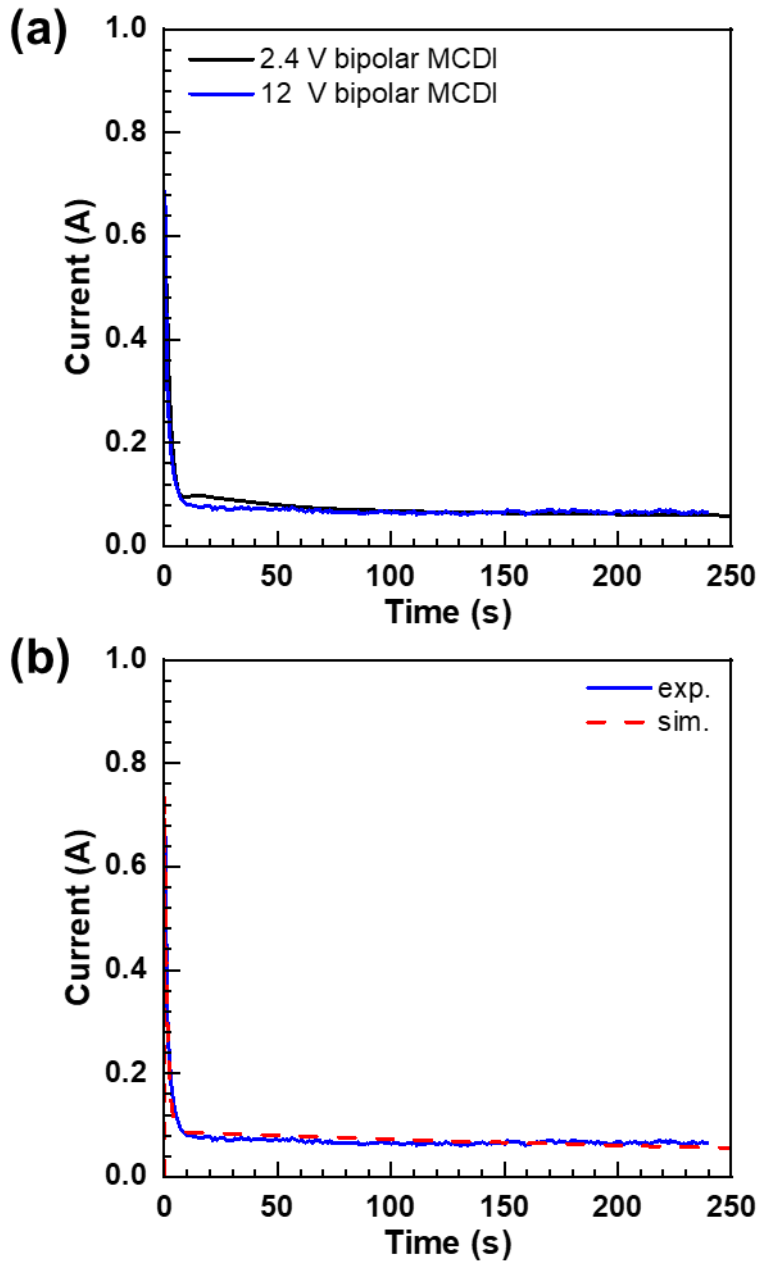

Figure 3-8. Comparison of charging current between (a) 2.4 V and 12 V Bipolar MCDI, and (b) experimental and simulation results of 12 V module.

Table 3-1. Summary of charging parameter in modified two branches model for 2.4 V and 12 V Bipolar MCDI.

Parameter	**2.4 V**	**12 V**	**Ratio** (12 V/2.4 V)
R_{s1}	2.8	16.3	**5.83**
R_{s2}	26.1	134.7	**5.16**
R_p	237.2	1183.7	**4.99**
C_1	0.41	0.08	**0.20**
C_2	15.09	3.10	**0.21**

Figure 3-9 shows the current profile of Bipolar MCDI during the direct energy recovery step. During direct connection with the second module, a current similar to constant voltage charging is observed. The peak current (*i(0)*) was lower than the constant voltage charging current. In the direct energy recovery step,

The potential difference between two Bipolar MCDI modules causes the current from the first Bipolar MCDI to the second Bipolar MCDI. the charging current in the second Bipolar MCDI with the same level as the discharging current in the first Bipolar MCDI. In other words, the second Bipolar MCDI is charged using the first Bipolar MCDI as a voltage source. In the aspect of the electrical circuit, the charged capacitor component in the first Bipolar MCDI act as a voltage source, and the current flow through the two resistors (R_{S1} of the first Bipolar MCDI and R_{S2} of the second Bipolar MCDI) into the capacitor component of second Bipolar MCDI. Therefore, the peak current during direct connection is lower than the peak current of constant voltage charging. This result indicates that energy recovery can be directly applied just by adding a switching circuit to the conventional control system.

In addition, the current of direct energy recovery in the 12 V system was almost the same with the 2.4 V system (**Figure 3-9b**). This result means that

the current during the direct energy recovery step will not increase as the number of electrode stacks increases for the same reason as mentioned in the charging current. Therefore, the results indicate that the direct energy recovery method can be applied in the Bipolar MCDI system without significant electrical risk.

The charged energy in the Bipolar MCDI can also be transferred to other devices, such as a supercapacitor and a battery, that are not the second Bipolar MCDI. In the case of the supercapacitor, it has lower resistance than the Bipolar MCDI, which is about 0.5 ohm or less. As shown in **Figure 3-10a**, the energy recovery efficiency decreases as the resistance between the charged Bipolar MCDI and connected energy-accepting devices increases. The series resistance of our system was 3 Ω or less. Nevertheless, there was little difference in energy recovery efficiency in this range of resistance, which was about 0.0012 times lower value than that of 0.5 Ω. Interestingly, the energy recovery efficiency significantly changed according to the difference in capacitance of capacitor components.

As shown in **Figure 3-10b**, the maximum energy recovery efficiency was reached when the Bipolar MCDI and energy acceptor had the same capacitance. This analysis indicates that the electrochemical parameters must be derived, and the appropriate electrical component must be selected to

efficiently implement direct energy recovery with a supercapacitor. On the other hand, since the second Bipolar MCDI has the same capacitance as the charged Bipolar MCDI and acceptable resistance, direct energy recovery can be applied without special effort.

Furthermore, additional energy loss may occur to utilize the energy stored in the supercapacitor for work, but in the case of the second Bipolar MCDI, it is more efficient because it performs spontaneous ion adsorption during the direct energy recovery step.

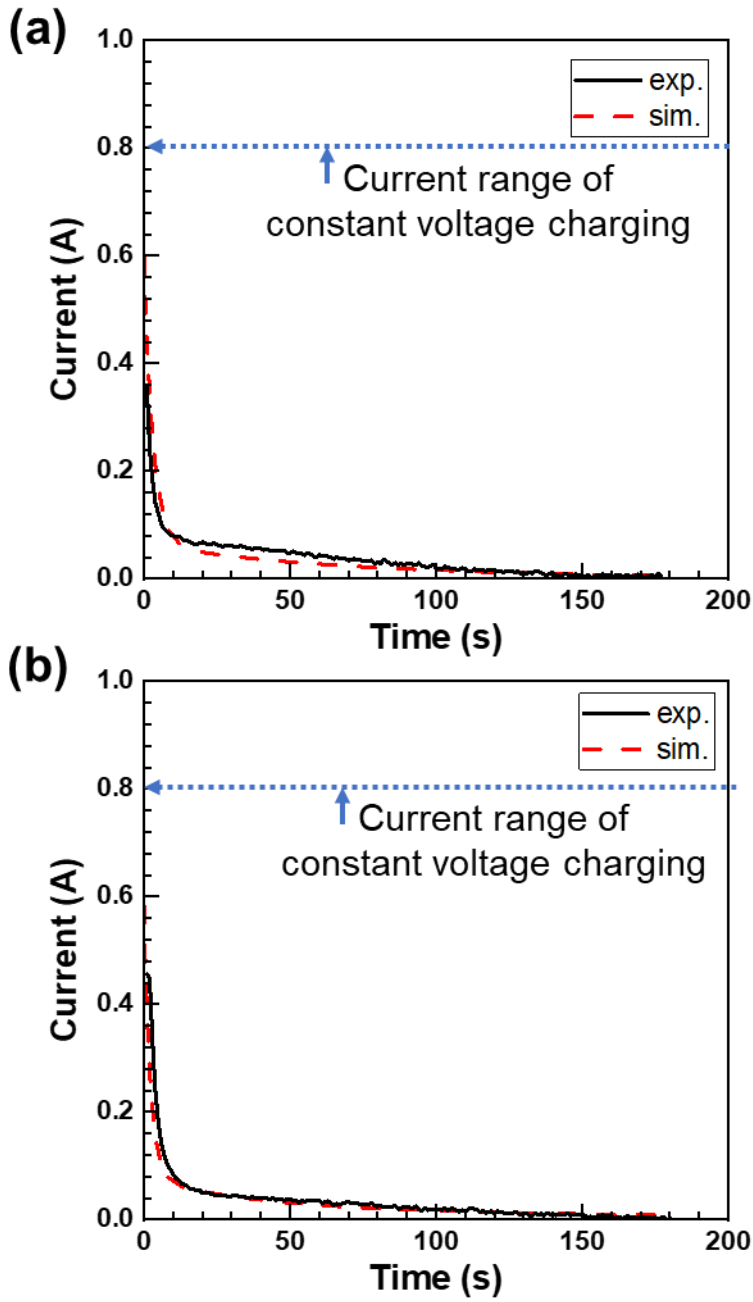

Figure 3-9. Representative current profile of Bipolar MCDI during direct energy recovery in (a) 2.4 V system and (b) 12 V system.

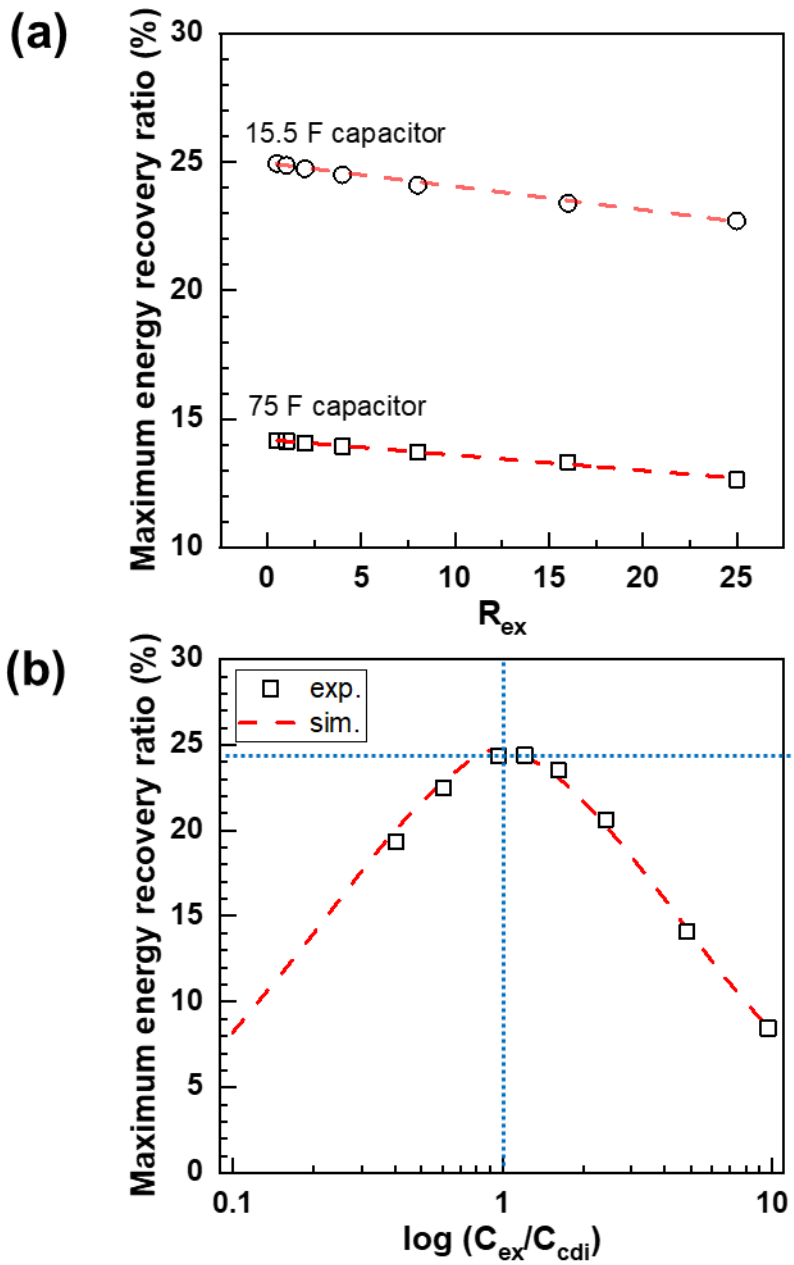

Figure 3-10. Energy recovery efficiency of direct energy recovery with (a) resistance of external energy acceptor (R_{ex})and (b) capacitance external energy acceptor (C_{ex}).

3.4. Summary

In this study, an equivalent circuit model was proposed to simulate the charge/discharge and direct energy recovery step. To improve the accuracy of the simulation, the modified two branches model was adopted for the charging model, and the classical model was adopted for the discharging model. The simulation results were in good agreement with the experimental results in not only the charge/discharge step but also the direct energy recovery step. In addition, it was confirmed that the direct energy recovery operates below the current of constant voltage operation, which indicates that the direct energy recovery of the Bipolar MCDI can be safely performed with a constant voltage operation system.

4. Investigation of Operation Characteristic for Bipolar MCDI System with Direct Energy recovery

4.1. Introduction

The electrochemical separation method has received large attention as promising water remediation and resource recovery process due to its environmentally benign and energy-efficient operation [38,93,109,110]. In particular, as the water crisis has become a growing global concern, significant research strides have been made in electrochemical desalination technology. Among the electrochemical desalination technology, capacitive deionization (CDI), membrane (MCDI), and electrodialysis has been extensively studied for industrial application [111,112]. Especially, MCDI is widely studied for treating relatively low salinity water streams such as brackish waters due to its simple implementation [4,22]. Furthermore, the potential of MCDI as a technology for a specific purpose such as selective removal of ions has been attracted [113–115]. The ion removal performance of MCDI has been enhanced with the introduction of various electrode materials such as functionalized carbon electrodes [116–119], intercalating materials [53,120–122], and integrating with redox materials [48,55,57,59,123,124]. The modification of cell construction [43–45,125], and optimization of the operation method [42,95,100,126] has also enhanced the performance of MCDI. In addition, efforts have also been made to develop

efficient energy recovery and scale-up methods in MCDI systems that are believed to be necessary for the successful commercial application of this technology [6,28,104,127].

The MCDI modules extend their desalination capacity via stack-up of the electrode as well as the extension of the electrode size [7,8]. Typically, the stacked electrodes are connected in parallel, which can be defined as a unipolar type. For this unipolar MCDI, all electrode pairs require a terminal to connect with an external power supply, which increases the complexity of module assemblies with a larger number of stacked electrodes [8]. In addition, the current is proportionally increased with the number of electrodes in the stack since the total current of the system is distributed at one point to each electrode pair to apply the same voltage (e.g., 1.2 V). Thus, a thick conducting wire is required to control the high current, which can increase the investment cost of the electrical systems and their size [7,9]. Furthermore, for unipolar MCDI, two types of electrodes sandwiched between cation exchange membranes and anion exchange membranes are alternately stacked between conventional electrodes pairs [10]. These characteristics make the unipolar MCDI module complex, bulky, expensive, as the scale of the module increases.

Recently, the Bipolar MCDI module has gained much attention, in which

stacked electrodes are connected in series without conducting wiring (**Figure 4-1**). As compared in **Figure 4-1a and b**, contrary to unipolar MCDI, there is no requirement for terminals for applying electrical energy, since the bipolar electrodes (inner electrode of the module) are evenly polarized via the applied electric field through the outermost electrode pair [105,107]. Thus, the Bipolar MCDI module is operated under a high voltage without increasing current depending on the number of stacked electrodes, which does not require a thick conducting wire [9,11]. Furthermore, in the Bipolar MCDI module, only one type of electrode sandwiched between the cation exchange membrane and the anion exchange membrane is stacked as the inner electrode [9]. Therefore, the Bipolar MCDI system can be operated with a low investment cost compared to the unipolar MCDI. In this regard, Bipolar MCDI is expected to be a more suitable process for real implementation in industrial and environmental applications. However, for the further success of Bipolar MCDI, it is still necessary to improve its energy efficiency during desalination. Nevertheless, to date, there are few studies to improve the energy efficiency of Bipolar MCDI significantly limiting its practical application.

Therefore, this study aimed to propose the desalination process of a Bipolar MCDI system including direct energy transfer for energy recovery

and assess its potential with a lab-scale and a pilot-scale module. In this study, various Bipolar MCDI modules were employed to assess the energy recovery process, such as a lab-scale module with a single stack and nine stacks of the bipolar electrode (i.e., 2.4 V and 12 V system) and a pilot-scale module with 250 stacks (i.e., 300 V system). Because the energy was recovered via a direct energy transfer between two Bipolar MCDI modules, this step was denoted as direct P2P (direct energy transfer from MCDI process to MCDI process). The overall process was performed as follows (**Figure 4-1c**). First, as a pretreatment process before energy recovery, the Bipolar MCDI modules were operated in an alternating manner with constant cell voltage operation. For example, the first Bipolar MCDI module was operated by applying a constant cell voltage of 2.4 V for desalination while the second Bipolar MCDI module was operated by applying a reverse voltage of –2.4 V for regeneration. Consequently, the invested energy can be simultaneously charged at both Bipolar MCDI modules up to cell voltages of 2.4 V and –2.4 V, respectively, during the desalination and regeneration phase. Second, as shown in **Figure 4-1c**, the energy was transferred between both Bipolar MCDI modules by a direct connection leading to energy recovery (first direct P2P). Since the transferred energy is not sufficient to perform a full-cycle operation, this energy partially supports the initial ion adsorption at the first Bipolar MCDI

module (desalination) and ion desorption at the second Bipolar MCDI module (regeneration) by controlling the duration of their electrical connection. Then, additional energy was invested to complete the full cycle operation via an external power source (charging for energy input). For consecutive operations, these processes were alternatively operated between two Bipolar MCDI modules via a second direct P2P and reverse charging.

To optimize the direct P2P, the effect of the duration of direct P2P on the energy efficiency and desalination performance of Bipolar MCDI operation within 5 min of half-cycle time in a lab-scale module (i.e., 2.4 V and 12 V systems) was examined. Additionally, the potential of direct P2P was assessed with a pilot-scale module (i.e., 300 V system).

4.2. Experimental Section

4.2.1 Bipolar MCDI module configuration

In the Bipolar MCDI module, the bipolar carbon electrodes were coated by cation and anion exchange resins on both sides. The bipolar carbon electrodes were placed between a pair of conventional activated carbon electrodes with an anion exchange membrane and cation exchange membrane (refer to **Figure 3-1**). The nonconductive nylon cloth was used as a spacer providing a water stream.

Contrary to conventional MCDI stacked with unipolar electrodes, only the outermost electrodes are connected to the external circuit in the Bipolar MCDI module (refer to **Figure 4-1a**) [9,11]. A high voltage is applied to the outermost electrode pair to distribute the desired voltage to each cell, as shown in **Figure 4-1b**. By the electric field applied through the outmost electrode pair, inner electrodes are evenly polarized. Namely, the voltage between each cell is the same but the potential difference between the 1st electrode and others increases as away from the 1st electrode. For example, the Bipolar MCDI module consisted of a pair of carbon electrodes, and one sheet of bipolar carbon electrodes was operated with a cell voltage of 2.4 V to evenly distribute cell voltage of 1.2 V for each electrode (1.2 V/cell × 2 cells). In addition, the Bipolar MCDI module with nine sheets of bipolar

carbon electrode was operated with a cell voltage of 12 V (1.2 V/cell × 10 cells).

The outermost electrode pair of the lab-scale Bipolar MCDI module consisted of a pair of activated carbon electrodes (Siontech Co., Ltd., Republic of Korea), and ion exchange membranes (AEM/CEM Type 1, FUJIFILM Europe, Japan). One or nine sheets of the resin-coated bipolar electrodes (Siontech Co., Ltd., Republic of Korea) were inserted between the outermost electrode pair for the 2.4 V and 12 V systems, respectively. All components were cut to 10 cm in diameter and had a 1 cm hole in the center for water flow.

The pilot-scale Bipolar MCDI module (Model SDI-C2, Siontech Co., Ltd., Republic of Korea) was purchased, which is assembled with two-unit modules having a diameter of 23 cm, and a height of 31.2 cm. In the unit module, approximately 250 sheets of the resin-coated bipolar electrodes were stacked, which were the same product as the materials in the lab-scale module. The module is designed with a rated flow rate of 20 L min^{-1}, and rated input voltage and current of 300 V and 2 A, respectively.

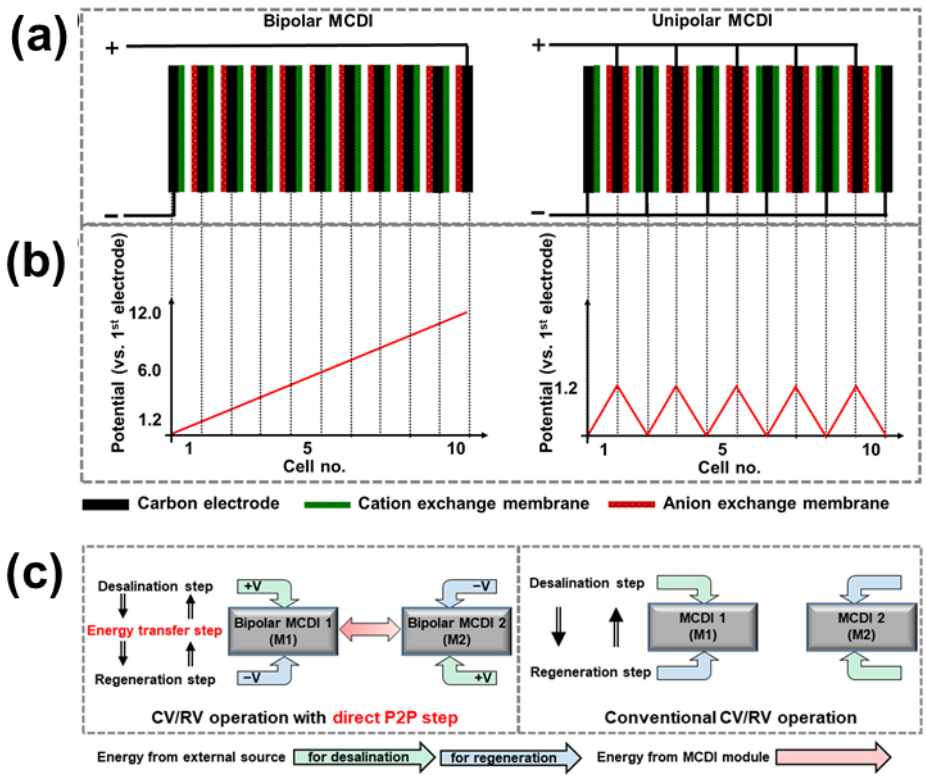

Figure 4-1. Schematic illustration of (a) Bipolar MCDI and unipolar MCDI in stack configuration and (b) the standard curve of electrode potential distribution, and (c) comparison of constant voltage desalination/reverse voltage regeneration (CV/RV operation) with and without direct energy transfer from MCDI process to MCDI process (direct P2P).

4.2.2 Operation of Bipolar MCDI with direct energy recovery

The desalination and regeneration of two Bipolar MCDI modules were repeatedly performed under constant voltage and reverse voltage regeneration (CV/RVD operation). In contrast with classical CV/RVD operation of MCDI, in order to recover energy, the direct connection of two Bipolar MCDI modules was conducted between the desalination step and regeneration step (**Figure 4-1c**). Namely, the following four sequential steps were repeatedly performed, as shown in **Figure 4-2**.

In the first step, the reverse charged Bipolar MCDI module (first Bipolar MCDI module) and the charged Bipolar MCDI modules (second Bipolar MCDI module) were directly connected, which were prepared as a result of the previous desalination and regeneration phase. The energy was transferred between two Bipolar MCDI modules leading to desalination of the first Bipolar MCDI module and regeneration of the second Bipolar MCDI module, which is denoted as direct P2P (direct energy transfer from MCDI process to MCDI process). However, the energy transfer is insufficient to operate the full- cycle of two Bipolar MCDI modules since their cell voltages will be equalized by energy transfer [17,19,21,105]. Thus, the energy transfer only allows initial ion adsorption at the first Bipolar MCDI module (for desalination) and ion desorption at the second Bipolar MCDI module (for

regeneration).

In the second step, the insufficient energy was compensated for by applying a constant voltage from an external power source leading to full desalination and regeneration phases of two Bipolar MCDI modules. Thus, the charged first Bipolar MCDI module and the reverse charged second Bipolar MCDI module were prepared by this step.

Then, the third and final steps were performed in the same manner as the first and second steps, but the roles of the two modules were switched.

For the consecutive operation of these steps, a simple switch circuit was employed as shown in **Figure 4-3**. The circuit changes the electrical connection between the external power source and two Bipolar MCDI modules according to the operational step.

To optimize the operational cycle with direct P2P, the energy efficiency was estimated with various durations for direct P2P and desalination/regeneration (**Table 4-1**). The half-cycle time was employed at 5 min for the desalination and regeneration phase (total operation time was 10 min). The direct P2P time was varied from 0 min to 4 min corresponding to the introduction of additional energy by the external power source. For example, when the direct P2P time had a duration of 1 min, the time for constant voltage operation was 4 min. The operational conditions were

denoted as P_xC_y, where P means the direct P2P, C means a charging (constant voltage and reverse voltage), and x and y are the duration of direct P2P and the charging, respectively.

To investigate the voltage difference after charging and reverse charging Bipolar MCDI modules, the open-circuit voltage (OCV) of the Bipolar MCDI module was measured after charging and reverse charging by a constant voltage of 2.4 V for 1, 2-, 3-, 4-, and 5-min. Note that the Bipolar MCDI module was completely short-circuited before charging and reverse charging.

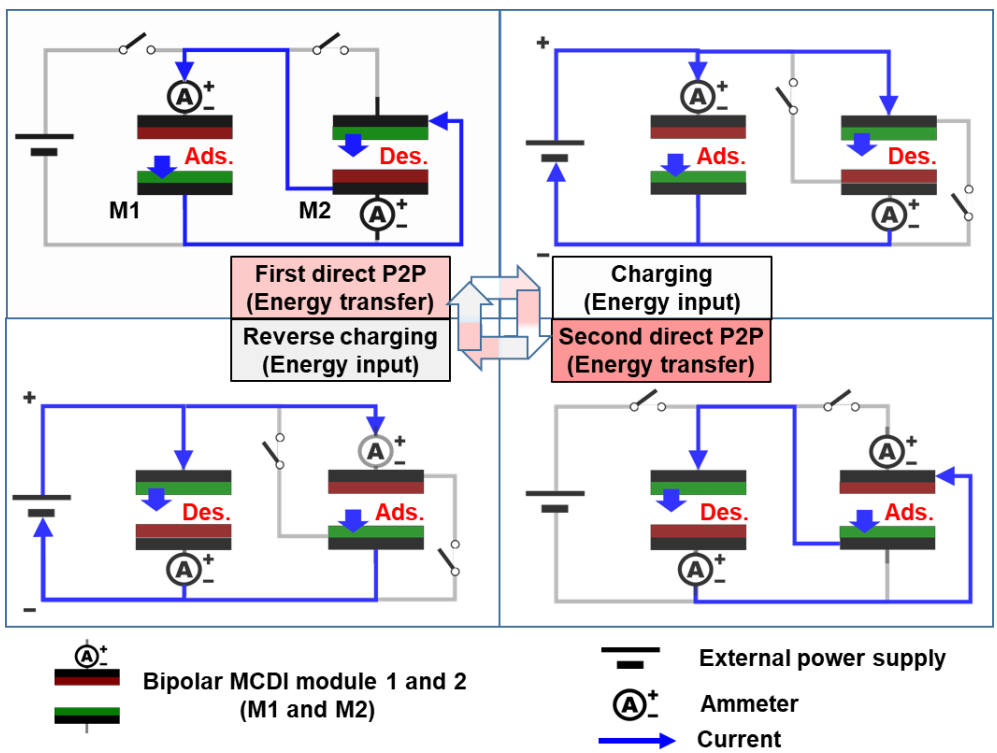

Figure 4-2. Schematic simple circuit diagram of the Bipolar MCDI operation cycle including the direct P2P step.

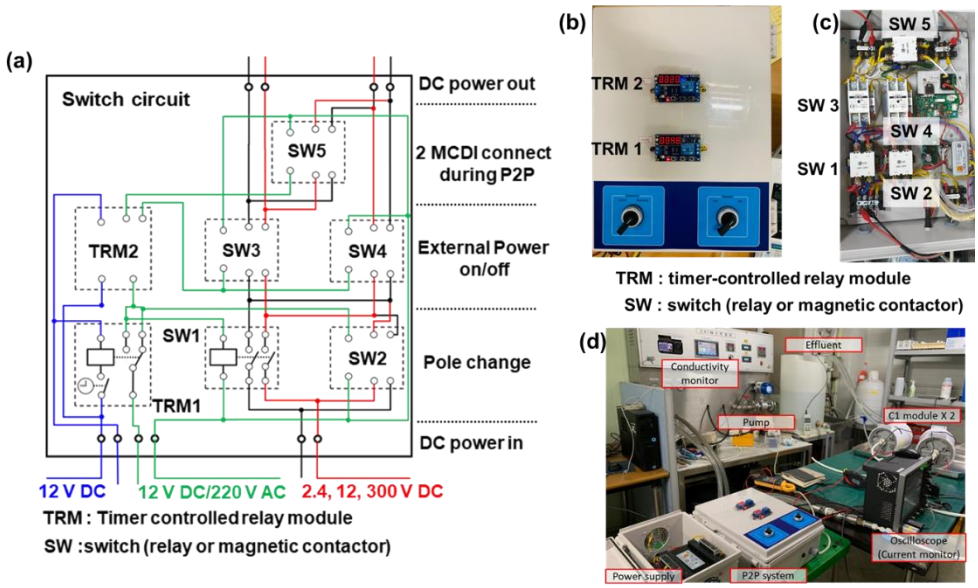

Figure 4-3. Schematic (a) electric circuit diagram of the simple switch circuit for MCDI operation including direct P2P, and its photograph for the pilot-scale module (300 V system); (b) front view, (c) inside view, and (d) its desalination test system.

Table 4-1. Duration of steps depending on the combination, where P means the direct P2P, C means charging, and x and y are, respectively, the duration of direct P2P and the charging.

Combination	Desalination (regeneration) phase time (min)	
	First Direct P2P (Second direct P2P)	Charging (Reverse charging)
$\mathbf{P_0C_5}$	0	5
$\mathbf{P_1C_4}$	1	4
$\mathbf{P_2C_3}$	2	3
$\mathbf{P_3C_2}$	3	2
$\mathbf{P_4C_1}$	4	1

4.2.3 Experimental conditions and performance indicator

Feedwater with 10.27 mM NaCl solution was supplied to each module with flow rates of 8-, 40-, and 1,340 ml min^{-1}, in 2.4 V, 12 V, and 300 V system, respectively, by a gear pump (75211-15, Cole-Parmer, USA). The effluent concentration of the Bipolar MCDI module was measured using a conductivity meter (3574-10C, HORIBA, Japan). The current was measured at the anode terminal of each Bipolar MCDI module by an oscilloscope (wavesurfer 44MXs-B, LeCroy, USA) with a current probe (CP150, LeCroy, USA) during not only the charge/discharge step but also the direct P2P step.

The desalination performance of various operation combinations was evaluated through the number of adsorbed ions over the desalination phase, the average salt adsorption rate, the average concentration reduction, and molar energy consumption.

The adsorbed ions (ΔN, μmol g^{-1}) in the desalination phase can be calculated from

$$\Delta N = \frac{\int_0^t Q(C_i - C_o)dt}{nm}, \quad (4\text{-}1)$$

where Q is the volumetric flow rate of the feed stream (ml min^{-1}), C_i and C_o are the influent and effluent concentrations (mM), respectively, n is the number of electrode pairs (cell) in the Bipolar MCDI module, m is the mass of activated carbon in an electrode pair (g). The ΔN over the charging step

was calculated by subtracting the ΔN at the end of the direct P2P from the ΔN at the end of the full desalination phase.

The average salt adsorption rate (ASAR, μmol min^{-1} cm^{-2}) can be calculated from

$$ASAR = \frac{\int_0^t Q(C_i - C_o)dt}{nA\Delta t}, \quad (4\text{-}2)$$

where A is the electrode area of the one cell (cm^{-2}), and Δt is the operation time over which a process was performed.

the average concentration reduction ($\Delta\overline{C}$, mM) represents the average difference in salt concentration between the effluent stream and feed [60]. This indicator indicates the concentration of produced water obtained from a desalination process. As expressed in Equation (4-3, $\Delta\overline{C}$ is calculated by dividing ΔN by the total volume of water supplied over time.

$$\Delta\overline{C} = \frac{\int_0^t Q(C_i - C_o)dt}{\int_0^t Q dt}, \quad (4\text{-}3)$$

The $\Delta\overline{C}$ at the end of the desalination phase is defined as $\Delta\bar{C}_d$, which indicates the final concentration of produced water.

The energy efficiency of the operational combinations was evaluated by comparing the molar energy consumption (E_m, kJ mol^{-1}). E_m during the total process was calculated by dividing the energy supplied during the charging

and discharging steps (E_c and E_d) by the number of adsorbed ions, as expressed in Equation (4-4)

$$E_m = \frac{E_c + E_d}{\int_0^c Q(C_i - C_o)dt}, \quad (4\text{-}4)$$

where the energy (E) supplied during each step is a value obtained by integrating the product of voltage-current over the time of the step, given by,

$$E = \int Vidt, \quad (4\text{-}5)$$

4.3. Results and Discussion

4.3.1 Bipolar MCDI with direct energy recovery step in 2.4 V system

Figure 4-4 shows the representative effluent concentration and current profile of the first Bipolar MCDI module in 2.4 V systems in various durations of first direct P2P, charging (+V), second direct P2P, and reverse charging (–V).

As shown in **Figure 4-4a**, the effluent concentration profile of the first Bipolar MCDI module with various direct P2P steps (i.e., P_4C_1, P_3C_2, P_2C_3, and P_1C_4) showed a bimodal curve for ion adsorption and desorption, while P_0C_5 had a typical effluent profile of CV/RV operation (black line in Figure 4-4a). Accordingly, as shown in **Figure 4-4b**, the current profile of the operation with a direct P2P step also revealed double peaks in the desalination and regeneration phase compared to the typical current profile of CV/RV operation (black line in **Figure 4-4b**).

Considering that the direct P2P step was skipped in the P_0C_5 operation, it is plausible that the bimodal curves are likely due to the energy transfer between two Bipolar MCDI modules. In particular, the measured current in the direct P2P proves the energy transfer between two Bipolar MCDI modules because both modules were connected only to each other in this step. This energy transfer occurs due to the voltage difference of two Bipolar MCDI

modules formed by the previous charging and reverse charging steps. For example, in the first direct P2P step, the reverse charged first Bipolar MCDI module (i.e., with lower voltage) and forward charged second Bipolar MCDI module (i.e., with higher voltage) were electrically connected. This connection causes a positive current to flow in the first Bipolar MCDI module to equalize the voltages of the two modules. Thus, the first Bipolar MCDI module can perform partial desalination. At the same time, the second Bipolar MCDI module can perform partial regeneration with a negative current, and the desalination profile of the second Bipolar MCDI module compared with the first Bipolar MCDI module is presented in **Figure 4-5**.

After completing the first direct P2P, forward and reverse voltages were applied to the first and second Bipolar MCDI modules, respectively, by the external power source to operate full desalination and regeneration of two Bipolar MCDI modules. By this step, the voltage difference of two Bipolar MCDI modules, which might be insufficient to transfer the energy in the second direct P2P, was compensated for similar to the start of the operational cycle, and the polarity was reversed. Thus, in the second direct P2P step, the negative current flows in the first Bipolar MCDI module with the regeneration, and partial adsorption and desorption were similar to that in the first direct P2P.

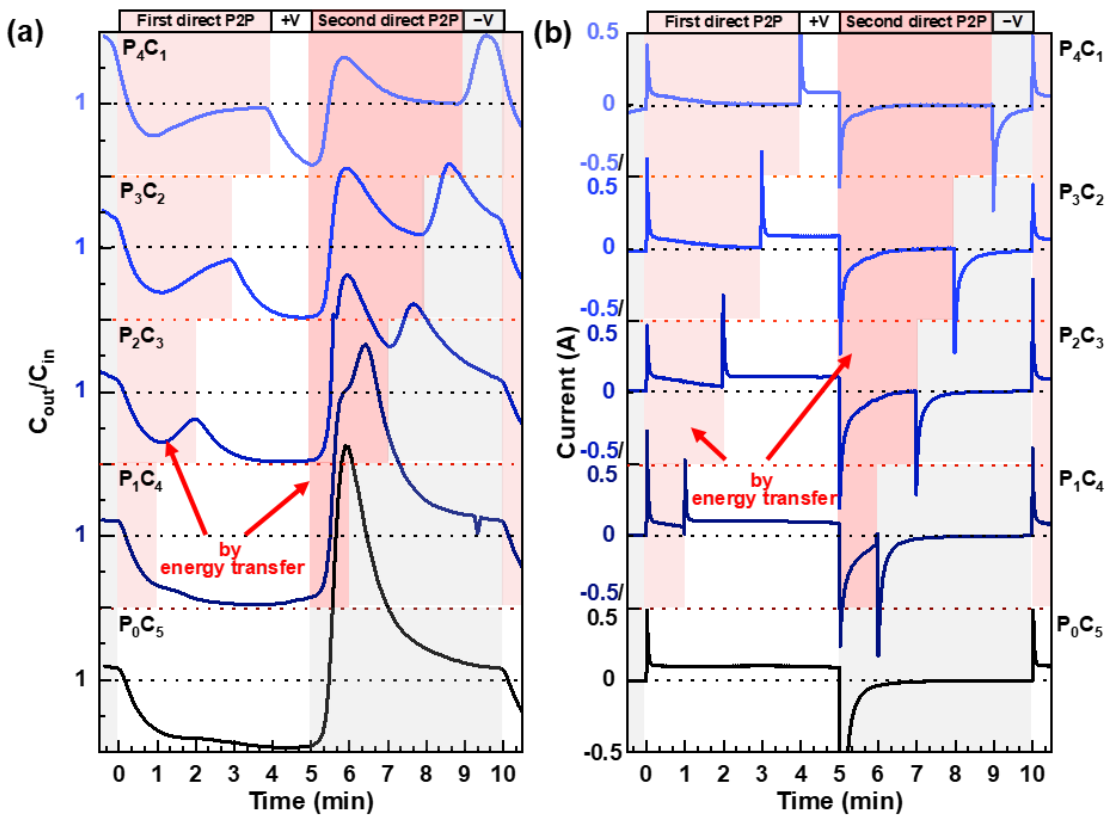

Figure 4-4. Representative effluent concentration (a) and current profile (b) of first Bipolar MCDI module with various time combinations of four steps. The duration of each step was combined within a half-cycle time of 5 min. The color of the panel indicates the step labeled on top of the panel, where +V is the charging step with a constant voltage of 2.4 V, and –V is the reverse charging step with a constant voltage of –2.4 V.

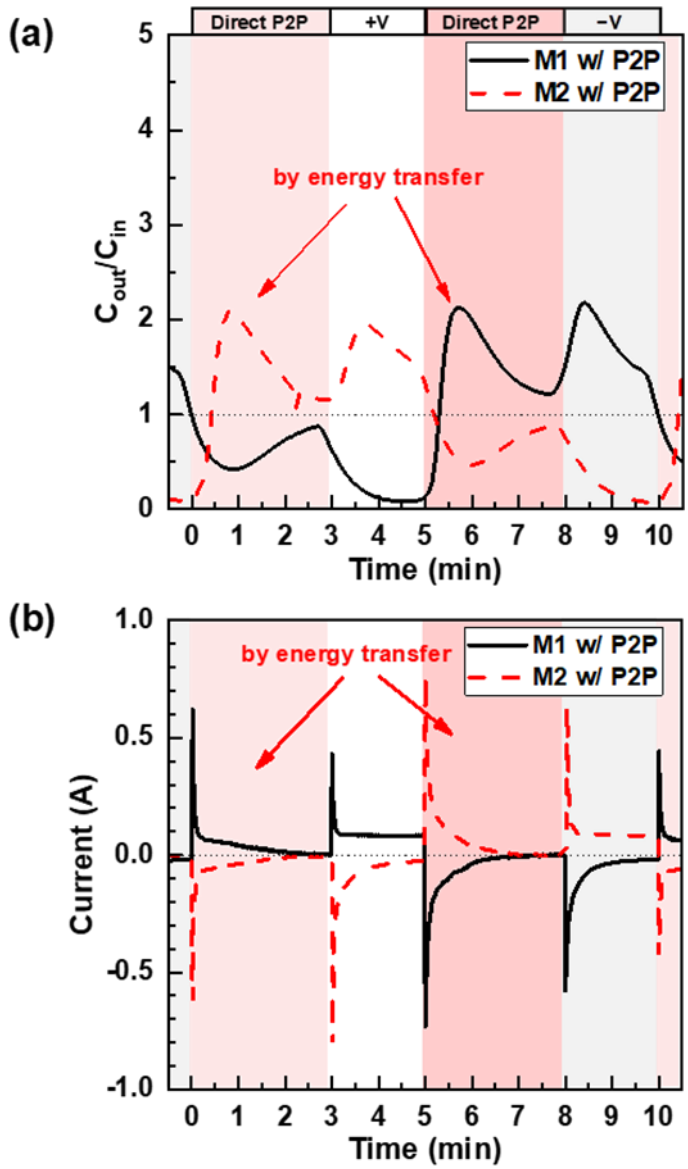

Figure 4-5. Representative (a) the effluent concentration of two Bipolar MCDI modules during operation including direct P2P, and (b) the current profile. The background color in all graph panels means the step is denoted as the same color in (a and b).

4.3.2 Performance analysis of Bipolar MCDI with direct P2P

As shown in **Figure 4-6**, with direct P2P, the energy efficiency of the first Bipolar MCDI module was significantly improved during the regeneration (the red bar) and desalination (the black bar) phase. For example, E_m of P_2C_3 was reduced to 207 kJ mol^{-1} over the full operation cycle, which was 43% lower than the E_m of 361 kJ mol^{-1} in P_0C_5. This is attributed to the ions being partially ad/desorbed without supplying external power during the desalination and regeneration phase. For instance, the partial desorption of ions via direct P2P could cause energy reduction in the reverse charging step. As illustrated by the red circle in **Figure 4-7a**, the operational combinations including direct P2P (i.e., P_1C_4, P_2C_3, P_3C_2, and P_4C_1) were reverse charged with significantly lower energy than P_0C_5 operation. Since the stored charge on the bipolar electrode decreased by partial desorption during the second direct P2P step, the reverse charging step could be performed at a lower initial current than the P_0C_5 operation (refer to the negative current in **Figure 4-7b**). Note that the relation between direct P2P and change in the current profile requires further study. In the case of the charging step, the supplied energy linearly decreased as the charging time (duration of supplying external energy) decreased (the black square in **Figure 4-7a**). Furthermore, the decrease rate of the supplied energy with the duration of the charging step was almost the

same as that of adsorbed ions (see the black square in **Figure 4-8a**). The results indicate that the energy efficiency in the charging step was barely affected by the introduction of direct P2P (refer to **Figure 4-8b**). Accordingly, the reduction of E_m in the regeneration phase was higher than that in the desalination phase.

On the other hand, the partially adsorbed ions also contributed to the reduction of E_m in the full operation cycle. As illustrated by the red circle in Figure 4-8a, the adsorbed ions (ΔN) over the direct P2P step increased in P_1C_4 and P_2C_3 operations, and thus the E_m of P_1C_4 and P_2C_3 was significantly reduced compared with P_0C_5 not only in the regeneration phase but also in the desalination phase (refer to the stacked bar in Figure 4-6). In addition, the reduction of E_m in the desalination phase shows the same trend as that of the additional ion adsorption in the direct P2P.

Interestingly, ΔN over the direct P2P step was smaller in P_3C_2 and P_4C_1 than P_2C_3 leading to a higher E_m than P_2C_3. This result indicates that the optimized duration of the charging and direct P2P steps should be combined to efficiently reduce the energy consumption of Bipolar MCDI. For example, a short charging step would cause a low adsorption capacity during direct P2P even if the direct P2P step is performed for a long time because the stored charging on the electrode is small. Moreover, a decrease in ΔN over the full

operation cycle, which would result from the change in the duration of the charging and direct P2P steps, affects the quality of the produced water (i.e., the concentration of desalinated water). As shown in **Figure 4-9**, the average concentration reduction at the end of the desalination phase ($\Delta\bar{C}_d$) gradually decreased as operational combination changed from P_0C_5 to P_4C_1. For example, $\Delta\bar{C}_d$ of P_4C_1 was 3.05 mM in contrast with 8.18 mM of P_0C_5, where $\Delta\bar{C}_d$ means the difference in concentration between feed water and final product. Namely, by replacing the 4 min charging time with direct P2P, the P_4C_1 operation obtained 63% less desalted water than P_0C_5.

We believe that the result mainly is due to two reasons (refer to **Figure 4-10**). First, the short charging step causes a low voltage difference between both Bipolar MCDI modules after completing charging, which induces a low adsorption rate during direct P2P. For example, as shown in **Figure 4-10**, the open-circuit voltage (OCV) of the Bipolar MCDI module was measured to be 2.21 V and –2.16 V, respectively, by charging and reverse charging under a constant voltage of 2.4 V for 5 min. The OCV decreased as the charging time decreased. Thus, the OCV difference between charged and reverse charged Bipolar MCDI modules decreased from 4.37 V to 3.32 V, as the charging/reverse charging time decreased from 5 min to 1 min (see V_{P2P} of inset graph in **Figure 4-10**). Since the difference in OCV between the charged

and reverse charged Bipolar MCDI modules is the driving force for ion adsorption in the direct P2P step, the desalination performance during the direct P2P step decreased as the charging time decreased (refer to **Figure 4-11**).

Second, an excessively long direct P2P step can be one of the main factors to decrease desalination performance. As shown in Figure 4-11a, the current during direct P2P converged to zero since the driving force for ion adsorption during direct P2P was gradually exhausted. Thus, ion adsorption indirect P2P gradually decreased with time, which represented a decrease in the average concentration reduction (**Figure 4-11b**).

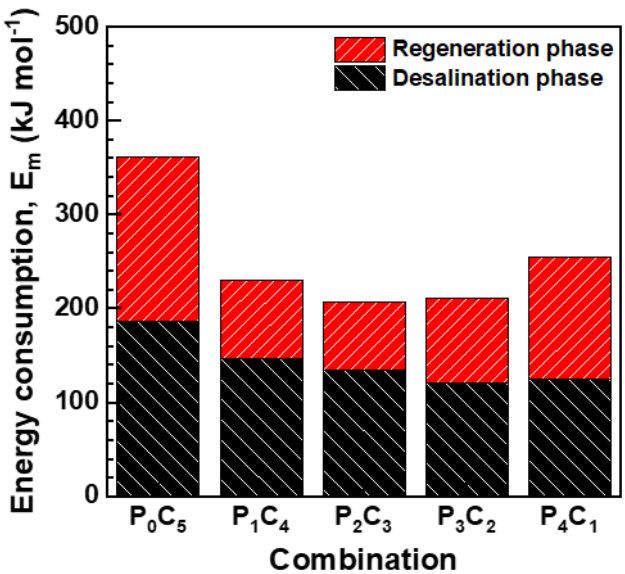

Figure 4-6. Representative the molar energy consumption (E_m) in the desalination and regeneration phase of first Bipolar MCDI with various operation combinations in the 2.4 V system.

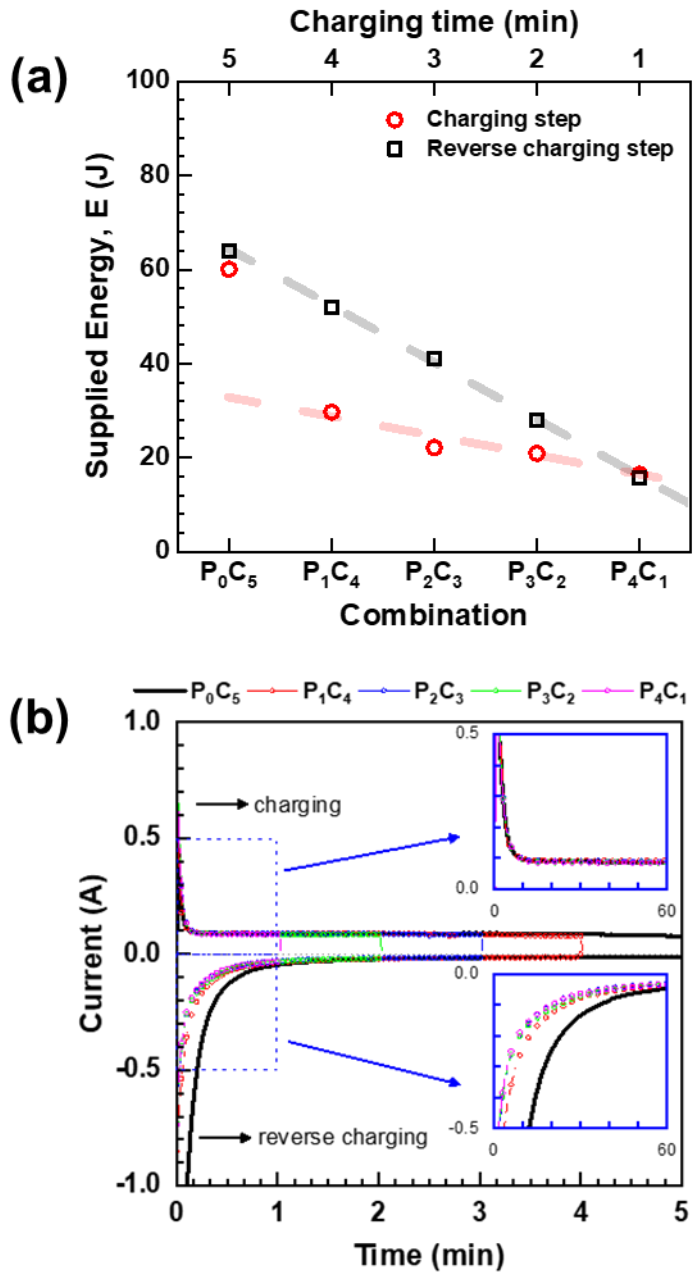

Figure 4-7. Representative (a) supplied energy (*E*) during the charging and reverse charging step and (b) comparison of current profile in charging (positive current) and reverse charging (negative current) step.

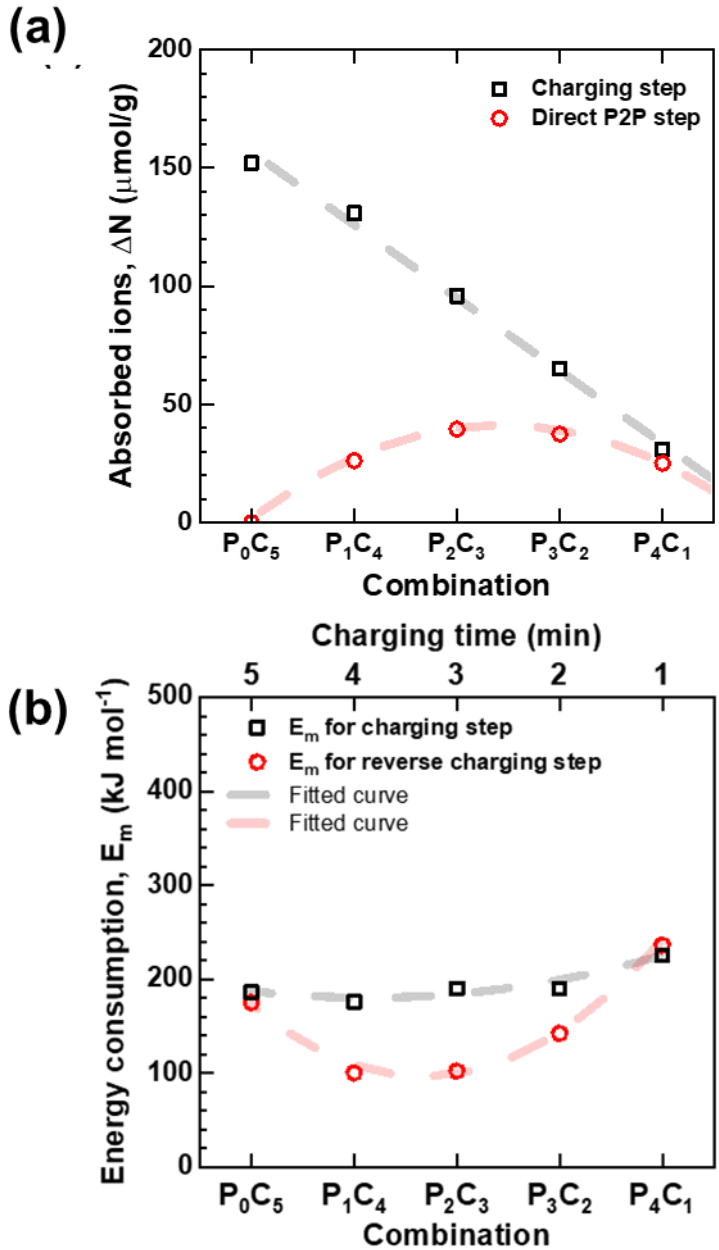

Figure 4-8. (a) Adsorbed ion (ΔN) over the charging step and direct P2P step of first Bipolar MCDI with various operation combinations in the 2.4 V system and (b) the molar energy consumption (E_m) over the charging and reverse charging step

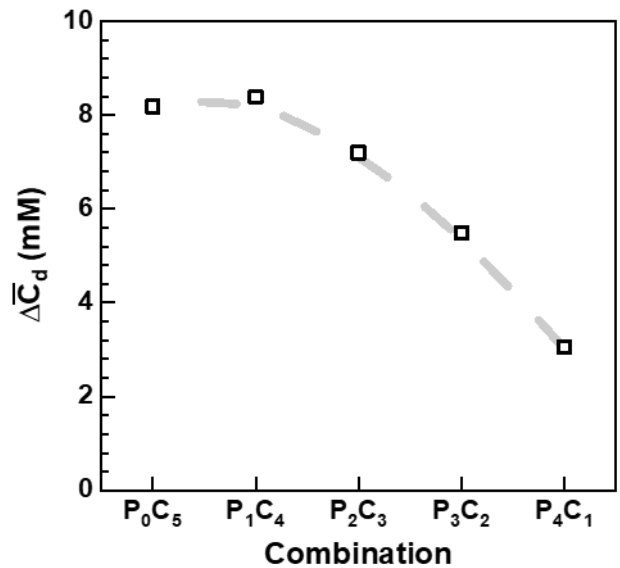

Figure 4-9. The average concentration reduction at the end of the desalination phase ($\Delta\overline{\boldsymbol{C}}_{\boldsymbol{d}}$) of first Bipolar MCDI with various operation combinations in the 2.4 V.

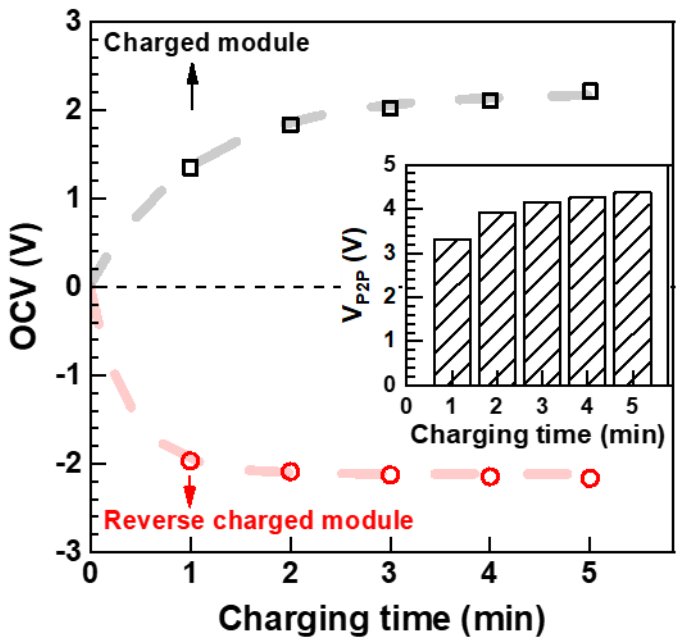

Figure 4-10. Representative open-circuit voltage (OCV) of Bipolar MCDI module which charged, and reverse charged for various charging times. V_{P2P} of the inset graph is the difference in OCV between charged and reverse charged Bipolar MCDI module**.**

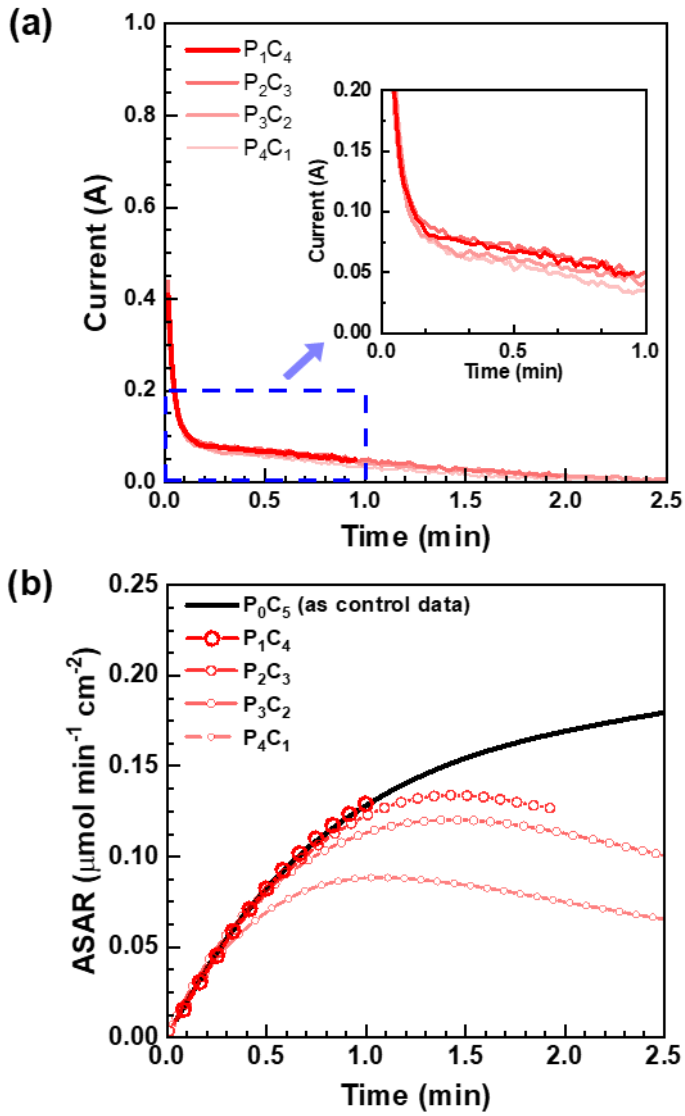

Figure 4-11. Representative (a) current profile and (b) the change in the average salt adsorption rate (ASAR) of first Bipolar MCDI module in the first direct P2P step.

4.3.3 Application into scaled-up system to 12 V and 300 V modules

As shown in **Figure 4-12** and **Figure 4-13**, the operation combinations including the direct P2P were well performed even in the 12 V Bipolar MCDI system, showing the same desalination behavior as the 2.4 V system.

For example, as shown in **Figure 4-14a,** the energy supplied during the charging step decreased linearly as the charging time decreased (the black square in **Figure 4-14a**). In addition, the energy supplied during the reverse charging step was significantly reduced by introducing the direct P2P compared with the P_0C_5 operation (the red circle in **Figure 4-14a**). The results were the same behavior with the 2.4 V system. Interestingly, the energy supplied during the charging step of the 12 V system was approximately five times higher than that of the 2.4 V system as the module scale was expanded by a factor of 5. In contrast with that of the charging step, a large increase in energy supplied during the reverse charging step was observed in the 12 V system compared with the 2.4 V system, which was due to a high reverse charging current (refer to **Figure 4-14b**). Note that a high reverse charging current might originate from the rapid discharging characteristic of the Bipolar MCDI [9].

As shown in **Figure 4-15a**, the trend of adsorbed ions during charging and direct P2P steps was similar to that in the 2.4 V system. The adsorbed

ions during the charging step decreased linearly as the duration of the charging step decreased. In addition, as in the 2.4 V system, the adsorbed ions during direct P2P were highest in P_2C_3 operation and gradually decreased. Notably, the 12 V system could adsorb 1.2- to 1.8-fold more ions per mass of activated carbon than the 2.4 V system for the same duration time, showing rapid and high ion adsorption during the direct P2P step (refer to **Figure 4-15b**).

According to previous research, the bipolar electrode stack showed an enhanced ion adsorption rate and capacity compared to the unipolar electrode stack [107]. This improvement is believed to originate from the high voltage induced across the Bipolar MCDI modules. For the same reason, it is plausible that the ion adsorption rate and capacity in direct P2P were improved. This result implies that Bipolar MCDI would be favorable for the application of direct P2P.

Figure 4-16 shows the molar energy consumption (E_m) and the average concentration reduction at the end of the desalination phase ($\Delta\bar{C}_d$) in operation combinations of a 12 V system, which were based on the supplied energy and adsorbed ions. As shown in **Figure 4-16,** the direct P2P reduced the energy consumption of the Bipolar MCDI system up to 47% compared with the P_0C_5 operation. However, the operation combination with a long direct P2P step

and a short charging step caused a decrease in $\Delta\bar{C}_d$. For example, $\Delta\bar{C}_d$ of P_3C_2 and P_4C_1 was 7.85 and 4.74 mM, respectively, while the $\Delta\bar{C}_d$ of P_0C_5 was 9.49 mM. Interestingly, P_2C_3 operation not only consumed significantly less energy, at 41% lower than P_0C_5 operation, but also, achieved consistent $\Delta\bar{C}_d$. Thus, we consider P_2C_3 to be the optimized operation combination to increase energy efficiency while maintaining desalination performance.

According to the result on the desalination operation of the 12 V system, the P_2C_3 combination was employed to operate the pilot-scale Bipolar MCDI modules and compared with conventional constant voltage desalination and reverse voltage regeneration (i.e., P_0C_5).

Figure 4-17 shows the representative molar energy consumption (E_m) with an average concentration reduction of the first Bipolar MCDI module at the end of the desalination phase ($\Delta\bar{C}_d$) in the 300 V system. Besides, the effluent concentration and current profile of the 300 V Bipolar MCDI system were presented in **Figure 4-18**. As shown in **Figure 4-18**, the effluent concentration and current profile in the 300 V Bipolar MCDI module with direct P2P (red line) is the same as conventional Bipolar MCDI operation (black line) during the desalination phase

This result indicates the successful application of the direct P2P to the pilot-scale system using the simple switching circuit. Moreover, as shown in

Figure 4-17, the operation combination including direct P2P (P_2C_3 operation) achieved significantly lower energy consumption than conventional operation (P_0C_5), which was 40% lower than the P_0C_5 energy consumption of 2,150 kJ/mol. In addition, the $\Delta\bar{C}_d$ of P_2C_3 was 8.97 mM, which was similar to the 9.37 mM of conventional operation (P_0C_5). Note that the flow rate of the feed water stream, which was lower than the rated flow rate, might affect the high energy consumption of the 300 V system compared with the conventional MCDI system. This could be solved by applying the appropriate operating conditions. Therefore, we ignored this fact in this paper to focus on the feasibility of applying Bipolar MCDI with direct P2P to an industrial-scale process. Nevertheless, the results indicate that Bipolar MCDI with direct P2P can be an option to improve the energy efficiency of MCDI operation not only for a lab-scale process but also for an industrial-scale process at a modest cost.

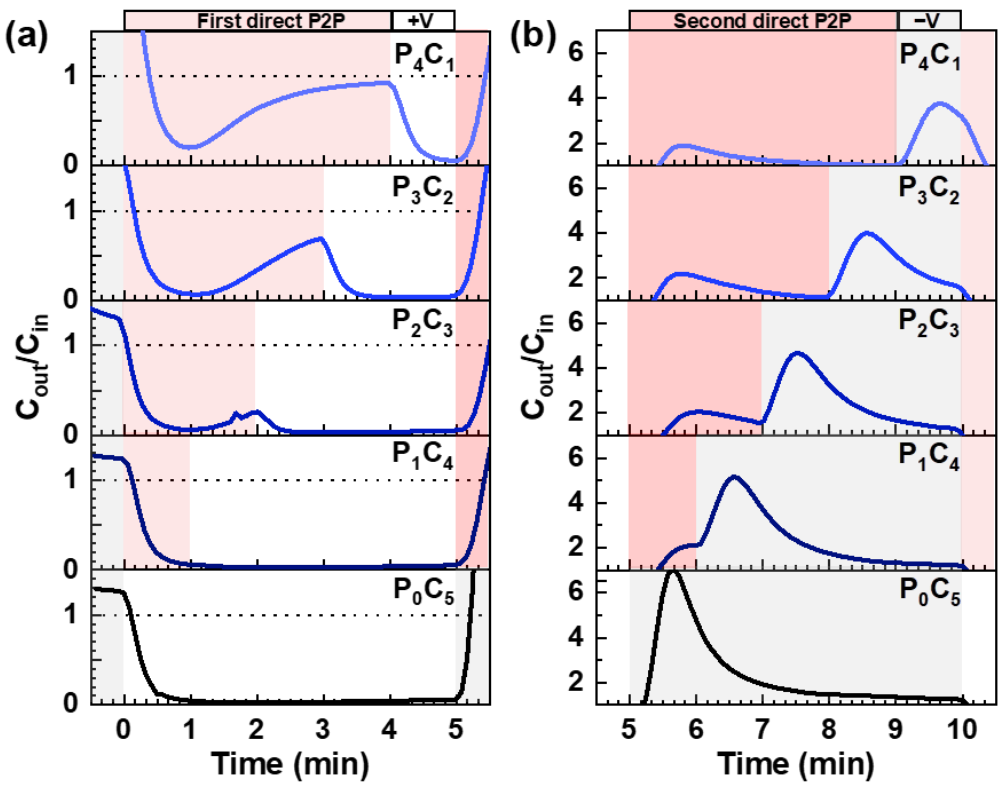

Figure 4-12. Representative desalination profile of first Bipolar MCDI module with the various operational combination in 12 V system: (a) the effluent concentration during desalination phase, (b) the effluent concentration during regeneration phase.

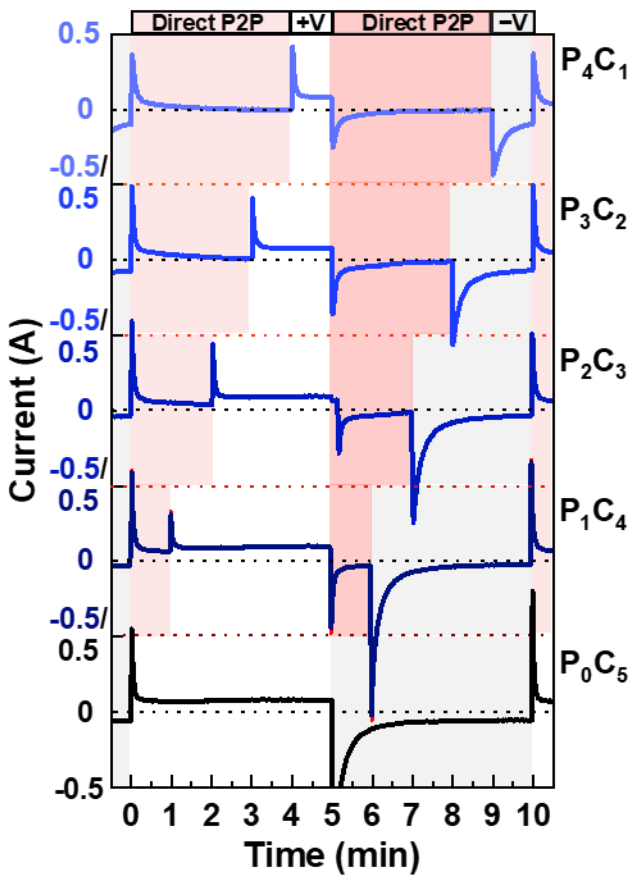

Figure 4-13. Representative current profile of first Bipolar MCDI module with the various operational combination in 12 V system during the entire cycle.

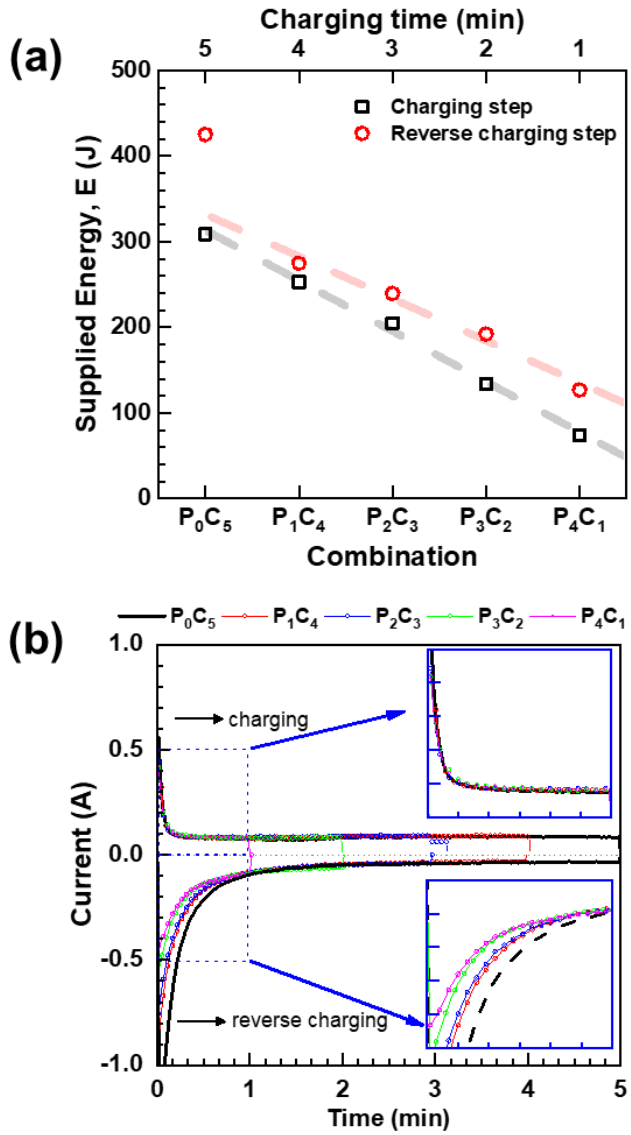

Figure 4-14. Representative desalination performance of first Bipolar MCDI module with various operation combinations in the 12 V system: (a) energy supplied during the charging and reverse charging step and (b) comparison of current profile in charging (positive current) and reverse charging (negative current) step.

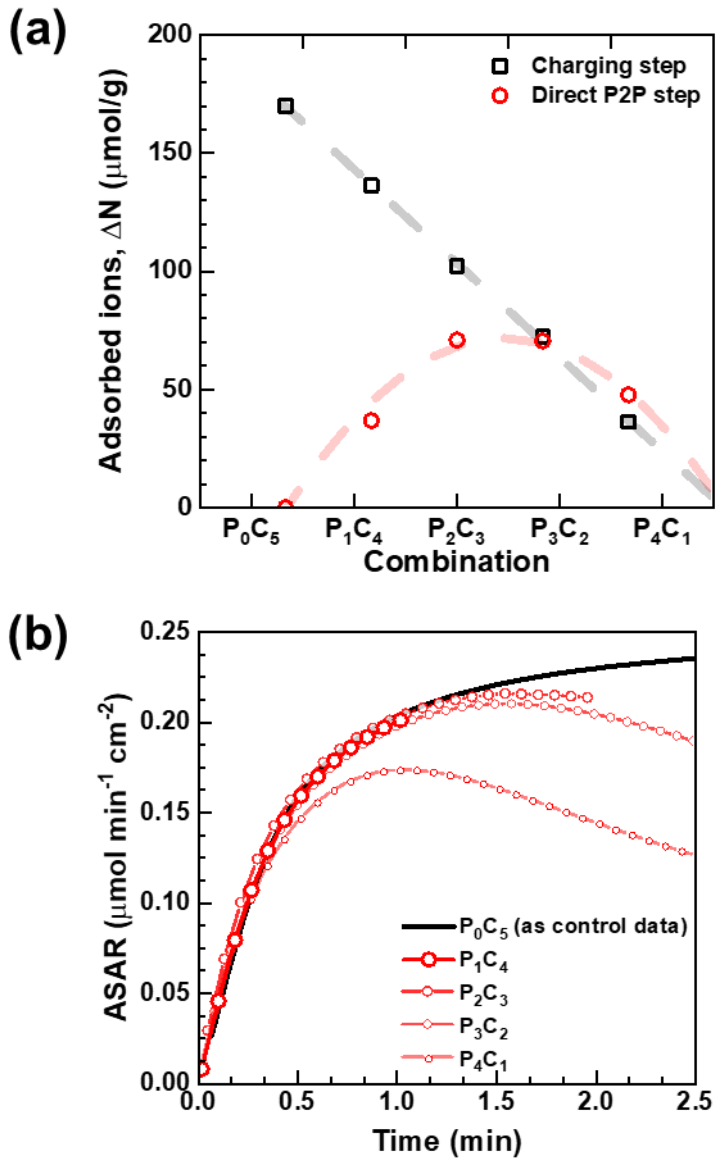

Figure 4-15. Representative (a) adsorbed ion (***ΔN***) over the charging step and direct P2P step of first Bipolar MCDI module with various operation combination in 12 V system and (b) the change of the average salt adsorption rate (ASAR).

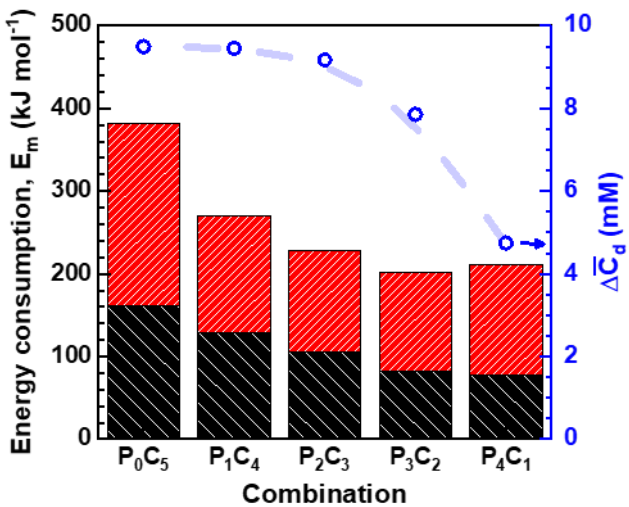

Figure 4-16. The molar energy consumption ($\boldsymbol{E_m}$) in the desalination and regeneration phase and the average concentration reduction at the end of the desalination phase ($\Delta\bar{\boldsymbol{C}}_{\boldsymbol{d}}$) of the 12 V Bipolar MCDI system.

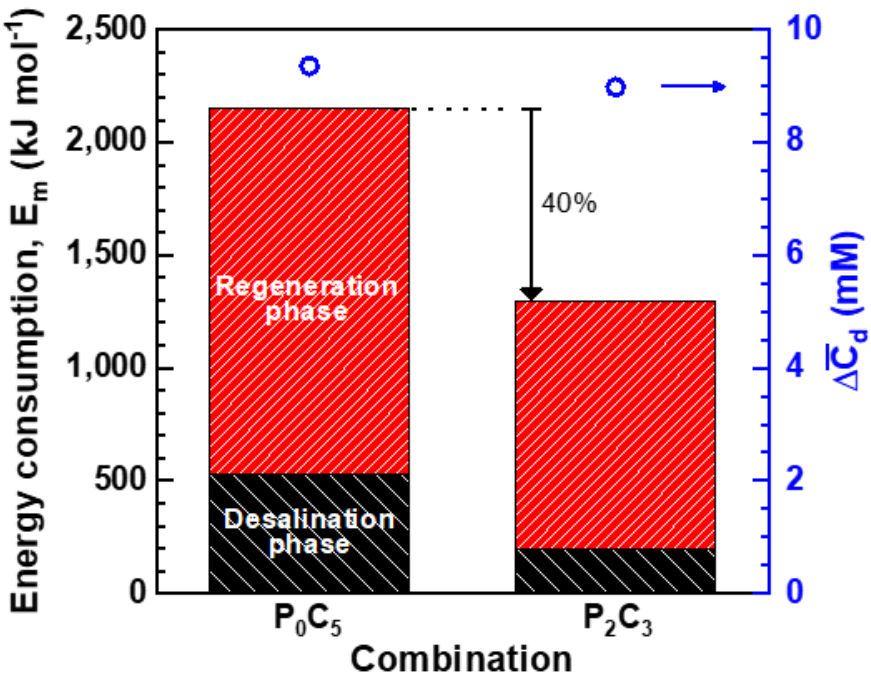

Figure 4-17. Representative comparison of molar energy consumption ($\boldsymbol{E_m}$) and average concentration reduction at the end of the desalination phase ($\Delta\overline{\boldsymbol{C}}_{\boldsymbol{d}}$) between the P_0C_5 and P_2C_3 operation in the 300 V system.

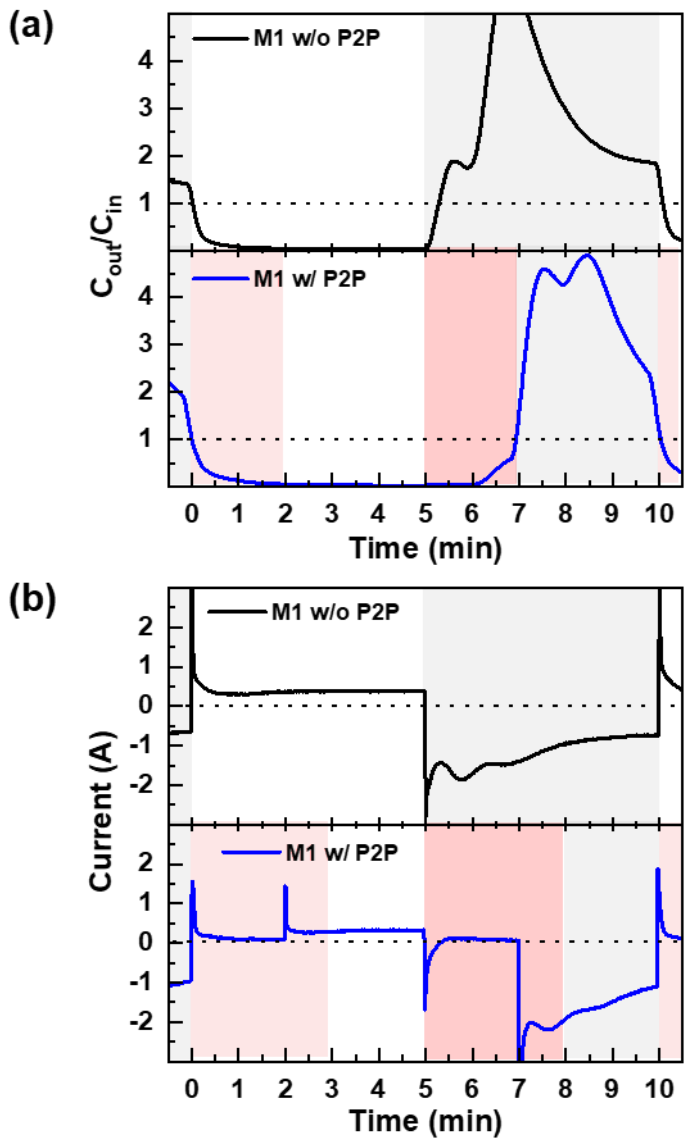

Figure 4-18. Representative (a) effluent concentration and (b) current profile of 300 V bipoalr MCDI module.

4.4. Summary

In this study, the operation characteristics of the Bipolar MCDI including the direct energy recovery step were investigated for the actual system. The optimized operation based on the lab-scale investigation was applied to the pilot-scale process. As a major result, energy consumption was reduced by 43% and 41%, respectively, at the laboratory scale (2.4 V and 12 V system) compared to the conventional constant voltage charge/discharge operation by the introduction of the direct energy recovery step. In addition, the energy consumption was reduced by 40% without deterioration of the desalination performance even in the pilot scale. Therefore, we envision that Bipolar MCDI with direct energy transfer can be a major stepping-stone to enhancing the energy efficiency of the MCDI system even on an industrial scale.

5. Conclusion

In this dissertation, a Bipolar MCDI system with direct energy recovery was developed by simulation and practical implementation.

In the first part, the charge/discharge and direct energy recovery steps were simulated by an equivalent circuit model. To improve the accuracy of the simulation, the modified two branches model was adopted for the charging model, and the classical model was adopted for the discharging model. The equivalent circuit model successfully simulates the charging/discharging and direct energy recovery steps. According to simulation, the direct energy recovery operates below the current of constant voltage operation, which indicates that the direct energy recovery of the Bipolar MCDI can be safely performed with a constant voltage operation system.

In the second part, the operation characteristics of the Bipolar MCDI including the direct energy recovery step were investigated for the actual system. The optimized operation based on the lab-scale investigation was applied to the pilot-scale process. As a major result, energy consumption was reduced by 43% and 41%, respectively, at the laboratory scale (2.4 V and 12 V system) compared to the conventional constant voltage charge/discharge operation by the introduction of the direct energy recovery step. In addition,

the energy consumption was reduced by 40% without deterioration of the desalination performance even in the pilot scale.

Therefore, the Bipolar MCDI system with direct energy recovery can be an energy-efficient alternative that can be applied to real industrial environments. In addition, the development process from simulation to application is expected to be of great help in expanding laboratory-scale research to an industrial scale.

6. References

[1] W.A. Jury, H.J. Vaux, The Emerging Global Water Crisis: Managing Scarcity and Conflict Between Water Users, in: Adv. Agron., 2007: pp. 1–76. https://doi.org/10.1016/S0065-2113(07)95001-4.

[2] M. a Shannon, P.W. Bohn, M. Elimelech, J.G. Georgiadis, B.J. Mariñas, A.M. Mayes, Science and technology for water purification in the coming decades., Nature. 452 (2008) 301–10. https://doi.org/10.1038/nature06599.

[3] IEA, Net Zero by 2050: A Roadmap for the Global Energy Sector, OECD Publishing, Paris, 2021. https://doi.org/10.1787/c8328405-en.

[4] M.E. Suss, S. Porada, X. Sun, P.M. Biesheuvel, J. Yoon, V. Presser, Water desalination via capacitive deionization: What is it and what can we expect from it?, Energy Environ. Sci. 8 (2015) 2296–2319. https://doi.org/10.1039/c5ee00519a.

[5] C. Tan, C. He, W. Tang, P. Kovalsky, J. Fletcher, T.D. Waite, Integration of photovoltaic energy supply with membrane capacitive deionization (MCDI) for salt removal from brackish waters, Water Res. 147 (2018) 276–286. https://doi.org/10.1016/j.watres.2018.09.056.

[6] C. Tan, C. He, J. Fletcher, T.D. Waite, Energy recovery in pilot scale membrane CDI treatment of brackish waters, Water Res. 168 (2020)

115146. https://doi.org/10.1016/j.watres.2019.115146.

[7] T.J. Welgemoed, C.F. Schutte, Capacitive Deionization Technology™: An alternative desalination solution, Desalination. 183 (2005) 327–340. https://doi.org/10.1016/j.desal.2005.02.054.

[8] Y. Oren, Capacitive deionization (CDI) for desalination and water treatment — past, present and future (a review), Desalination. 228 (2008) 10–29. https://doi.org/10.1016/j.desal.2007.08.005.

[9] S.-K. Park, J.-H. Choi, Desalination characteristics in a membrane capacitive deionization stack with carbon electrodes connected in series, Sep. Purif. Technol. 209 (2019) 152–158. https://doi.org/10.1016/j.seppur.2018.07.032.

[10] Y.Y. Shen, S.H. Sun, S.W. Tsai, T.H. Chen, C.H. Hou, Development of a membrane capacitive deionization stack for domestic wastewater reclamation: A pilot-scale feasibility study, Desalination. 500 (2021) 114851. https://doi.org/10.1016/j.desal.2020.114851.

[11] J.K. Lee, Y.E. Kim, J. Kim, S. Chung, D. Ji, J. Lee, Comparable mono and bipolar connection of capacitive deionization stack in NaCl treatment, J. Ind. Eng. Chem. 18 (2012) 763–766. https://doi.org/10.1016/j.jiec.2011.11.119.

[12] E. García-Quismondo, R. Gómez, F. Vaquero, A.L. Cudero, J. Palma,

M. Anderson, New testing procedures of a capacitive deionization reactor., Phys. Chem. Chem. Phys. 15 (2013) 7648–56. https://doi.org/10.1039/c3cp50514f.

[13] P. Dlugolecki, A. van der Wal, Energy Recovery in Membrane Capacitive Deionization, Environ. Sci. Technol. 47 (2013) 4904–4910. https://doi.org/10.1021/es3053202.

[14] R. Zhao, S. Porada, P.M. Biesheuvel, A. Van der Wal, Energy consumption in membrane capacitive deionization for different water recoveries and flow rates, and comparison with reverse osmosis, Desalination. 330 (2013) 35–41. https://doi.org/10.1016/j.desal.2013.08.017.

[15] L. Chen, X. Yin, L. Zhu, Y. Qiu, Energy recovery and electrode regeneration under different charge/discharge conditions in membrane capacitive deionization, Desalination. 439 (2018) 93–101. https://doi.org/10.1016/j.desal.2018.04.012.

[16] D.I. Oyarzun, S.A. Hawks, P.G. Campbell, A. Hemmatifar, A. Krishna, J.G. Santiago, M. Stadermann, Energy transfer for storage or recovery in capacitive deionization using a DC-DC converter, J. Power Sources. 448 (2020) 227409. https://doi.org/10.1016/j.jpowsour.2019.227409.

[17] M. Alkuran, M. Orabi, Utilization of a buck boost converter and the

method of segmented capacitors in a CDI water purification system, in: 2008 12th Int. Middle-East Power Syst. Conf., IEEE, 2008: pp. 470–474. https://doi.org/10.1109/MEPCON.2008.4562311.

[18] A.M. Pernía, M.J. Prieto, J.A. Martín-Ramos, P.J. Villegas, F.J. Álvarez-González, Energy Recovery in Capacitive Deionization Technology, in: Desalin. Water Treat., InTech, 2018. https://doi.org/10.5772/intechopen.75537.

[19] Y.-W. Chen, J.-F. Chen, C.-H. Lin, C.-H. Hou, Integrating a supercapacitor with capacitive deionization for direct energy recovery from the desalination of brackish water, Appl. Energy. 252 (2019) 113417. https://doi.org/10.1016/j.apenergy.2019.113417.

[20] A. Omosebi, Z. Li, N. Holubowitch, X. Gao, J. Landon, A. Cramer, K. Liu, Energy recovery in capacitive deionization systems with inverted operation characteristics, Environ. Sci. Water Res. Technol. 6 (2020) 321–330. https://doi.org/10.1039/C9EW00797K.

[21] M. Alkuran, M. Orabi, N. Scheinberg, Highly efficient Capacitive De-Ionization (CDI) water purification system using a buck-boost converter, in: 2008 Twenty-Third Annu. IEEE Appl. Power Electron. Conf. Expo., IEEE, 2008: pp. 1926–1930. https://doi.org/10.1109/APEC.2008.4522991.

[22] M. a. Anderson, A.L. Cudero, J. Palma, Capacitive deionization as an electrochemical means of saving energy and delivering clean water. Comparison to present desalination practices: Will it compete?, Electrochim. Acta. 55 (2010) 3845–3856. https://doi.org/10.1016/j.electacta.2010.02.012.

[23] A.M. Pernía, J.G. Norniella, J.A. Martín-Ramos, J. Díaz, J.A. Martínez, Up–Down Converter for Energy Recovery in a CDI Desalination System, IEEE Trans. Power Electron. 27 (2012) 3257–3265. https://doi.org/10.1109/TPEL.2011.2180926.

[24] A. Pernía, F. J. Alvarez-González, J. Díaz, P. Villegas, F. Nuño, Optimum Peak Current Hysteresis Control for Energy Recovering Converter in CDI Desalination, Energies. 7 (2014) 3823–3839. https://doi.org/10.3390/en7063823.

[25] A.M. Pernia, F.J. Alvarez-Gonzalez, M.A.J. Prieto, P.J. Villegas, F. Nuno, New Control Strategy of an Up–Down Converter for Energy Recovery in a CDI Desalination System, IEEE Trans. Power Electron. 29 (2014) 3573–3581. https://doi.org/10.1109/TPEL.2013.2280814.

[26] H. Mehrabian-Nejad, B. Farhangi, S. Farhangi, S. Vaez-Zadeh, DC-DC converter for energy loss compensation and maximum frequency limitation in capacitive deionization systems, 7th Power Electron. Drive

Syst. Technol. Conf. PEDSTC 2016. (2016) 211–216. https://doi.org/10.1109/PEDSTC.2016.7556863.

[27] F.J. Alvarez-Gonzalez, J.A. Martin-Ramos, J. Diaz, J.A. Martinez, A.M. Pernia, Energy-Recovery Optimization of an Experimental CDI Desalination System, IEEE Trans. Ind. Electron. 63 (2016) 1586–1597. https://doi.org/10.1109/TIE.2015.2494015.

[28] J. Kang, T. Kim, H. Shin, J. Lee, J.I. Ha, J. Yoon, Direct energy recovery system for membrane capacitive deionization, Desalination. 398 (2016) 144–150. https://doi.org/10.1016/j.desal.2016.07.025.

[29] H. Strathmann, Electrodialysis, a mature technology with a multitude of new applications, Desalination. 264 (2010) 268–288. https://doi.org/10.1016/j.desal.2010.04.069.

[30] T. Xu, C. Huang, Electrodialysis-Based Separation Technologies : A Critical Review, AIChE J. 54 (2008) 3147–3159. https://doi.org/10.1002/aic.

[31] M. Sadrzadeh, T. Mohammadi, Treatment of sea water using electrodialysis: Current efficiency evaluation, Desalination. 249 (2009) 279–285. https://doi.org/10.1016/j.desal.2008.10.029.

[32] M. Andelman, Flow Through Capacitor basics, Sep. Purif. Technol. 80 (2011) 262–269. https://doi.org/10.1016/j.seppur.2011.05.004.

[33] E. García-Quismondo, R. Gómez, F. Vaquero, A.L. Cudero, J. Palma, M. Anderson, New testing procedures of a capacitive deionization reactor., Phys. Chem. Chem. Phys. 15 (2013) 7648–56. https://doi.org/10.1039/c3cp50514f.

[34] S. Evans, W.S. Hamilton, The Mechanism of Demineralization at Carbon Electrodes, J. Electrochem. Soc. 113 (1966) 1314. https://doi.org/10.1149/1.2423813.

[35] G.W. Murphy, D.D. Caudle, Mathematical theory of electrochemical demineralization in flowing systems, Electrochim. Acta. 12 (1967) 1655–1664. https://doi.org/10.1016/0013-4686(67)80079-3.

[36] A. Soffer, M. Folman, The electrical double layer of high surface porous carbon electrode, J. Electroanal. Chem. Interfacial Electrochem. 38 (1972) 25–43. https://doi.org/10.1016/S0022-0728(72)80087-1.

[37] A.M. Johnson, J. Newman, Desalting by Means of Porous Carbon Electrodes, J. Electrochem. Soc. 118 (1971) 510–517. https://doi.org/10.1149/1.2408094.

[38] H. Yoon, J. Lee, S. Kim, J. Yoon, Review of concepts and applications of electrochemical ion separation (EIONS) process, Sep. Purif. Technol. 215 (2019) 190–207. https://doi.org/10.1016/j.seppur.2018.12.071.

[39] J.-B. Lee, K.-K. Park, H.-M. Eum, C.-W. Lee, Desalination of a thermal

power plant wastewater by membrane capacitive deionization, Desalination. 196 (2006) 125–134. https://doi.org/10.1016/j.desal.2006.01.011.

[40] H. Li, Y. Gao, L. Pan, Y. Zhang, Y. Chen, Z. Sun, Electrosorptive desalination by carbon nanotubes and nanofibres electrodes and ion-exchange membranes., Water Res. 42 (2008) 4923–8. https://doi.org/10.1016/j.watres.2008.09.026.

[41] P.M. Biesheuvel, a. van der Wal, Membrane capacitive deionization, J. Memb. Sci. 346 (2010) 256–262. https://doi.org/10.1016/j.memsci.2009.09.043.

[42] S. Jeon, J. Lee, K. Jo, C. Kim, C. Lee, J. Yoon, Novel Reuse Strategy in Flow-Electrode Capacitive Deionization with Switch Cycle Operation To Enhance Desalination Performance, Environ. Sci. Technol. Lett. 6 (2019) 739–744. https://doi.org/10.1021/acs.estlett.9b00541.

[43] S. Jeon, J. Yeo, S. Yang, J. Choi, D.K. Kim, Ion storage and energy recovery of a flow-electrode capacitive deionization process, J. Mater. Chem. A. 2 (2014) 6378–6383. https://doi.org/10.1039/c4ta00377b.

[44] S. Jeon, H. Park, J. Yeo, S. Yang, C.H. Cho, M.H. Han, D.K. Kim, Desalination via a new membrane capacitive deionization process utilizing flow-electrodes, Energy Environ. Sci. 6 (2013) 1471–1475.

https://doi.org/10.1039/c3ee24443a.

[45] C. Kim, J. Lee, P. Srimuk, M. Aslan, V. Presser, Concentration-Gradient Multichannel Flow-Stream Membrane Capacitive Deionization Cell for High Desalination Capacity of Carbon Electrodes, ChemSusChem. 10 (2017) 4914–4920. https://doi.org/10.1002/cssc.201700967.

[46] C. Kim, P. Srimuk, J. Lee, M. Aslan, V. Presser, Semi-continuous capacitive deionization using multi-channel flow stream and ion exchange membranes, Desalination. 425 (2018) 104–110. https://doi.org/10.1016/j.desal.2017.10.012.

[47] C. Kim, P. Srimuk, J. Lee, V. Presser, Enhanced desalination via cell voltage extension of membrane capacitive deionization using an aqueous/organic bi-electrolyte, Desalination. 443 (2018) 56–61. https://doi.org/10.1016/j.desal.2018.05.016.

[48] N. Kim, J. Lee, S. Kim, S.P. Hong, C. Lee, J. Yoon, C. Kim, Short Review of Multichannel Membrane Capacitive Deionization: Principle, Current Status, and Future Prospect, Appl. Sci. 10 (2020) 683. https://doi.org/10.3390/app10020683.

[49] N. Kim, J. Lee, S.P. Hong, C. Lee, C. Kim, J. Yoon, Performance analysis of the multi-channel membrane capacitive deionization with porous carbon electrode stacks, Desalination. 479 (2020) 114315.

https://doi.org/10.1016/j.desal.2020.114315.

[50] J. Lee, K. Jo, J. Lee, S.P. Hong, S. Kim, J. Yoon, Rocking-Chair Capacitive Deionization for Continuous Brackish Water Desalination, ACS Sustain. Chem. Eng. 6 (2018) 10815–10822. https://doi.org/10.1021/acssuschemeng.8b02123.

[51] K.C. Smith, R. Dmello, Na-Ion Desalination (NID) Enabled by Na-Blocking Membranes and Symmetric Na-Intercalation: Porous-Electrode Modeling, J. Electrochem. Soc. 163 (2016) A530–A539. https://doi.org/10.1149/2.0761603jes.

[52] S. Porada, A. Shrivastava, P. Bukowska, P.M. Biesheuvel, K.C. Smith, Nickel Hexacyanoferrate Electrodes for Continuous Cation Intercalation Desalination of Brackish Water, Electrochim. Acta. 255 (2017) 369–378. https://doi.org/10.1016/j.electacta.2017.09.137.

[53] J. Lee, S. Kim, J. Yoon, Rocking Chair Desalination Battery Based on Prussian Blue Electrodes, ACS Omega. 2 (2017) 1653–1659. https://doi.org/10.1021/acsomega.6b00526.

[54] J. Ahn, S. Kim, S. il Jeon, C. Lee, P.M. Biesheuvel, J. Lee, J. Yoon, New method for electrochemical ion separation (ElONS) for chloride/nitrate separation using Ag/AgCl electrodes with a cation exchange membrane, J. Environ. Chem. Eng. 9 (2021) 106876.

https://doi.org/10.1016/j.jece.2021.106876.

[55] D. Ahn, D. Kim, J.H. Park, N. Kim, E. Lim, C. Kim, Enhanced desalination performance of nitrogen-doped porous carbon electrode in redox-mediated deionization, Desalination. 520 (2021) 115333. https://doi.org/10.1016/j.desal.2021.115333.

[56] J. Ma, D. He, W. Tang, P. Kovalsky, C. He, C. Zhang, T.D. Waite, Development of Redox-Active Flow Electrodes for High-Performance Capacitive Deionization, Environ. Sci. Technol. 50 (2016) 13495–13501. https://doi.org/10.1021/acs.est.6b03424.

[57] N. Kim, S.P. Hong, J. Lee, C. Kim, J. Yoon, High-Desalination Performance via Redox Couple Reaction in the Multichannel Capacitive Deionization System, ACS Sustain. Chem. Eng. 7 (2019) 16182–16189. https://doi.org/10.1021/acssuschemeng.9b03121.

[58] K.B. Hatzell, M. Boota, E.C. Kumbur, Y. Gogotsi, Flowable Conducting Particle Networks in Redox-Active Electrolytes for Grid Energy Storage, J. Electrochem. Soc. 162 (2015) A5007–A5012. https://doi.org/10.1149/2.0011505jes.

[59] E.S. Beh, M.A. Benedict, D. Desai, J.B. Rivest, A Redox-Shuttled Electrochemical Method for Energy-Efficient Separation of Salt from Water, ACS Sustain. Chem. Eng. 7 (2019) 13411–13417.

https://doi.org/10.1021/acssuschemeng.9b02720.

[60] H. Li, L. Zou, L. Pan, Z. Sun, Novel Graphene-Like Electrodes for Capacitive Deionization, Environ. Sci. Technol. 44 (2010) 8692–8697. https://doi.org/10.1021/es101888j.

[61] D. Zhang, L. Shi, J. Fang, K. Dai, X. Li, Preparation and desalination performance of multiwall carbon nanotubes, Mater. Chem. Phys. 97 (2006) 415–419. https://doi.org/10.1016/j.matchemphys.2005.08.036.

[62] G. Wang, C. Pan, L. Wang, Q. Dong, C. Yu, Z. Zhao, J. Qiu, Activated carbon nanofiber webs made by electrospinning for capacitive deionization, Electrochim. Acta. 69 (2012) 65–70. https://doi.org/10.1016/j.electacta.2012.02.066.

[63] H.-J. Oh, J.-H. Lee, H.-J. Ahn, Y. Jeong, Y.-J. Kim, C.-S. Chi, Nanoporous activated carbon cloth for capacitive deionization of aqueous solution, Thin Solid Films. 515 (2006) 220–225. https://doi.org/10.1016/j.tsf.2005.12.146.

[64] J. Li, X. Wang, Q. Huang, S. Gamboa, P.J. Sebastian, Studies on preparation and performances of carbon aerogel electrodes for the application of supercapacitor, J. Power Sources. 158 (2006) 784–788. https://doi.org/10.1016/j.jpowsour.2005.09.045.

[65] Z. Peng, D. Zhang, L. Shi, T. Yan, S. Yuan, H. Li, R. Gao, J. Fang,

Comparative Electroadsorption Study of Mesoporous Carbon Electrodes with Various Pore Structures, J. Phys. Chem. C. 115 (2011) 17068–17076. https://doi.org/10.1021/jp2047618.

[66] W. Tang, J. Liang, D. He, J. Gong, L. Tang, Z. Liu, D. Wang, G. Zeng, Various cell architectures of capacitive deionization: Recent advances and future trends, Water Res. 150 (2019) 225–251. https://doi.org/10.1016/j.watres.2018.11.064.

[67] J. Ahn, A Study on the Improvement of Desealination Capacity and Stability of Ion Reactive Battery Desalination (DB) (unpublished doctoral dissertation), Seoul National University, 2022.

[68] K.Y. Foo, B.H. Hameed, A short review of activated carbon assisted electrosorption process: an overview, current stage and future prospects., J. Hazard. Mater. 170 (2009) 552–9. https://doi.org/10.1016/j.jhazmat.2009.05.057.

[69] P.M. Biesheuvel, S. Porada, M. Levi, M.Z. Bazant, Attractive forces in microporous carbon electrodes for capacitive deionization, J. Solid State Electrochem. 18 (2014) 1365–1376. https://doi.org/10.1007/s10008-014-2383-5.

[70] X. Gao, A. Omosebi, J. Landon, K. Liu, Voltage-Based Stabilization of Microporous Carbon Electrodes for Inverted Capacitive Deionization, J.

Phys. Chem. C. 122 (2018) 1158–1168. https://doi.org/10.1021/acs.jpcc.7b08968.

[71] T. Kim, J.E. Dykstra, S. Porada, A. van der Wal, J. Yoon, P.M. Biesheuvel, Enhanced charge efficiency and reduced energy use in capacitive deionization by increasing the discharge voltage, J. Colloid Interface Sci. 446 (2015) 317–326. https://doi.org/10.1016/j.jcis.2014.08.041.

[72] P.M. Biesheuvel, H.V.M. Hamelers, M.E. Suss, Theory of Water Desalination by Porous Electrodes with Immobile Chemical Charge, Colloids Interface Sci. Commun. 9 (2015) 1–5. https://doi.org/10.1016/j.colcom.2015.12.001.

[73] X. Gao, A. Omosebi, N. Holubowitch, J. Landon, K. Liu, Capacitive Deionization Using Alternating Polarization: Effect of Surface Charge on Salt Removal, Electrochim. Acta. 233 (2017) 249–255. https://doi.org/10.1016/j.electacta.2017.03.021.

[74] J. Yu, K. Jo, T. Kim, J. Lee, J. Yoon, Temporal and spatial distribution of pH in flow-mode capacitive deionization and membrane capacitive deionization, Desalination. 439 (2018) 188–195. https://doi.org/10.1016/j.desal.2018.04.011.

[75] C. Zhang, D. He, J. Ma, W. Tang, T.D. Waite, Faradaic reactions in

capacitive deionization (CDI) - problems and possibilities: A review, Water Res. 128 (2018) 314–330. https://doi.org/10.1016/j.watres.2017.10.024.

[76] Marc D. Andelman, Gregory S. Walker, Charge barrier flow-through capacitor, US 6,709,560 B2, 2004.

[77] E. Avraham, Y. Bouhadana, A. Soffer, D. Aurbach, Limitation of Charge Efficiency in Capacitive Deionization, J. Electrochem. Soc. 156 (2009) P95. https://doi.org/10.1149/1.3115463.

[78] E. Avraham, M. Noked, Y. Bouhadana, A. Soffer, D. Aurbach, Limitations of Charge Efficiency in Capacitive Deionization, J. Electrochem. Soc. 156 (2009) P157. https://doi.org/10.1149/1.3193709.

[79] E. Avraham, M. Noked, Y. Bouhadana, A. Soffer, D. Aurbach, Limitations of charge efficiency in capacitive deionization processes III: The behavior of surface oxidized activated carbon electrodes, Electrochim. Acta. 56 (2010) 441–447. https://doi.org/10.1016/j.electacta.2010.08.056.

[80] I. Cohen, E. Avraham, M. Noked, A. Soffer, D. Aurbach, Enhanced Charge Efficiency in Capacitive Deionization Achieved by Surface-Treated Electrodes and by Means of a Third Electrode, J. Phys. Chem. C. 115 (2011) 19856–19863. https://doi.org/10.1021/jp206956a.

[81] M.E. Suss, T.F. Baumann, W.L. Bourcier, C.M. Spadaccini, K. a. Rose, J.G. Santiago, M. Stadermann, Capacitive desalination with flow-through electrodes, Energy Environ. Sci. 5 (2012) 9511–9519. https://doi.org/10.1039/c2ee21498a.

[82] X. Gao, A. Omosebi, J. Landon, K. Liu, Enhanced Salt Removal in an Inverted Capacitive Deionization Cell Using Amine Modified Microporous Carbon Cathodes, Environ. Sci. Technol. 49 (2015) 10920–10926. https://doi.org/10.1021/acs.est.5b02320.

[83] X. Gao, A. Omosebi, J. Landon, K. Liu, Surface charge enhanced carbon electrodes for stable and efficient capacitive deionization using inverted adsorption–desorption behavior, Energy Environ. Sci. 8 (2015) 897–909. https://doi.org/10.1039/C4EE03172E.

[84] S. Yang, S. Il Jeon, H. Kim, J. Choi, J.G. Yeo, H.R. Park, D.K. Kim, Stack Design and Operation for Scaling Up the Capacity of Flow-Electrode Capacitive Deionization Technology, ACS Sustain. Chem. Eng. 4 (2016) 4174–4180. https://doi.org/10.1021/acssuschemeng.6b00689.

[85] S. Yang, J. Choi, J. Yeo, S. Jeon, H. Park, D.K. Kim, Flow-Electrode Capacitive Deionization Using an Aqueous Electrolyte with a High Salt Concentration, Environ. Sci. Technol. 50 (2016) 5892–5899.

https://doi.org/10.1021/acs.est.5b04640.

[86] C.J. Linnartz, A. Rommerskirchen, M. Wessling, Y. Gendel, Flow-Electrode Capacitive Deionization for Double Displacement Reactions, ACS Sustain. Chem. Eng. 5 (2017) 3906–3912. https://doi.org/10.1021/acssuschemeng.6b03086.

[87] K.B. Hatzell, M.C. Hatzell, K.M. Cook, M. Boota, G.M. Housel, A. McBride, E.C. Kumbur, Y. Gogotsi, Effect of Oxidation of Carbon Material on Suspension Electrodes for Flow Electrode Capacitive Deionization, Environ. Sci. Technol. 49 (2015) 3040–3047. https://doi.org/10.1021/es5055989.

[88] H. Park, J. Choi, S. Yang, S.J. Kwak, S. Jeon, M.H. Han, D.K. Kim, Surface-modified spherical activated carbon for high carbon loading and its desalting performance in flow-electrode capacitive deionization, RSC Adv. 6 (2016) 69720–69727. https://doi.org/10.1039/C6RA02480G.

[89] P. Liang, X. Sun, Y. Bian, H. Zhang, X. Yang, Y. Jiang, P. Liu, X. Huang, Optimized desalination performance of high voltage flow-electrode capacitive deionization by adding carbon black in flow-electrode, Desalination. 420 (2017) 63–69. https://doi.org/10.1016/j.desal.2017.05.023.

[90] S. Yang, H. Park, J. Yoo, H. Kim, J. Choi, M.H. Han, D.K. Kim, Plate-

Shaped Graphite for Improved Performance of Flow-Electrode Capacitive Deionization, J. Electrochem. Soc. 164 (2017) E480–E488. https://doi.org/10.1149/2.1551713jes.

[91] H. Boo, S. Park, B. Ku, Y. Kim, J.H. Park, H.C. Kim, T.D. Chung, Ionic Strength-Controlled Virtual Area of Mesoporous Platinum Electrode, J. Am. Chem. Soc. 126 (2004) 4524–4525. https://doi.org/10.1021/ja0398316.

[92] A. Rommerskirchen, Y. Gendel, M. Wessling, Single module flow-electrode capacitive deionization for continuous water desalination, Electrochem. Commun. 60 (2015) 34–37. https://doi.org/10.1016/j.elecom.2015.07.018.

[93] P. Srimuk, X. Su, J. Yoon, D. Aurbach, V. Presser, Charge-transfer materials for electrochemical water desalination, ion separation and the recovery of elements, Nat. Rev. Mater. 5 (2020) 517–538. https://doi.org/10.1038/s41578-020-0193-1.

[94] L. Wang, Y. Zhang, K. Moh, V. Presser, From capacitive deionization to desalination batteries and desalination fuel cells, Curr. Opin. Electrochem. 29 (2021) 100758. https://doi.org/10.1016/j.coelec.2021.100758.

[95] Y. Qu, P.G. Campbell, L. Gu, J.M. Knipe, E. Dzenitis, J.G. Santiago, M.

Stadermann, Energy consumption analysis of constant voltage and constant current operations in capacitive deionization, Desalination. 400 (2016) 18–24. https://doi.org/10.1016/j.desal.2016.09.014.

[96] L. Wang, J.E. Dykstra, S. Lin, Energy Efficiency of Capacitive Deionization, Environ. Sci. Technol. 53 (2019) 3366–3378. https://doi.org/10.1021/acs.est.8b04858.

[97] J. Kang, T. Kim, K. Jo, J. Yoon, Comparison of salt adsorption capacity and energy consumption between constant current and constant voltage operation in capacitive deionization, Desalination. 352 (2014) 52–57. https://doi.org/10.1016/j.desal.2014.08.009.

[98] L. Han, K.G. Karthikeyan, K.B. Gregory, Energy Consumption and Recovery in Capacitive Deionization Using Nanoporous Activated Carbon Electrodes, J. Electrochem. Soc. 162 (2015) E282–E288. https://doi.org/10.1149/2.0431512jes.

[99] J.-H. Choi, Comparison of constant voltage (CV) and constant current (CC) operation in the membrane capacitive deionisation process, Desalin. Water Treat. 56 (2015) 921–928. https://doi.org/10.1080/19443994.2014.942379.

[100] R. Zhao, P.M. Biesheuvel, A. van der Wal, Energy consumption and constant current operation in membrane capacitive deionization, Energy

Environ. Sci. 5 (2012) 9520. https://doi.org/10.1039/c2ee21737f.

[101] R. Zhao, O. Satpradit, H.H.M. Rijnaarts, P.M. Biesheuvel, A. van der Wal, Optimization of salt adsorption rate in membrane capacitive deionization., Water Res. 47 (2013) 1941–52. https://doi.org/10.1016/j.watres.2013.01.025.

[102] J.E. Dykstra, S. Porada, A. van der Wal, P.M. Biesheuvel, Energy consumption in capacitive deionization – Constant current versus constant voltage operation, Water Res. 143 (2018) 367–375. https://doi.org/10.1016/j.watres.2018.06.034.

[103] L. Wang, S. Lin, Membrane Capacitive Deionization with Constant Current vs Constant Voltage Charging: Which Is Better?, Environ. Sci. Technol. 52 (2018) 4051–4060. https://doi.org/10.1021/acs.est.7b06064.

[104] J. Landon, X. Gao, J.K. Neathery, K. Liu, Energy Recovery in Parallel Capacitive Deionization Operations, ECS Trans. 53 (2013) 235–243. https://doi.org/10.1149/05330.0235ecst.

[105] G.L. Andres, Y. Yoshihara, A capacitive deionization system with high energy recovery and effective re-use, Energy. 103 (2016) 605–617. https://doi.org/10.1016/j.energy.2016.03.021.

[106] G.L. Andres, T. Mizugami, Y. Yoshihara, Simulation of an electric behavior of the CDI system, Desalination. 419 (2017) 211–218.

https://doi.org/10.1016/j.desal.2017.06.011.

[107] Y.A. Chen, C.S. Fan, C.H. Hou, Optimizing the energetic performance of capacitive deionization devices with unipolar and bipolar connections under constant current charging, J. Taiwan Inst. Chem. Eng. 93 (2018) 201–210. https://doi.org/10.1016/j.jtice.2018.06.039.

[108] J. Yang, H. Zhao, C. Li, X. Li, A direct energy reuse strategy for absorption air-conditioning system based on electrode regeneration method, Renew. Energy. 168 (2021) 353–364. https://doi.org/10.1016/j.renene.2020.12.012.

[109] A. Román Santiago, P. Baldaguez Medina, X. Su, Electrochemical remediation of perfluoroalkyl substances from water, Electrochim. Acta. 403 (2022) 139635. https://doi.org/10.1016/j.electacta.2021.139635.

[110] N. Kim, J. Jeon, R. Chen, X. Su, Electrochemical separation of organic acids and proteins for food and biomanufacturing, Chem. Eng. Res. Des. 178 (2022) 267–288. https://doi.org/10.1016/j.cherd.2021.12.009.

[111] H. Strathmann, Electrodialysis, a mature technology with a multitude of new applications, Desalination. 264 (2010) 268–288. https://doi.org/10.1016/j.desal.2010.04.069.

[112] G. Folaranmi, M. Bechelany, P. Sistat, M. Cretin, F. Zaviska, Towards Electrochemical Water Desalination Techniques: A Review on Capacitive Deionization, Membrane Capacitive Deionization and Flow Capacitive Deionization, Membranes (Basel). 10 (2020) 96. https://doi.org/10.3390/membranes10050096.

[113] J.W. Palko, D.I. Oyarzun, B. Ha, M. Stadermann, J.G. Santiago, Nitrate removal from water using electrostatic regeneration of functionalized adsorbent, Chem. Eng. J. 334 (2018) 1289–1296. https://doi.org/10.1016/j.cej.2017.10.161.

[114] Q. Dong, X. Guo, X. Huang, L. Liu, R. Tallon, B. Taylor, J. Chen, Selective removal of lead ions through capacitive deionization: Role of ion-exchange membrane, Chem. Eng. J. 361 (2019) 1535–1542. https://doi.org/10.1016/j.cej.2018.10.208.

[115] D.I. Kim, P. Dorji, G. Gwak, S. Phuntsho, S. Hong, H. Shon, Reuse of municipal wastewater via membrane capacitive deionization using ion-selective polymer-coated carbon electrodes in pilot-scale, Chem. Eng. J. 372 (2019) 241–250. https://doi.org/10.1016/j.cej.2019.04.156.

[116] A.S. Yasin, A.Y. Mohamed, I.M.A. Mohamed, D.Y. Cho, C.H. Park, C.S. Kim, Theoretical insight into the structure-property relationship of mixed transition metal oxides nanofibers doped in activated carbon and

3D graphene for capacitive deionization, Chem. Eng. J. 371 (2019) 166–181. https://doi.org/10.1016/j.cej.2019.04.043.

[117] J. Kim, J. Kim, J.H. Kim, H.S. Park, Hierarchically open-porous nitrogen-incorporated carbon polyhedrons derived from metal-organic frameworks for improved CDI performance, Chem. Eng. J. 382 (2020) 122996. https://doi.org/10.1016/j.cej.2019.122996.

[118] J. Ma, T. Gao, Y. He, K. Zuo, Q. Li, P. Liang, Enhanced Charge Efficiency and Electrode Separation Utilizing Magnetic Carbon in Flow Electrode Capacitive Deionization, ACS ES&T Eng. 1 (2021) 340–347. https://doi.org/10.1021/acsestengg.0c00044.

[119] L. Wang, Y. Liang, L. Zhang, Enhancing Performance of Capacitive Deionization with Polyelectrolyte-Infiltrated Electrodes: Theory and Experimental Validation, Environ. Sci. Technol. 54 (2020) 5874–5883. https://doi.org/10.1021/acs.est.9b07692.

[120] H. Younes, F. Ravaux, N. El Hadri, L. Zou, Nanostructuring of pseudocapacitive MnFe2O4/Porous rGO electrodes in capacitive deionization, Electrochim. Acta. 306 (2019) 1–8. https://doi.org/10.1016/j.electacta.2019.03.097.

[121] J. Ahn, S. Kim, S. il Jeon, C. Lee, J. Lee, J. Yoon, Nafion-coated Prussian blue electrodes to enhance the stability and efficiency of battery

desalination system, Desalination. 500 (2021) 114778. https://doi.org/10.1016/j.desal.2020.114778.

[122] J. Ahn, J. Lee, S. Kim, C. Kim, J. Lee, P.M. Biesheuvel, J. Yoon, High performance electrochemical saline water desalination using silver and silver-chloride electrodes, Desalination. 476 (2020) 114216. https://doi.org/10.1016/j.desal.2019.114216.

[123] N. Kim, X. Su, C. Kim, Electrochemical lithium recovery system through the simultaneous lithium enrichment via sustainable redox reaction, Chem. Eng. J. 420 (2021) 127715. https://doi.org/10.1016/j.cej.2020.127715.

[124] X. Hou, Q. Liang, X. Hu, Y. Zhou, Q. Ru, F. Chen, S. Hu, Coupling desalination and energy storage with redox flow electrodes, Nanoscale. 10 (2018) 12308–12314. https://doi.org/10.1039/C8NR02737D.

[125] J. Lee, S. Kim, C. Kim, J. Yoon, Hybrid capacitive deionization to enhance the desalination performance of capacitive techniques, Energy Environ. Sci. 7 (2014) 3683–3689. https://doi.org/10.1039/C4EE02378A.

[126] K. Tang, Y. ha Kim, J. Chang, R.T. Mayes, J. Gabitto, S. Yiacoumi, C. Tsouris, Seawater desalination by over-potential membrane capacitive deionization: Opportunities and hurdles, Chem. Eng. J. 357

(2019) 103–111. https://doi.org/10.1016/j.cej.2018.09.121.

[127] Y. Wang, I. Vázquez-Rodríguez, C. Santos, E. García-Quismondo, J. Palma, M.A. Anderson, J.J. Lado, Graphite felt 3D framework composites as an easy to scale capacitive deionization electrode for brackish water desalination, Chem. Eng. J. 392 (2020) 123698. https://doi.org/10.1016/j.cej.2019.123698.

국문 초록

기후위기 극복을 위한 탄소중립사회로의 전환을 위해 에너지 효율적이고 친환경적인 물 확보 기술의 개발이 중요하며, 저에너지 친환경 담수화 기술인 막 축전식 탈염 (membrane capacitive deionization, MCDI) 기술이 주목받고 있다. MCDI 기술이 실제 산업에 적용되기 위해서는 MCDI 모듈의 확장과 에너지 회수 기술의 탑재가 필수적이지만, 기존 확장 방식은 시스템에서 큰 에너지 손실이 발생하며, 에너지 회수 기술도 비효율적이다.

본 논문은 직접 에너지 회수 단계를 포함하는 양극성 전극 기반 막 축전식 탈염 (bipolar electrode based MCDI, Bipolar MCDI) 시스템을 개발하는 것을 목적으로 한다. 이를 위해 두가지 접근 방식을 적용하였다. 첫 번째는 직렬 연결로 적층된 전극인 양극성 전극을 통하여 이를 해결하였다. 양극성 전극 기반 막축전식 탈염(bipolar electrode based MCDI, Bipolar MCDI)은 높은 전압, 낮은 전류로 운전되기 때문에 산업 규모에서의 에너지 손실을 줄일 수 있다. 두 번째는 직접 에너지 회수 방식을 채용하여 시스템의 에너지 소비를 줄일 수 있었다. 그러나 이 두 개념의 성공적인 조합을 위해서는 전기적 안전성 확보가 우선해야 한다. 높은 운전 전압으로 작동하는 두 개의 Bipolar MCDI 모듈이 에너지 회수를 위

해 직접 연결될 경우, 시스템의 허용 전류보다 높은 전류가 흐를 가능성이 높고, 이는 전기 폭발이나 장치 손상으로 나타날 수 있다.

우선, Bipolar MCDI 모듈의 충/방전 및 직접 에너지 회수 단계를 모사하기 위하여 등가회로 모델을 적용하였다. 주요 모사 결과는 충/방전 단계는 물론 직접 에너지 회수 단계에 대해서도 실제 실험결과와 매우 잘 맞았다. 또한 직접에너지 회수가 정전압 운전의 전류 범위 이내에서 작동함을 확인하였고, 이는 Bipolar MCDI의 직접에너지 회수가 정전압 시스템에 안전하게 작동할 수 있음을 나타낸다.

둘째, 직접 에너지 회수 단계를 포함하는 Bipolar MCDI 시스템의 운전 특성을 조사하였고, 이를 토대로 최적화된 운전 방식을 파일럿 규모 공정에도 확장하였다. 주요 결과로 실험실 규모의 장치 (2.4 V와 12 V 시스템)에서 기존의 정전압 충/방전 운전에 비해 각각 43%와 41%의 에너지를 저감할 수 있었다. 게다가 파일럿 규모의 공정에서도 탈염 성능의 저하없이 40%의 에너지를 감축하였다.

요약하면 본 연구에서는 MCDI 기술의 산업적 응용을 위해 MCDI 모듈 확장과 에너지 회수 기술을 양극성 전극 그리고 직접 에너지 회수 기술을 적용하여 파일럿 공정에도 적용되는 Bipolar MCDI 시스템을 성공적으로 개발하였다. 본 연구를 통해 개발한 직접 에너지 회수 단계를

포함하는 Bipolar MCDI 시스템이 실제 산업 환경에서 에너지 효율적인 대안이 될 수 있으며, 개발과정은 향후 실험실 규모의 연구가 산업 규모로 확장하는 것에 도움을 줄 수 있을 것으로 기대 된다.

주요어: 전기화학적 이온분리; 축전식 탈염; 양극성 전극; 에너지 회수; 등가회로;

학번: 2017-34898